PhD-Thesis

Eukaryotic Translation Initiation Factors in Non-Small Cell Lung Cancer

submitted by

Nadine Gantenbein, MSc. BSc.

for the Academic Degree of

Doctor of Philosophy (PhD)

at the

Medical University of Graz

Diagnostic & Research Center, Institute of Pathology

under the Supervision of

Prof. Dr.med. univ. Dr.sc.nat. Johannes Haybaeck

October, 2018

“Declaration

I hereby declare that this thesis is my own original work and that I have fully acknowledged by name all of those individuals and organizations that have contributed to the research for this thesis. Due acknowledgement has been made in the text to all other material used. Throughout this thesis and in all related publications I followed the “Standards of Good Scientific Practice and Ombuds Committee at the Medical University of Graz”.
1st of October, 2018”.

_____

Nadine Gantenbein, MSc. BSc.

Parts of this thesis have been published in:

Influence of eukaryotic translation initiation factor 6 on non-small cell lung cancer development and progression

Nadine Gantenbein [1,2], Eva Bernhart [3], Ines Anders [1], Nicole Golob-Schwarzl [1,2], Stefanie Krassnig [1], Christina Wodlej [1,2], Luka Brcic [1], Joerg Lindenmann [4], Nicole Fink-Neuboeck [4], Franz Gollowitsch [1], Elvira Stacher-Priehse [1], Martin Asslaber [1], Margit Gogg-Kamerer [1], Jana Rolff [5], Jens Hoffmann [5], Alessandra Silvestri [6], Christian Regenbrecht [6], Christoph Reinhard [7], Anna-Maria Pehserl [8], Martin Pichler [8], Olga Sokolova [9], Michael Naumann [9], Valentin Mitterer [10], Brigitte Pertschy [10], Helmut Bergler [10], Helmut Popper [1], Wolfgang Sattler [3], Johannes Haybaeck [1,2,11]

1 Diagnostic and Research Institute of Pathology, Medical University of Graz, Neuestiftingtalstrasse 6, 8010 Graz, Austria
2 Center for Biomarker Research in Medicine, Stiftingtalstrasse 5, 8010 Graz, Austria
3 Gottfried Schatz Research Center for Cell Signaling, Metabolism and Aging, Molecular Biology and Biochemistry, Medical University of Graz, Neuestiftingtalstrasse 6, 8010 Graz, Austria
4 Division of Thoracic and Hyperbaric Surgery, Medical University of Graz, Auenbruggerplatz 29, 8036 Graz, Austria
5 Experimental Pharmacology & Oncology Berlin GmbH-Berlin-Buch, Robert-Rössle-Str. 10, 13125 Berlin-Buch, Germany
6 Cpo - Cellular Phenomics & Oncology Berlin-Buch GmbH, Robert-Rössle-Str. 10, 13125 Berlin-Buch, Germany
7 Eli Lilly & Company, Lilly Corporate Center, 46285 Indiana, Indianapolis, USA
8 Division of Oncology, Medical University of Graz, Auenbruggerplatz 15, 8036 Graz, Austria
9 Institute of Experimental Internal Medicine, Otto-von-Guericke-University Magdeburg, Leipziger Str. 44, 39120 Magdeburg, Germany
10 Institute of Molecular Biosciences, Karl-Franzens-University of Graz, Humboldtstraße 50, 8010 Graz, Austria
11 Department of Pathology, Medical Faculty, Otto-von-Guericke-University Magdeburg, Leipziger Str. 44, 39120 Magdeburg, Germany

„Es gibt keine Probleme, lediglich Herausforderungen. Nur müssen wir bereit sein, sie zu erkennen, zu bewerten und zu bewältigen. Gelingt uns das einmal nicht, muss dies nicht gleichbedeutend mit einer Niederlage sein. Vielleicht müssen wir dann nur unser Ziel ändern.” Wladimir Klitschko [1]

Acknowledgements

Finally, this work is coming to an end, I would like to thank the PhD MolMed program for giving me the opportunity to do my PhD at the Medical University of Graz. I would also like to thank the PhD program and the CBmed GmbH for funding my project.
I would like to thank my supervisor Prof. Johannes Haybaeck, his support and the freedom he gave me with my project was perfect.
My thesis committee, Prof. Wolfgang Sattler and Prof. Peter Neumeister supported me and guided me perfectly on my way to finalizing this work. Specially, many thanks go to Wolfgang, who welcomed me in his lab, supported me and had every time an open ear for me.
Eva Bernhart, thank you for all the time you sacrificed showing me new protocols and the friendship which developed during the last three years.
I also want to thank my lab collogues, it was an unforgettable time!
My biggest thanks go to my mum, who helped me every minute during the PhD, which were not always easy minutes - despair and joy were close together! Mum, you made my time in Graz the best time in my life. Thank you for your relentless support, I love you!
Thanks are nearly not enough to describe his support and love he gave me, since we met! I'm grateful to have you by my side, Chris.
Mariella and Bernadette, my best friends, the time we had together during this PhD time was very limited, but you both were my airbag and my friends in good and bad times, thank you both my two lovely girls!!
Fabienne, my little sis, I could not wish for a better sister, for your relentless love and support.
My godfather Werner and his wife Eli, welcomed me in their family like her own child. I could always count on them, thank you for the last unforgettable 11 years we spent together in Graz.
My beloved grandparents, who were the reason for moving to Graz, thank you for all the happy and precious moments we shared together!
Zoey my little dog, who became part of our family two years ago and her happy nature made me smile every day, thank you Joyli!
Last but not least, thanks to my family, friends and all people who believed in me!

Table of Content

Abbreviations

ADC	Adeno carcinoma
Alk	Anaplastic lymphoma kinase
BRAF	V-raf murine sarcoma viral oncogene homolog B
Casp 3	Caspase 3
cDNA	Complementary deoxyribonucleic acid
CK20	Cytokeratin 20
CK7	Cytokeratin 7
CT	Computed tomography scan
DNA	Deoxyribonucleic acid
EGFR	Epidermal growth factor receptor
eIFs	eukaryotic translation initiation factor
ER	Endoplasmatic reticulum
EtOH	Ethanol
ETS	External spacer
FACS	Fluorescence activated cell sorter
FDA	Food and Drug Administration
G1	Grade 1
G2	Grade 2
G3	Grade 3
GDP	Guanosine-diphosphate
GTP	Guanosine-triphosphate
HER2	Human epidermal growth factor receptor 2
HKG	House keeping gene
IC_{50}	Half maximal inhibitory concentration
IHC	Immunohistochemistry
IRES	Internal ribosome entry site
ITS	Internal spacer
KRAS	Kirsten rat sarcoma viral oncogene
LC	Large cell carcinoma
MAPK	Mitogen-activated protein kinase
MEK	Mesenchymal-epithelial transition kinase
MET	Mesenchymal epithelial transition factor
MRI	Magnetic resonance imaging
mRNA	Messenger ribonucleic acid

mTOR	Mechanistic target of Rapamycin
NGS	New generation sequencing
NNT	Non-neoplastic tissue
NRG1	Neuregulin 1
NSCLC	Non-small cell lung cancer
NTRK1	Neurotrophic receptor tyrosine kinase 1
OS	Overall survival
PARP	Poly (ADP-ribose) polymerase
PD-L1	Programmed death ligand 1
PERK	Protein kinase R (PKR)-like endoplasmic reticulum kinase (PERK)
PIK3	Phosphatidylinositol 3-kinase
Pol I-III	Polymerarse 1
RET	Receptor tyrosine kinase
RNA	Ribonucleic acid
ROS1	Proto-oncogene tyrosine-protein kinase
RPL	Ribosomal proteins of the large subunit of the ribosome
RPS	Ribosomal proteins of the small subunit of the ribosome
rRNA	Ribosomal ribonucleic acid
SBDS	Shwachman–Bodian–Diamond syndrome
SCLC	Small cell carcinoma
SDHA	Succinate dehydrogenase complex, subunit A
SEM	Standard error of means
siRNA	Silencing ribonucleid acid
SQC	Squamous cell carcinoma
TCGA	The Cancer Genome Atlas
TMA	Tissue micro array
TNM	Classification of Malignant Tumours
tRNA	Transfere ribonucleic acid
$_{met}$tRNAi	Initiator transfere ribonucleic acid
TTF1	Thyroide transkriptionfactor 1
USA	United States of America
UTR	Untranslated region
VEGF	Vascular Endothelial Growth Factor
WHO	World health organisation

List of Figures

List of Tables

Zusammenfassung

Nicht-kleinzelligem Lungenkrebs (NSCLC) gehört zu den am häufigsten diagnostizierten Krebstypen und ist eine der führenden Ursachen für krebsbedingte Todesfälle weltweit. NSCLC hat zwei große histologische Subtypen, Adenokarzinom (ADC) und Plattenepithelkarzinom (SQC). Die Zukunft für Patienten mit NSCLC ist trist, mit einer 5-Jahres-Überlebensrate von 15%. Daher ist ständige Forschung erforderlich, um zukünftige Patienten besser zu versorgen.

Die Dysregulation der Proteinsynthese hat als ein wichtiger Schritt in der Krebsentwicklung und -progression beträchtliche Aufmerksamkeit erhalten. Die Proteinsynthese wird auf mehreren Stufen reguliert, einschließlich der Translation von mRNA in Proteine. Einige Studien legen nahe, dass die ribosomale Proteinsynthese eine direkte Rolle während der Tumorinitiation spielt.

Entscheidend für diesen Translationsprozess sind eukaryotische Initiationsfaktoren (eIFs), die die korrekte 80S-Ribosomenassemblierung sicherstellen. eIFs sind mit den MAPK- und mTOR-Signalwegen verbunden, die zu wichtigen Zielen in der Krebstherapie geworden sind. Mutationen oder deregulierte Expression von eIFs beeinflussen das Zellwachstum und die Zellproliferation und tragen zur Karzinogenese bei.

Die vorliegende Arbeit basiert auf der Hypothese, dass eIFs potentielle Biomarker bei NSCLC darstellen und dass spezifische Mitglieder zum neoplastischen Wachstum beitragen. Die Analyse der eIF-Expression in NSCLC-frisch gefrorenem Gewebe durch Western Blot und qRT-PCR zeigte eine veränderte eIF-Expression im ADC und im SQC im Vergleich zu gesundem nicht-neoplastischem Gewebe. Zusätzlich zeigten Überlebensanalysen von Affymetrix- und TCGA-Daten, dass die eIF-Expression tatsächlich mit dem Gesamtüberleben der Patienten assoziiert ist. Paclitaxel-Behandlung von A549-Zellen (eine Zelllinie, die für ADC repräsentativ ist) zeigte, dass die eIF-Expression durch Behandlung mit dieser chemotherapeutischen Verbindung moduliert werden kann. Nach einer allgemeinen Expressionsanalyse verschiedener eIFs bei NSCLC entschied ich mich, mich auf eIF1A und eIF6 zu konzentrieren, da diese eindeutig das Überleben der Patienten vorhersagten.

Ein Knockdown von eIF1A in A549- und H520-Zellen reduzierte die Proliferationsraten. Apoptose-, Seneszenz- und Polysomeprofile waren durch eIF1A-Knockdown nicht beeinflusst und ähnelten den Kontrollbedingungen. Die

Mechanismen, die für den beobachteten Wachstumsdefekt als Reaktion auf RNAi verantwortlich sind, sind noch nicht klar.

eIF6 ist in NSCLC überexprimiert und mit schlechterem Gesamtüberleben des Patienten bei ADC assoziiert. Depletion von eIF6 in A549 und H520 Lungenkrebszellen verminderte Proliferation und induzierte Apoptose. Dieser Teil meiner Arbeit liefert mechanistische Einblicke in die Konsequenzen der eIF6-Depletion auf das Wachstum von Lungenkrebszellen, die Defekte in der rRNA-Prozessierung und der ribosomalen 60S-Reifung aufzeigen.

Zusammenfassend zeigen die in dieser Studie präsentierten Daten, dass einige Mitglieder der eIF-Familie signifikant hochreguliert sind und mit einem schlechteren Gesamtüberleben bei NSCLC-Patienten assoziiert sind, was einen wichtigen Beitrag von eIFs zur Entwicklung und Progression von Lungenkarzinomen nahelegt. Ein besseres Verständnis der molekularen Mechanismen in der Lungenkarzinogenese könnte die Entwicklung neuer Behandlungsstrategien erleichtern.

Abstract English

Non-small cell lung cancer (NSCLC) belongs to the most frequently diagnosed cancer entity and is one of the leading causes of cancer-related death worldwide. NSCLC has two major histological subtypes, adenocarcinoma (ADC) and squamous (SQC) cell carcinoma. The future for patients suffering from NSCLC is dismal, with a 5-year overall survival rate of 15%. Therefore, constant research is needed to provide better care for future patients.

Dysregulation of protein synthesis has received considerable attention as a major step in cancer development and progression. Protein synthesis is regulated at multiple stages, including translation of mRNA into proteins. Some studies suggest that ribosomal protein synthesis plays a direct role during tumor-initiation.

Eukaryotic initiation factors (eIFs), which ensure the correct 80S ribosome assembly, are crucial to this translation process. eIFs are linked to the MAPK and the mTOR signaling pathways, which have become major targets in cancer therapy. Mutations or deregulated expression of eIFs influence cell growth and proliferation, and contribute to carcinogenesis.

The present thesis was based on the hypothesis that eIFs represent potential biomarkers in NSCLC and that specific members contribute to neoplastic growth. Analysis of eIF expression in NSCLC fresh frozen tissue by Western Blot and qRT-PCR showed altered eIF expression for ADC and SQC compared to healthy non-neoplastic tissue. In addition, survival analyses of Affymetrix and TCGA data sets revealed that eIF expression is indeed associated with overall patient survival. Paclitaxel treatment of A549 cells (a cell line representative for ADC) revealed that eIF expression can be modulated by treatment with this chemotherapeutic compound. Following a general expression analysis of different eIFs in NSCLC, I decided to focus on eIF1A and eIF6 because these were clearly predictive for patient survival.

Knockdown of eIF1A in A549 and H520 cells reduced proliferation rates. Apoptosis, senescence and polysome profiles were unaffected by eIF1A knockdown and similar to control conditions. The mechanism(s) being responsible for the observed growth defect in response to RNAi are still not clear.

eIF6 is overexpressed in NSCLC and associated with worse patient overall survival in ADC. Depletion of eIF6 in A549 and H520 lung cancer cells reduced proliferation and induced apoptosis. This part of my thesis provides mechanistic insights into the

consequences of eIF6 depletion on lung cancer cell growth revealing defects in rRNA processing and ribosomal 60S maturation.

In conclusion, the data presented in this study demonstrate that some members of the eIF family are significantly upregulated and associated with worse overall survival in NSCLC patients, suggesting an important contribution of eIFs to the development and progression of lung carcinomas. A better understanding of the molecular mechanisms in pulmonary carcinogenesis could facilitate the development of novel treatment strategies.

1 Introduction

1.1 Non-Small Cell Lung Cancer

The lung is an essential, highly organized organ responsible for respiration. It consists of a left lung with two lung lobes and a right lung with three lobes. In total, every human has 1.500 – 2000 km of airways and 50m^2 inner lung surface. The inhaled air is first filtered by lung cilia, then immune cells and phagocytes eliminate infectious particles [2]. The lung is a key player in the body, and disturbances or dysfunctions have severe consequences for patients and their quality of life.

One of the leading causes of death worldwide is cancer with over ~ 8 million deaths per year [3,4]. Of the cancer-related deaths, cancer of the lung & bronchus , besides prostate and colorectal cancer, is the most common cause of death worldwide [5,6]. One major problem of lung cancer is that once the clinical symptoms have manifested and a diagnosis has been made, patients already have developed metastasis and therefore have a very poor survival prognosis [2].

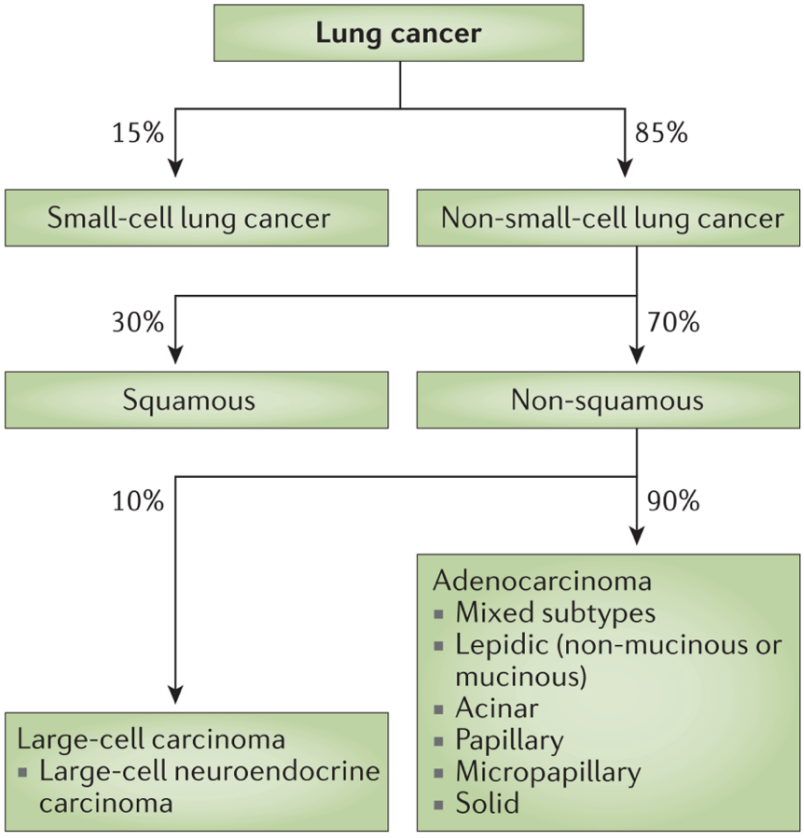

Figure 1 Overview on lung cancer subtypes. Lung cancer can be divided in two major subtypes: small cell lung cancer and NSCLC. Furthermore, SCLC comprises two histological subtypes, namely SQC and Non-squamous carcinoma. The non-squamous

subtype is further divided into ADC and large cell carcinoma and their histological subtypes [2,7]. Reproduced from [2] with permission of publisher Springer Nature.

Newly diagnosed lung cancer can be divided in two major histological subtypes, of which ~85% are non-small cell lung cancer (NSCLC) and ~15% are small cell lung cancer (SCLC) (*Figure 1*) [2,8,9]. This study focuses on NSCLC, which comprises three histological subtypes, including adenocarcinoma (ADC), squamous cell carcinoma (SQC) and large cell carcinoma (LC) (*Figure 2*) [8,10]. ADC and SQC are the most common diagnosed cancers, therefore the focus was on these two subtypes. Currently, ADC is more often diagnosed in women than in men. In contrast, the incidence for men diagnosed with SQC is higher than for women [5,11]. The current perspectives for patients with NSCLC are poor. Despite a large arsenal of treatment options the total overall survival (OS) is approximately 15-18% upon treatment, [5,11]. The quality of life for patients with NSCLC is poor. They show symptoms like cough, dyspnea, pain, anorexia and fatigue. The median OS is 10-12 months [2,12].

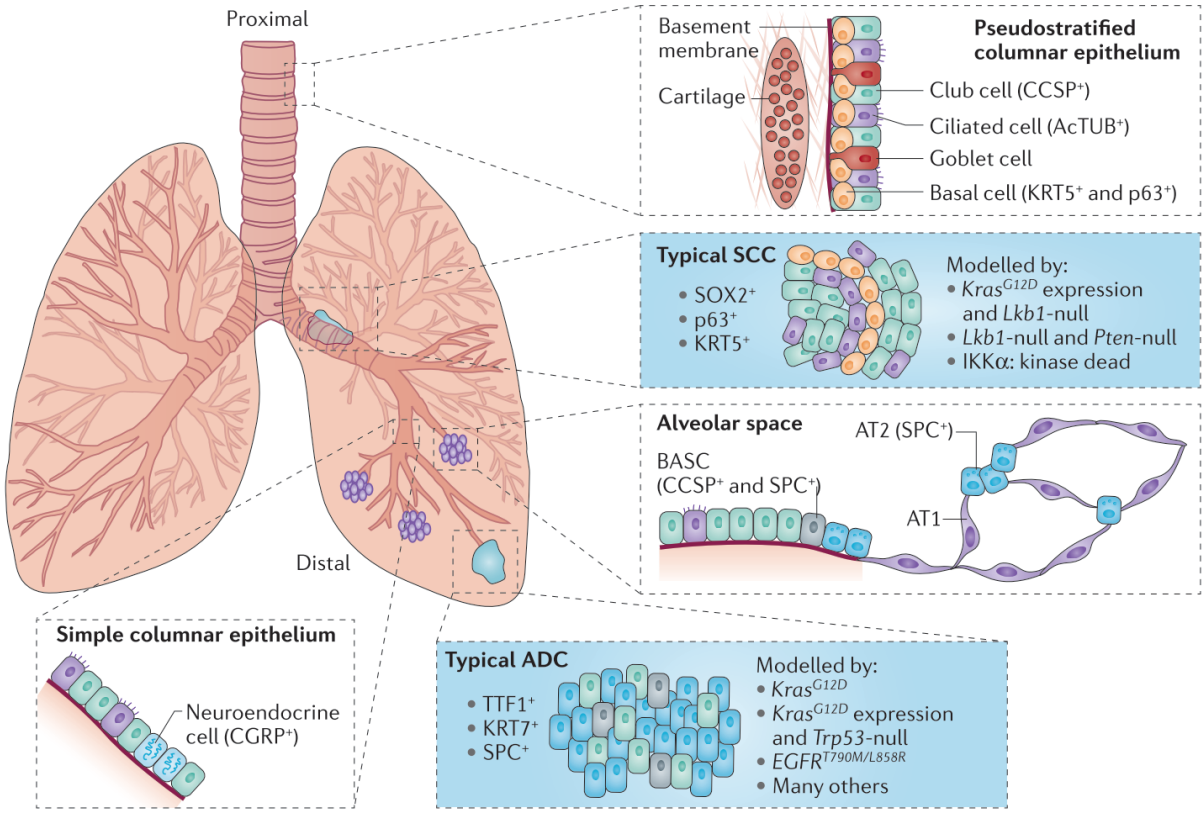

Figure 2 Scheme of the two major histological NSCLC subtypes, ADC and SQC and molecular markers [10]. Reproduced from [10] with permission of publisher Springer Nature.

The predominant risk factor for developing lung cancer is smoking. Over 80% of lung cancer incidences in USA and other countries are associated with smoking [13]. All NSCLC subtypes have been reported to be strongly associated with smoking, but the relationship between smoking and cancer is strongest in SQC and LC [2,10,14]. Early detection of lung cancer, tobacco prevention and a more detailed understanding of the disease are urgently needed to prevent lung cancer incidences, to provide lung cancer patients with the best possible care and to disburden the public health care system.

1.1.1 Tumor/ Node/ Metastasis (TNM) Classification according to the International Association for the Study against Lung Cancer (IASLC) in NSCLC

The IASLC, founded in 1974, is a global organization dedicated to the study of lung cancer. This organization, which plays an essential role in lung cancer research and prevention, is part of the WHO classification for lung cancer and also proposed the TNM Classification. Its 8th edition was published in 2015. General classifications are very important to have the possibility of cohort comparison. In the present thesis the patient samples were classified according to the 8th edition of TNM classification *Table 1*. It is important to have such a guideline not only for a global TNM classification that allows for a comparison of cohorts, but also for the therapy of patients and their prognosis after diagnosis [9,15,16]. Staging lung cancer combines several disciplines like computer tomography (CT), magnetic resonance imaging (MRI), sonography, biopsy and pathology [9]. The latter plays a very important role for the new WHO classification. Immunohistochemistry is recommended not only for biopsies and cytology, but also for surgically resected specimens to guarantee an accurate staging and the best personalized medicine option [8].

Table 1 TNM staging according to the 8th Edition of the TNM Classification for Lung Cancer [17–23]. Reproduced from [21] with permission of publisher Elsevier.

Stage	T	N	M
Occult carcinoma	TX	N0	M0
0	Tis	N0	M0
IA1	T1mi	N0	M0
	T1a	N0	M0
IA2	T1b	N0	M0
IA3	T1c	N0	M0
IB	T2a	N0	M0
IIA	T2b	N0	M0
IIB	T1a	N1	M0
	T1b	N1	M0
	T1c	N1	M0
	T2a	N1	M0
	T2b	N1	M0
	T3	N0	M0
IIIA	T1a	N2	M0
	T1b	N2	M0
	T1c	N2	M0
	T2a	N2	M0
	T2b	N2	M0
	T3	N1	M0
	T4	N0	M0
	T4	N1	M0
IIIB	T1a	N3	M0
	T1b	N3	M0
	T1c	N3	M0
	T2a	N3	M0
	T2b	N3	M0
	T3	N2	M0
	T4	N2	M0
IIIC	T3	N3	M0
	T4	N3	M0
IVA	Any T	Any N	M1a
	Any T	Any N	M1b
IVB	Any T	Any N	M1c

1.1.2 Biology of lung adenocarcinoma

ADC, whose incidence is increasing constantly, is the most dominant histological subtype of all NSCLCs. ADC is the most common type diagnosed in non-smokers, females and Asian patients [24,25]. It is a malignant epithelial tumor with glandular differentiation and/or mucin production by the tumor cells and usually arises in the distal[1] airways of the lung. ADC comprises different growth patterns like acinar, papillary, bronchioalveolar and solid with mucus formation [7,26,27]. ADCs are tested immunohistochemically and mostly present the following pattern: thyroid transcription factor 1 (TTF1) and keratin 7 (CK7) positivity and keratin 20 (CK20) negativity [10,28]. By contrast, ADCs with mucinous bronchoalveolar features are TTF1-negative and CK20-positive [8,10,28]. Genetic alterations in lung ADC are described below.

1.1.3 Lung squamous cell carcinoma

SQC, a subtype of NSCLC, arises in the proximal[2] airways and is strongly associated with smoking [10,26,28]. The number of incidences for SQC is slowly decreasing, which is most probably due to the large anti-smoking campaigns and restrictions that resulted in a decline in tobacco consumption [26]. SQC is mostly a central lung tumor, originates from bronchial epithelial cells and has a squamous differentiation [10,26,28]. The immunohistochemical markers for SQC are TTF1-negative, keratin 5, keratin 6, p40 and p63-positive [8,28].

1.1.4 Risk factors for the Development of NSCLC

1.1.4.1 Tobacco smoke

The major risk factor for developing lung cancer is smoking; not only active smoking increases the risk of developing lung cancer, but also second- and third-hand smoke significantly correlates with lung cancer development. Generally 80% to 90% of men and women diagnosed with NSCLC are smokers or former smokers [2,29,30]. Smoking can be related to a variety of cancers, but lung cancer, together with cardiovascular diseases, is the leading cause of death associated with smoking [2,29,31]. Regularly, tobacco consume alters cancer biology, resulting in treatment resistance, which subsequently leads to worse patient survival [29,32]. It has also

[1] distal airways: < 2 mm in diameter, contribute to gas exchange [27]
[2] proximal airways: > 2mm in diameter, no gas exchange [27]

been shown that second-hand smoke increases the risk of developing lung cancer over 20%. All these facts should suffice to stop smoking and to prevent non-smokers form inhaling second-hand smoke. Unfortunately, in other countries, the authorities controlling tobacco consumption are subject to their governmental regulations, laws, taxation, social patterns and public awareness/ acceptance [29,33].

The tobacco consumption resulting in lung cancer is a heavy burden also encountered in our health insurance system. In Austria, especially in Styria, PDL-1 treatment is not always covered by the state health insurance, so a very promising Food and Drug Administration (FDA) -approved treatment option will not be administered to patients.

1.1.4.2 Hereditary factors

Genetic alterations might contribute to the risk of developing lung cancer especially in non-smokers. Smokers only rarely have a family history of lung cancers. In 2012 a pooled analysis investigating individuals with a family history of lung cancer revealed an increased risk of developing lung cancer [34]. The genetic component responsible for developing lung cancer is more common in ADC patients than in other histological subtypes. A germline mutation in exon 20 T790M encoding for EGFR and a mutation in *HER2* were found to be oncogenic and responsible for hereditary and sporadic ADC [2,35].

1.1.4.3 Radon

9% of lung cancer deaths and 2% of all cancer deaths are related to radon exposure and/or inhalation in Europe [2,36]. Radon is a gas that arises from to the decay of Uranium (^{238}U). The inhalation of radon normally results in immediate exhalation of radon. The major problem is that radon gas contains solid particles which are retained by the lung epithelium. There, α- decay damages DNA in situ [2,14,36].

1.1.5 Genetic alterations in NSCLC and its potential for personalized medicine

Historically NSCLC subtypes are defined according to their histological features and marker expression. This approach is still important, and recent advances achieved by molecular testing support the classification system. Nowadays, next generation sequencing (NGS) and molecular testing should be available in all hospitals. In the 1980s, the first genetic aberration in ADC was found. The Kirsten rat sarcoma viral

oncogene (KRAS) can be altered in ADC patients [37,38]. KRAS was followed by v-raf murine sarcoma viral oncogene homolog B (BRAF) mutation in NSCLC, which was reported in 2002 [39]. In 2004 it was found that patients with epidermal growth factor receptor (EGFR)-activating mutations respond well to EGFR inhibitor gefitinib; consequently, the third genetic aberration was discovered for NSCLC [40,41]. Since the discovery of these three genetic mutations in NSCLC, the list of genetic mutations has been growing. An overview on ALK [42], MET [43], HER2 [44], ROS1 [45], RET [46], NRG1 [47], NTRK1 [48], PIK3CA [49] and MEK [50] mutations in NSCLC is listed in *Figure 3*.

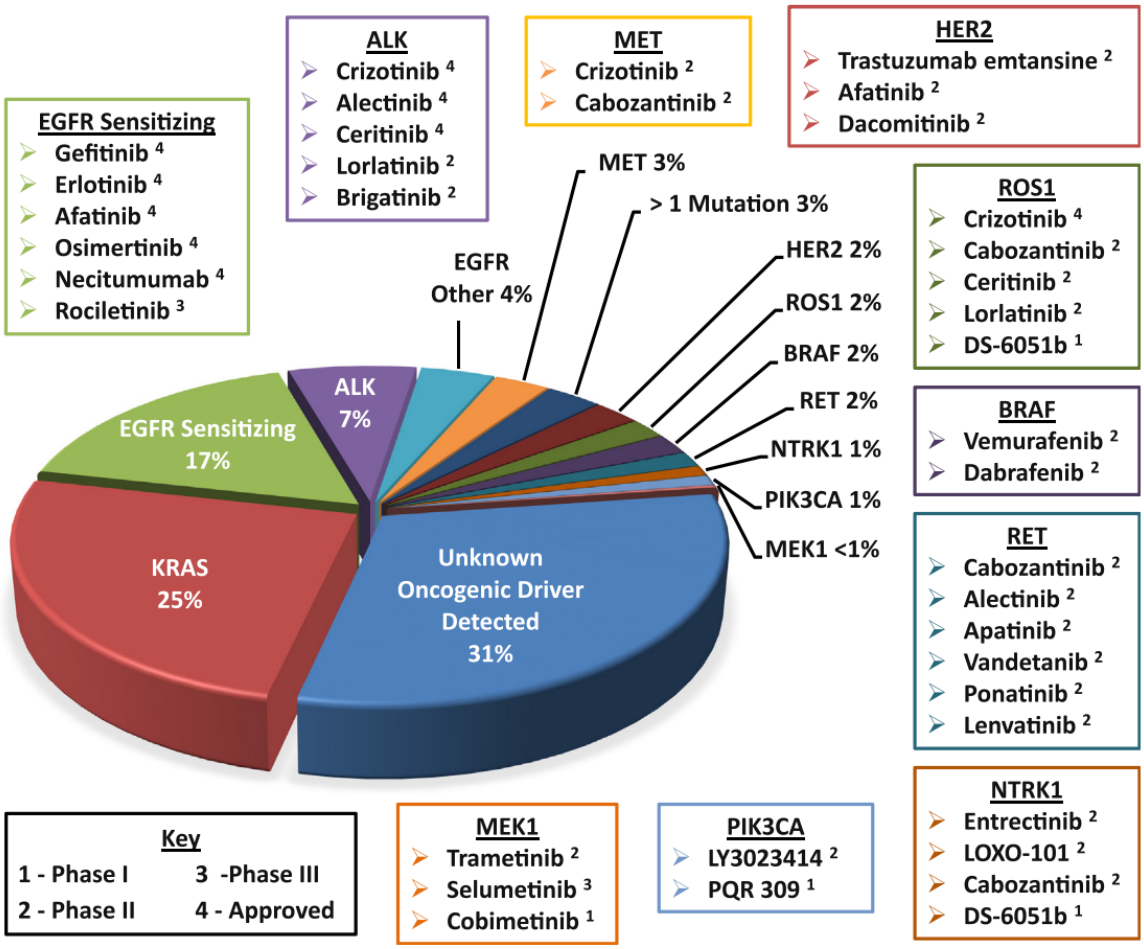

Figure 3 Driver genes in ADC and their targeted treatment options. ALK= Anaplastic lymphoma kinase, MET= Mesenchymal epithelial transition factor, HER2= Human epidermal growth factor receptor 2, ROS1= Proto-oncogene tyrosine-protein kinase, RET= Receptor tyrosine kinase, NRG1= Neuregulin 1, NTRK1= Neurotrophic receptor tyrosine kinase 1, PIK3CA= phosphatidylinositol 3-kinase, MEK= mesenchymal-epithelial transition kinase [29]. Reproduced from [29] with permission of publisher Elsevier.

1.1.5.1 *KRAS* mutation

Mutations in *KRAS* occur more often in smokers and ADC patients than in never smokers or SQC patients [29,51,52]. Approximately 25% of ADC and 4% of SQC patients have a KRAS mutation [29,53]. Still today, no FDA-approved targeted therapy is available.

1.1.5.2 *BRAF* mutation

NSCLC patients with *BRAF* mutations are very rare, approximately 2% of all patients carry a mutation in *BRAF* [9,29,53]. Some clinical trials investigating *BRAF* inhibitors for targeted therapy are ongoing, but until now the FDA-approved therapy against *BRAF* has been used only for metastatic NSCLC patients with *BRAF V600E* mutation [54].

1.1.5.3 *EGFR* mutation

In 2004 targeted therapy started to evolve for NSCLC patients with the finding of better sensitivity for EGFR tyrosine kinase (TKI) inhibitors [40,41]. Mutations in *EGFR* are typically found in ADC patients, no smoking history and females [9,55]. The most common *EGFR* mutations such as exon 19 deletion or exon 21 missense mutation are associated with higher sensitivity to TKIs [40,41]. Currently, different TKIs are FDA-approved and available for first line therapy like Erlotinib, Afatinib and Gefitinib [9]. Patients respond to TKIs but after 9-12 months they start to progress due to an acquired resistance mutation in exon 20 [9,56]. This mutation affects the drug efficacy in several ways. The tyrosine kinase domain shows more sensitivity to ATP than to TKIs and/or steric hindrance for TKIs [57,58]. To avoid the reprogression in NSCLC patients with *EGFR* mutation, third generation TKIs such as Osimertinib are now used in clinical trials. Osimertinib is an irreversible TKI and overcomes the resistance mechanism [9,57,59,60].

1.1.5.4 ALK and ROS1 translocation

2-7% of NSCLC patients have an ALK translocation and 1-2% a *ROS1* translocation, which leads to new fusion genes with transforming activity [9,61,62]. ALK and ROS1 are also receptors for tyrosine kinases. Resistance to ALK-TKIs is also found [63,64]. However, a variety of mechanisms, like mutations, amplifications

or an induction/upregulation of other signaling pathway bypasses ALK-receptors [57,64].

ALK and ROS1 share high homology in the kinase domain [57]. For ROS1 no targeted therapy is FDA-approved until now, but is often observed in second line therapy in which patients might benefit form ALK-TKIs as well [57].

1.1.5.5 Other alterations

RET rearrangement is found in 1-2 % of all NSCLC patients with light smoking history [29,65]. At present, no targeted therapy is available, but they respond well to other therapies available on the market [9]. 2% of NSCLC patients harbor a MET amplification with poor prognosis [29,66], and some FDA-approved MET inhibitors improve patient OS [9]. Further alterations in *HER2* and *NTRK* have been reported in NSCLC cases [9,57].

1.1.6 Immunotherapy and PDL-1 in NSCLC

Cancer cells can avoid recognition by the immune system. They bypass the activation of the specific T-cell-mediated immune response by expressing PDL-1 on their surface. PDL-1 binds to the receptors of the activated T-cell, B7.1 and PD1 and can subsequently inactivate the T-cell. Thereby cancer cells mask themselves as healthy cells. Under normal conditions, this process is important to keep immune response homeostasis stable, but in cancer it prohibits the activation of T-cell immune response.

Great effort and money were invested in processes preventing this binding to induce a functional T-cell response in cancer patients. As PDL-1-blocking antibodies prevent the binding of PDL-1 and PD1, T-cells do not recognize cancer cells as normal healthy cells and induce the T-cell-mediated immune response [9,10,57,67]. Currently, patients with NSCLC are immunohistochemically evaluated on the basis of their PDL-1 expression level. Patients with 50% positive staining for PDL-1 are regarded as high-level patients and are very likely to benefit from treatment. 1% PDL-1 staining is assumed low, and no notable benefits for patients are observed [9,10,57]. A major bias of this approach is that for each PDL-1 blocking antibody, better specified staining protocols should be recommended for deciding about the adequate treatment. The evaluation of PDL-1 expression and options for patient treatment option needs better systems to ensure the best treatment for NSCLC patients.

1.1.7 Biomarkers in NSCLC

Biomarkers can be molecular alterations linked to a disease. The World Health Organization (WHO) defines biomarker as “any substance, structure, or process that can be measured in the body or its products and influence or predict the incidence of outcome or disease” [68]. These alterations can therefore lead to changes in protein levels, expression of cellular markers and changes in circulating DNA amount; methylation status can also be a biomarker.

Targeted therapy for NSCLC patients is gaining momentum and each targeted therapy is linked to a biomarker in NSCLC. At present nearly all targeted therapies are accompanied by a matched diagnostic kit [69]. As described in the chapters above, biomarkers in NSCLC can vary from a gene mutation to overexpression of a protein.

1.1.8 Therapy and treatment options in NSCLC

Current therapy options for NSCLC patients are surgery, radiation, chemotherapy, targeted treatment and immunotherapy. In Austria patients without metastases undergo surgery. This mostly applies to patients with stage 1 and stage 2 NSCLC [9,29,70]. Additionally, chemotherapy is an option for patients with metastasis who cannot undergo surgery. Chemotherapy is also an option as adjuvant or neoadjuvant treatment after or before surgery. These patients are often additionally treated by radiation to control tumor growth. At late stage NSCLC, radiation is used for palliative care [2,9,12,29]. Furthermore, since the last decade, targeted therapy has also been available to specifically target for example EGFR or ALK. The latest therapy option is immune therapy, where PDL-1 is targeted with antibodies or inhibitors [2,9,29,71,72].

1.2 Human Ribosome and its Biogenesis

Ribosomes constitute the machinery that synthesizes proteins. This process is highly conserved and important to ensure continuous and regulated protein production. Eukaryotic ribosome biogenesis is well characterized in *S.cerevisiae*. In 2010, three research groups investigated the crystal structure of the eukaryotic 80S ribosome: M. Yusupov et al. in France, R. Beckmann et al. in Germany and Nenad Ban et al. in Switzerland [73–75]. The human ribosome consists of 80 ribosomal proteins and 4 ribosomal RNAs (rRNA; 5S, 5.8S, 18S, 28S) [76].

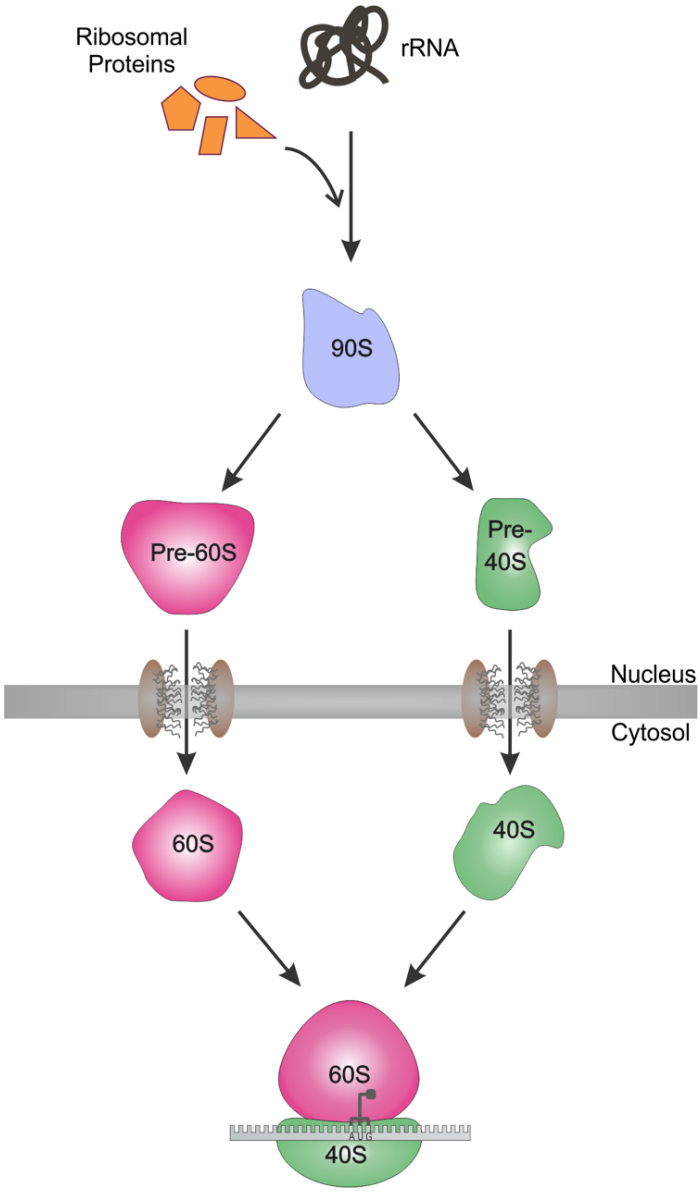

Figure 4 Eukaryotic Ribosome biogenesis at a glance. Ribosomal proteins, rRNA and assembly factors build the 90S ribosomal particle. After several maturation and processing steps the 90S is divided into pre-40S and pre-60S particles. Both particles are exported into the cytoplasm, where further maturation steps occur, before the translational competent 80S ribosome is formed.

In mammals, the mature ribosome consists of a small 40S subunit and a large 60S subunit. The biogenesis of the ribosome starts in the nucleolus, where non-ribosomal proteins and ribosomal maturation factors, together with rRNA, form the pre-90S particle. This pre-90S particle then undergoes several maturation steps leading to a separation of the pre-90S particle into pre-40S and pre-60S particle. After further maturation of the two particles they are exported into the cytosol, where the last maturation steps occur and a translational competent ribosome is formed (*Figure 4*) [76,77]. A multitude of proteins is involved in ribosome biogenesis, including ribosome assembly factor, maturation factors and eukaryotic translation initiation factors (eIF), to orchestrate the crucial steps [78,79].

1.2.1 Ribosomal RNA Processing

Forming a translational, competent ribosome involves synthesis of rRNA, its integration into the pre-90S and the processing of rRNA [76]. The 40S subunit has incorporated the 18S rRNA, and the 60S subunit contains: 25S, 5.8S and 5S rRNA [76,77,80].

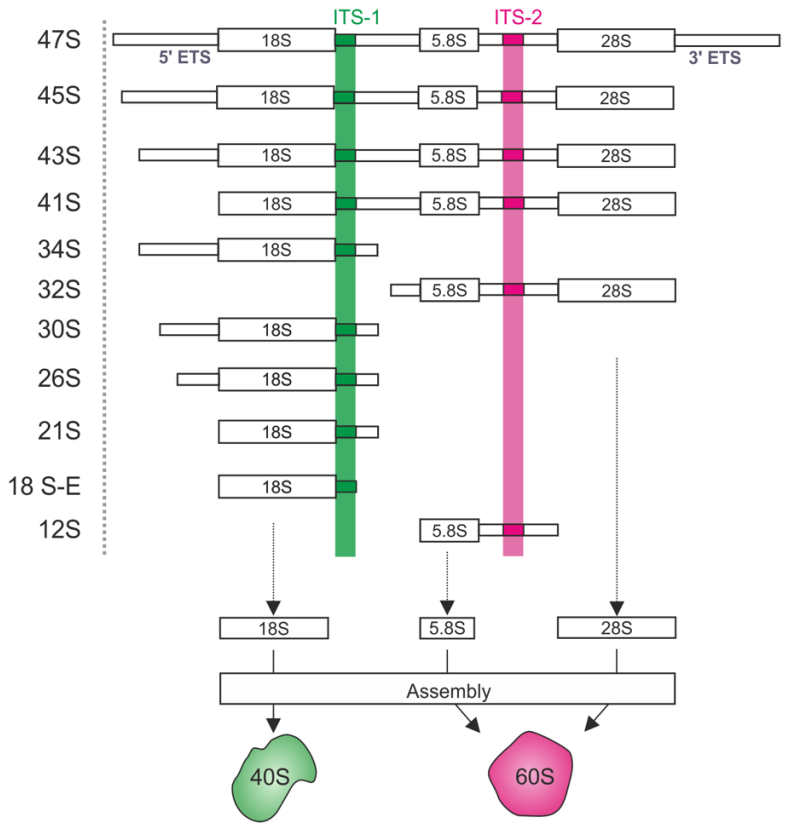

Figure 5 Scheme of major 47S pre- rRNA processing intermediates. The external cleavage sites 5´- external spacers (ETS) and 3´-ETS are displayed in grey. The rRNAs are separated at internal spacers, ITS-1 is highlighted in green and the ITS-2 is colored in pink. Scheme displayed is adapted from Gantenbein et al. 2018 [81]. Reproduced from [81] with permission of publisher Elsevier.

The RNA polymerases Pol I and Pol III synthesize the rRNA. Pol I transcribes a long 47S precursor rRNA (pre-rRNA) which is then further processed into 5.8S, 18S and 25S. 5S rRNA is transcribed separately by RNA Pol III [76,82,83]. After transcription of the pre-rRNAs, several cleavage steps and chemical modifications occur to remove internal spacers (ITS) and external spacers (ETS). *Figure 5* gives an overview of the most prominent cleavage steps and its intermediate pre-rRNAs [83,84]. The major processing sites, 5´-ETS, ITS1, ITS2 and 3´-ETS, were mapped with a combination of DNA sequencing techniques, Northern blotting, primer extension and 3´random amplification of cDNA [83,85–88]. In mammals the 47S pre-rRNA is processed via two possible pathways (pathway 1 or 2). A simplified scheme is shown in *Figure 6* [83,89,90].

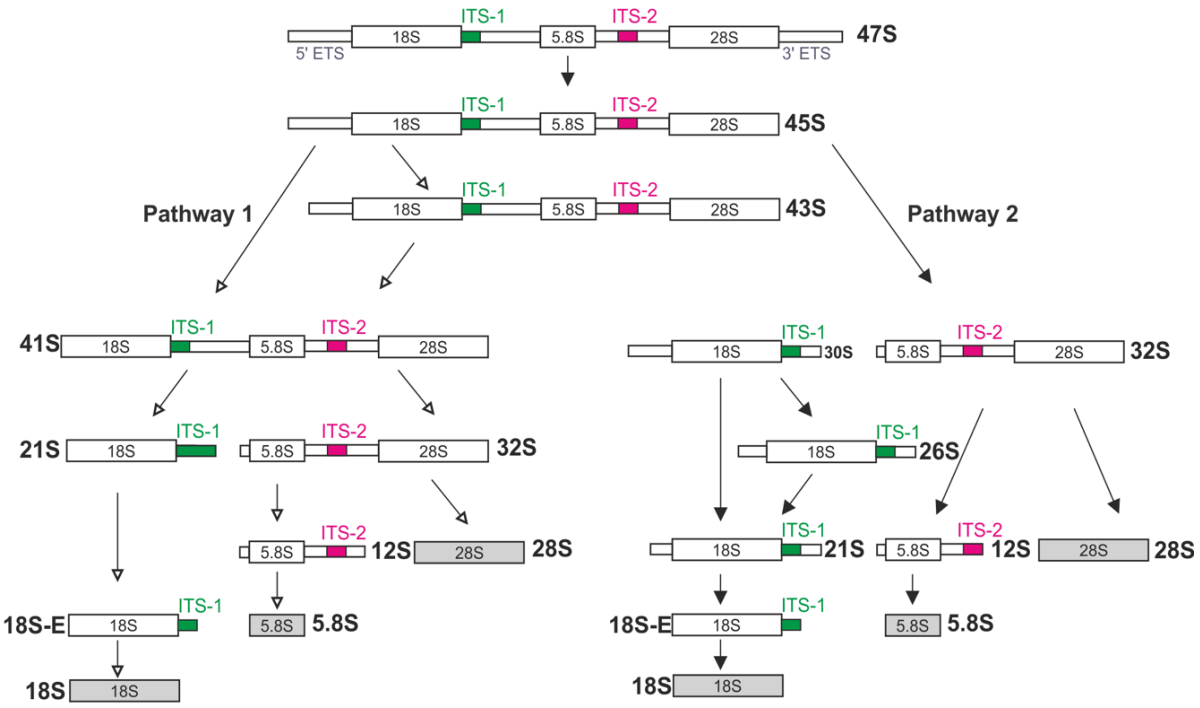

Figure 6 The two major rRNA processing pathways of 47S pre-RNA. The 47S pre-rRNA acts as template for the three final rRNA products, 18S, 5.8S and 28S rRNA. Pathway 1 is a minor pathway and pathway two is the major processing route to make mature rRNAs. Scheme displayed is adapted from Gantenbein et al. 2018 [81]. Reproduced from [81] with permission of publisher Elsevier.

1.3 Eukaryotic Translation Initiation

Translation in eukaryotes can be divided into four major steps: translation initiation, elongation, termination, and ribosomal recycling. Translating mRNA to the corresponding protein is one of the major activities in each cell and is strictly regulated. The first step, translation initiation is highly regulated. The major translation initiation pathway is the canonical pathway. There are also other pathways like the IRES mediated translation initiation pathway [91]. The eukaryotic translation initiation factors (eIFs) are crucial for initiation. They ensure correct assembly of the two ribosomal subunits [78]. Currently, 13 core eIFs consisting of several different subunits have been identified. A major upstream regulator of this process is the PI3K/AKT/mTOR pathway. This pathway is regulated by stimuli like hormones, cytokines and growth factors, and therefore plays an important role in protein synthesis and cell growth and subsequently in cancer development and progression [91,92].

The canonical initiation pathway starts when the 40S ribosomal subunit binds to eIF1A, eIF1, eIF5 and eFI3-complexes. These complexes then recruit the $_{met}$tRNAi-eIF2 complex, forming the 43S preinitiation complex. Then, the eIF4F complex, together with eIF4B, binds to the mRNA and the cap-proximal region is unwound by ATP-ases. Subsequently, the mRNA-eIF4F complex attaches to the 43S complex. When the mRNA is bound, scanning for the start codon AUG starts. The 48S complex is formed when AUG is at the right position (P-position) of the 40S subunit and the tRNA anticodon loop binds to the AUG. This step is facilitated by eIF1 and eIF1A. eIF2 is hydrolyzed and dissociates the initiation complex after the binding between AUG and tRNA. The 60S subunit is then recruited to the 48S initiation complex, followed by the joining of the 60S subunit and the 48S initiation complex. eIF5B and eIF6 accompany the 60S subunit, facilitate correct binding and dissociate after correct assembly of the two subunits. During this joining process of the 40S and 60S subunit, eIF2, eIF5, eIF1 and eIF3 detach. When a translational competent ribosome is formed, the last eIFs dissociate, eIF5B is hydrolyzed and detaches, and eIF1A is also released [78,79,93,94]. *Figure 7* provides a scheme of the eukaryotic translation initiation pathway.

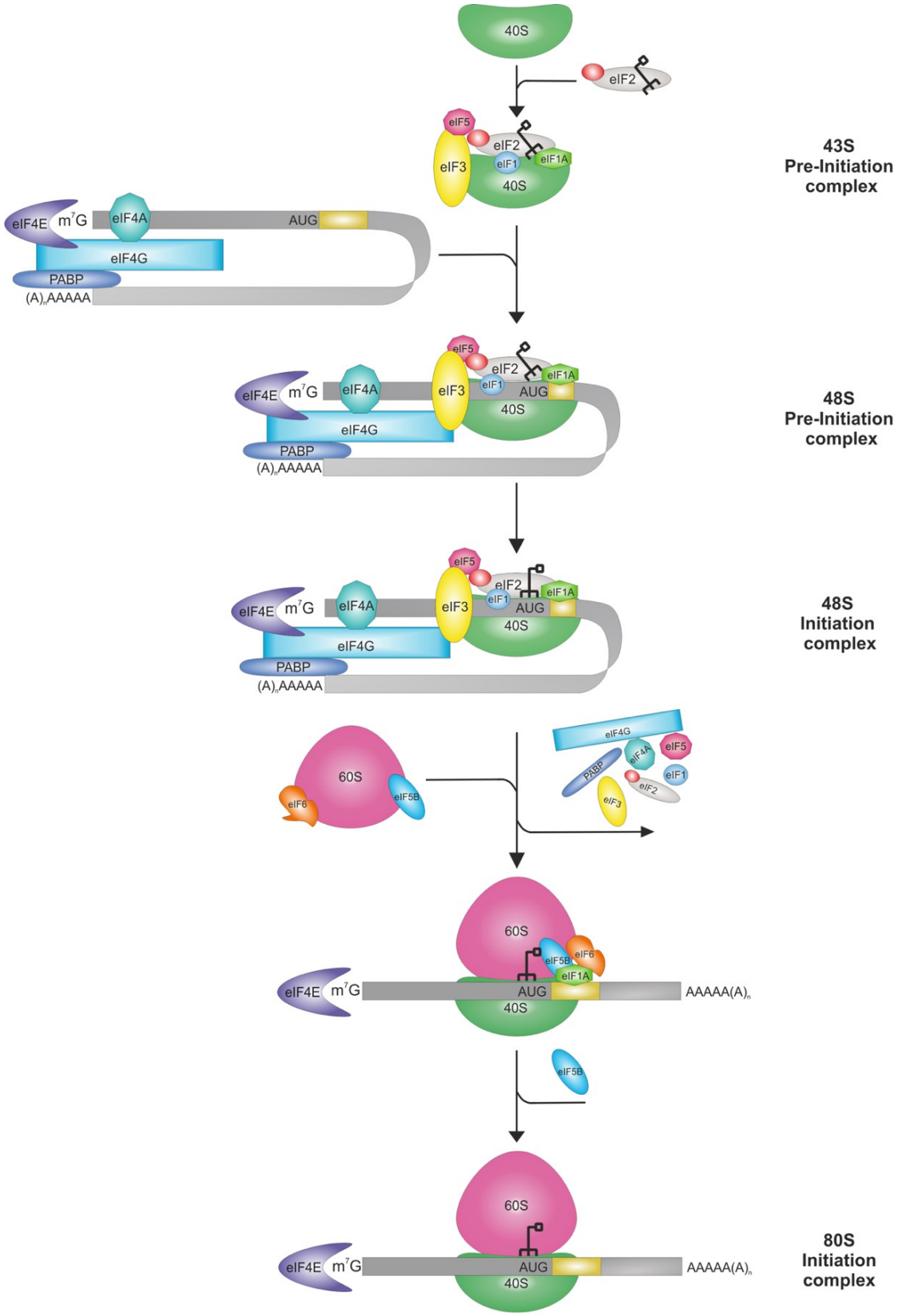

Figure 7 Eukaryotic translation initiation pathway. The first step is the 43S complex formation where eIFs and the small ribosomal subunit 40S join, followed by the binding of $_{met}$tRNAi. Then the mRNA bound to the eIF4F complex is recruited to the preinitiation complex. Next step is the scanning for the start codon AUG and the 48S initiation complex is formed. The large ribosomal subunit 60S joins the 48S initiation complex, eIFs dissociate and a translational competent ribosome is formed.

1.3.1 eIFs in detail and their role in cancer development

Protein translation is an essential process for all eukaryotic cells. eIFs ensure this process by managing the correct assembly of the two ribosomal subunits, the mRNA and the $_{met}$tRNAi to a translational competent ribosome. Deregulation of translation can lead to an abnormal gene expression which can result in uncontrolled cell growth and therefore in cancer. It has been previously reported that eIFs are altered in different tumor types. Information about the involvement of eIFs in cancer is given below, an overview is provided in *Table 2* and *Table 3*.

1.3.1.1 eIF1

The small protein eIF1 binds to the 40S subunit and is required for the 43S-pre-inintiation complex formation [95,96]. After scanning of the mRNA for the start codon, eIF1 is released when scanning is completed [97]. eIF1 binds to eIF3C and eIF5 [96,98]. eIF1 has been reported to be overexpressed in colorectal carcinoma tissue compared to healthy mucosa [96,99].

1.3.1.2 eIF1A

eIF1A, formerly known as eIF4C, has a size of 17kDa. There are two different forms of eIF1A, one encoded on the X-Chromosome (eIF1AX) and the other encoded on the Y-Chromosome (eIF1AY) [96,98]. Both eIF1 and eIF1A are required for the translation initiation and mRNA scanning, but eIF1A is essential for the pre-initiation complex formation [78,96,100]. In 2000, Battiste and colleagues were able to solve the crystal structure of human eIF1A displayed in *Figure 8* [101]. It has an oligonucleotide binding domain and two flexible intrinsically disordered tails. eIF1A binds to the small ribosomal subunit 40S at the A-site and dissociates as last eIF before translation can start [101].

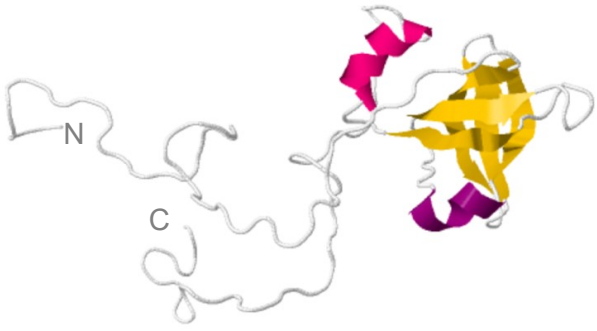

Figure 8 Crystal structure of human eIF1A. The beta barrel is highlighted in yellow and the alpha helices are colored in pink and violet. The eIF1A Protein Data Bank access code

is 1D7Q, structure is published in [101]. NGL Viewer (AS Rose et al. (2018) NGL viewer: web-based molecular graphics for large complexes. Bioinformatics dio:10.1093/ bioinformatics/bty419), and RCSB PDB.

1.3.1.3 eIF2

The heterotrimeric eIF2 has three subunits, eIF2α, eIF2β and eIF2γ. eIF2-GTP binds to the tRNAi. Stress kinases like eIF2AKs, GCN2, HRI, PERK and PKR can phosphorylate the eIF2α subunit at S^{51} [102]. PERK phosphorylates eIF2α upon ER stress. When nutritional stress occurs in a cell HRI kinase phosphorylates eIF2α [102,103]. The phosphorylation of eIF2α blocks eIF2B activity, resulting in an eIF2-GDP arrest [102]. eIF2 is not able to bind to the 40S subunit with this conformation, leading to a promotion of translation initiation. The involvement of eIF2 in cancer was described previously for bronchioalveolar carcinomas, melanocyte neoplasms, aggressive lymphomas and gastrointestinal cancer [104–107]. An overview of the role of eIF2 in cancer is provided in *Table 3*. There are some studies on eIF2 targeted cancer therapy, especially on the phosphorylation status of eIF2α, but further studies are needed before this can be considered a valid treatment [96,108]. The guanine nucleotide exchange factor which promotes GDP-GTP exchange for eIF2 consists of five subunits [96,109]. The catalytic subunit of eIF2B is upregulated in various tumors and is correlated to cancer development [96,110].

1.3.1.4 eIF3

The largest eIF complex is eIF3, with over 700 kDa and 13 subunits (eIF3A, eIF3B, eIF3C, eIF3D, eIF3E, eIF3F, eIF3G, eIF3H, eIF3I, eIF3J, eIF3K, eIF3L, eIF3M), six eIFs of which form the core unit [96,111–113]. The eIF3 complex is responsible for mRNA recruitment and stabilization of the pre-initiation complex. Furthermore, it is required for the IRES-dependent translation [96,111]. The different subunits have been described to be differently expressed in diverse cancer entities *Table 3*.

1.3.1.5 eIF4F-Complex

The eIF4F-complex consists of three eIFs: eIF4A, the DEAD-box helicase with ATP dependence, eIF4E, the Cap-binding protein and eIF4G, a scaffold protein [78,91,93]. eIF4E binds at the cap-region of the mRNA [91,114]. Erk1/2 or p38 MAPK is responsible for the phosphorylation of eIF4E at S^{209} [78,115].The eIF4E-binding protein-1 (4E-BP1) binds to eIF4E and regulates eIF4E activity. Phosphorylation of 4E-BP1 leads to release of eIF4E, which then binds to mRNA.

When the eIF4F-complex is recruited, eIF4A unwinds the secondary RNA structure within the 5'UTR region. The ATP-dependent helicase activity of eIF4A is enhanced by interaction with either eIF4H or eIF4B [78,93,96,116,117].

1.3.1.6 eIF4B and eIF4H

eIF4B and eIF4H do not have helicase activity, but promote RNA-binding capacity in absence of eIF4A and the helicase activity of eIF4A [96,116,118,119]. eIF4H is not as well characterized as other eIFs, but it was reported that eIF4H consists of two isoforms and displays sequence homology with eIF4B [116,118,120]. The phosphorylation of eIF4B is crucial for cap-dependent translation [96,116]. eIF4H lacks the C-terminal phosphorylation site [116,121]. Both eIFs have a homologous RNA recognition motive domain [116,118]. eIF4H was found to be overexpressed in NSCLC, colorectal cancer and esophagus caner tissue compared to normal control tissue [116,122].

1.3.1.7 eIF5

eIF5 has GTPase-activating (GAP) activity and forms a complex with eIF2, which is essential for translation initiation [96,123]. eIF2-GTP recruits the $_{met}$tRNAi to the 40S subunit. Hydrolysis of eIF2-GTP, after correct assembly with tRNA is performed by eIF5. Additionally, eIF5 is also involved in eIF2 recycling by inhibiting eIF2B [96,123]. eIF2 is not the only interaction partner of eIF5. Other partners are eIF1, eIF3 and eIF4G, which also bind to eIF5 [96,124]. A correlation between eIF5 and cancer development was recently described for colorectal carcinoma.

1.3.1.8 eIF5B

eIF5B is essential for the canonical translation initiation pathway. Together with eIF6, it accompanies the 60S ribosomal subunit to the pre-initiations complex [125]. It catalyzed the joining of 40S and 60S by promoting the dissociation of the eIFs previously bound to the 40S subunit [98,113]. Currently, no detailed information is available on eIF5B and its association with cancer.

1.3.1.9 eIF6

eIF6 accompanies the large ribosomal subunit to the 48S initiation complex. eIF6, a 27kDa protein, consists of 245 amino acids which are 70% identical between human and yeast [126,127]. In 2000, Groft et al. solved the crystal structure of eIF6 for *S.cerevisiae* [127,128]. eIF6 consists of five quasi identical α/β- subdomains arrayed around a five-fold axis of pseudosymmetry and is named pentein [127,128]. Crystal structure is displayed in *Figure 9*.

Figure 9 Crystal structure of eIF6 solved for S. cerevisiae. Five quasi-identical α/β-subunits that enclose a cavity. α-helices are marked in pink, beta-strands are highlighted in yellow. The *S.cerevisiae* eIF6 Protein Data Bank access code is 1G62, structure is published in [128]. NGL Viewer (AS Rose et al. (2018) NGL viewer: web-based molecular graphics for large complexes. Bioinformatics dio:10.1093/bioinformatics/bty419), and RCSB PDB. [127–130].

eIF6 was first described as an anti-association factor that prevents the joining of the 40S and the 60S ribosomal subunit [131]. Despite this mainly cytoplasmic function, eIF6 is also necessary for ribosome biogenesis in the nucleus [132]. The crucial role of eIF6 in ribosome biogenesis in mammals was shown in a study where mice with a total depletion of eIF6 had a lethal phenotype [133]. It was reported for different models (e.g. *Saccharomyces cerevisiae*, *Caenorhabditis elegans*, pleural mesothelioma, HeLa cells, ovarian carcinoma cells and mouse liver extracts) that eIF6 depletion results in reduced free 60S particles [134–138]. For the depletion of *eIF6* yeast homologue *TIF6* leads to reduced free 60S ribosomal subunits, and this

phenotype can be rescued by ectopic expression of human eIF6 [127,139,140]. The Shwachman-Bodian-Diamond syndrome, where patients suffer from bone marrow failure and a predisposition to leukemia, is caused by a deficiency in the Shwachman-Bodian-Diamond syndrome protein (SBDS). In yeast mutations in the SBDS orthologue, Sdo1 leads to 60S biogenesis defects, which can be rescued by *TIF6* overexpression [127,141].

Pulse-chase experiments in yeast have shown that *TIF6* depletion results in pre-rRNA processing defects for 25S and 5.8S [127,142]. The Lafontaine group performed a high throughput analysis to define the consequences of eIF knockdown and rRNA processing in human cell lines and found that eIF6 depletion leads to pre-rRNA processing defects [77].

eIF6 has been shown to be dysregulated in various cancer entities such as colon carcinoma [99], malignant pleural mesothelioma [134] and breast cancer [143]. Especially in colon carcinoma and malignant pleural mesothelioma an overexpression of eIF6, compared to non-neoplastic tissue was noted. This suggested a key contribution to carcinogenesis and a potential new biomarker [99,134].

Table 2 Function of eIFs [96]. Reproduced from [96] with permission of publisher Elsevier.

eIF	Subunits	Size [kDa]	Function	Refs.
eIF1	1	12.7	Binds to the 40S ribosome and assures the mRNA loading and start codon scanning, prevents premature eIF5 binding	[144][145]
eIF1A	1	16.5	Assures together with eIF1 the mRNA loading and start codon scanning on the 40S ribosome	[100][146]
eIF2	3 Subunits eIF2α eIF2β eIF2γ	 36,1 38.4 52	Binds and recruits the $_{met}$tRNAi and accompanies it to the 40S ribosome	[147][148]
eIF2B	5 Subunits eIF2B1α eIF2B2β eIF2B3γ eIF2B4δ eIF2B5ε	 26 39 58 67 82	GTP exchange factor for eIF2	[149][150]
eIF3	13 Subunits eIF3A* eIF3B* eIF3C* eIF3D eIF3E* eIF3F* eIF3G eIF3H* eIF3I eIF3J eIF3K eIF3L eIF3M	 170 116 110 66 48 47 44 40 36 35 28 67 43	* Subunits form the functional core of eIF3. eIF3 binds to the 40S ribosome and prevents premature binding of the 60S ribosome subunit and promotes mRNA recruitment	[151][111] [152]
eIF4F	3 Subunits eIF4A eIF4E eIF4G	 46 24.5 175.5	eIF4F: Cap-binding complex eIF4A: ATP helicase unwinds secondary mRNA structure eIF4E: Cap-binding activity eIF4G: scaffold protein	[117][153]
eIF4B	1	69.3	stimulates helicase activity of eIF4A	[154][155]
eIF4H	1	27.4	homologue N-terminal sequence to eIF4B, stimulates helicase activity of eIF4A	[122]
eIF5	1	49	inhibits GDP dissociation of eIF2	[156][157] [158]
eIF5B	1	138.9	GTPase, promotes 80S ribosome formation	[117]
eIF6	1	26.6	Binds 60S ribosomal subunit, involved on 60S biogenesis, anti-association factor preventing pre-mature binding of 60S and 40S	[127] [159]

Table 3 eIFs in Cancers [96]. Reproduced from [96] with permission of publisher Elsevier.

eIF	Expression	Cancer association	References
eIF1	Increased	Colorectal carcinoma	[99,160]
eIF2α	Increased	Malignant melanoma, colorectal carcinoma, lymphoma, brain tumors	[105,161]
eIF3A	Increased	Breast cancer, cervical cancer, esophageal cancer, hepatocellular carcinoma, lung and stomach cancer	[145,162–169]
eIF3B	Increased	Bladder cancer, breast cancer, hepatocellular carcinoma and prostate cancer	[169–171]
eIF3C	Increased	Meningioma, hepatocellular carcinoma and testicular seminoma	[169,172,173]
eIF3E	Decreased	Breast cancer, lung cancer and prostate cancer	[174–178]
eIF3F	Decreased	Breast cancer, colorectal carcinoma, ovarian carcinoma, pancreatic cancer, vulva cancer and melanoma	[179]
eIF3H	Increased	Breast cancer, colorectal carcinoma, hepatocellular carcinoma and prostate cancer	[169,180,181]
eIF3I	Increased	Breast cancer, head and neck cancer, hepatocellular carcinoma, melanoma and neuroblastoma	[182–185]
eIF3M	Increased	Colorectal carcinoma	[164]
eIF4A	Increased	Lung cancer and cervical cancer	[178,186]
eIF4E	Increased phosphorylation	Breast cancer, colorectal carcinoma, gastric cancer, lung cancer, hepatocellular carcinoma, meningioma, glioblastoma	[99,169,187–189]
eIF4G	Increased	Lung cancer, breast cancer, hepatocellular carcinoma, colorectal carcinoma and cervical cancer	[99,169,186,190]
eIF4H	Increased	Lung cancer colorectal cancer esophagus cancer	[116,122]

eIF	Dysregulation	Cancer association	References
eIF5A	Increased expression	Colorectal carcinoma, lung cancer and hepatocellular carcinoma	[191,192]
eIF5	Increased expression	Colorectal carcinoma	[99]
eIF6	Increased expression	Ovarian serous carcinoma, mesothelioma, head and neck carcinoma and colorectal carcinoma	[99,134,193,194]

1.3.1.11 eFIs in NSCLC

Eukaryotic translation initiation as potential drug target is also under scrutiny in NSCLC. The main focus lies on the eIF4F-complex and its main player, as well as on the eIF3-complex. PubMed reveals a constant increase in the number of studies dealing with dysregulation of eIFs or their description as therapy targets. Table 4 gives an overview of published articles on eIFs and NSCLC.

Table 4 eIFs investigated in NSCLC

eIF	Expression	References
eIF2α	Increased	[195,196]
eIF3A	Increased	[174]
eIF3E	Decreased	[175]
eIF3H	Increased	[176]
eIF4A	Increased	[178]
eIF4E	Increased	[197]
eIF4G	Increased	[178]
eIF4H	Increased	[116]
eIF5A	Increased	[198,199]

1.3.1.11.1 eIF4E and 4EBP1 in NSCLC

The Cap-binding protein eIF4E has been reported to display higher expression in different types of lung cancer and a correlation with a worse survival rate for NSCLC patients [195–201]. Knockdown of eIF4E in lung cancer cell lines leads to reduced growth and proliferation [200]. Moreover, it was reported that also Western Blot analysis revealed eIF4E overexpression in lung cancer tissue, as well as an increase in eIF4E mRNA levels in lung cancer tissue compared to normal lung control tissue [195,196,201]. eIF4E overexpression was mainly reported for ADC [161,201]. eIF4E ensures the selective increase in translation of mRNAs that code for proliferation, pro-survival and proangiogenic proteins like cyclin D1 and vascular endothelial growth factor (VEGF), which are also upregulated in lung cancer tissue [197,199,201,202].

Additionally, hints for dysregulation of eIF4E modulating proteins like eIF4E-binding-protein 1 and the kinases phosphorylating eIF4E reveal the importance of eIF4E in NSCLC. Increased phosphorylation of eIF4E results in enhanced Cap-binding of the eIF4F complex and consequently in an increase of translation of eIF4E, favoring mRNAs like cyclin D1, c-Myc and VEGF [197,201,203]. A second regulation of eIF4E activity is 4EBP1, which binds to eIF4E and prevents eIF4E binding to eIF4F-complex. mTOR phosphorylation of 4EBP1 leads to release of eIF4E, which then binds the eIF4F-complex. The mTOR pathway regulates phosphorylation of 4EBP1 [78,201]. Increased phosphorylation of 4EBP1 was shown to be associated with poor prognosis in ADC [201]. Tobacco smoking is the main risk factor for lung cancer development, and was found to have a causal link to 4EBP1. Since 4EBP1 increases the sensitivity to lung cancer development with tobacco smoke [201,204].

1.3.1.11.2 eIF3-complex in NSCLC

One of the major eIF3-complex members is eIF3a, which is overexpressed in breast cancer, cervical cancer, esophageal cancer, lung and stomach cancer. Experiments in lung cancer cell lines revealed that knockdown of eIF3a leads to decreased proliferation and tumorigenesis [96,174,201]. A link between chemosensitivity to platinum-based chemotherapeutics in lung cancer patients and eIF3a expression was demonstrated in cell experiments where low eIF3a levels lead to better chemosensitivity and eIF3a overexpression to chemo resistance [201,205].

Additionally, in lung cancer, correlation with an eIF3-complex member, eIF3E, was reported. Interestingly, eIF3E appears to be downregulated in lung cancer samples [164,201].

1.3.1.11.3 eIF2α in NSCLC

eIF2 is a cellular stress sensor detecting the phosphorylation status of eIF2α [102,103]. eIF2α is overexpressed in several types of lung cancer, but not in SQC [161,178]. Phosphorylation of eIF2α is inhibitory for translation and should therefore be beneficial for patients. Indeed, it was shown that patients with increased phosphorylation of eIF2α have better survival rates [201,206].

1.3.1.11.4 Further eIFs in NSCLC

In SQC eIF4G was found to be overexpressed compared to lung control tissue [178,201]. Comtesse et al. reported an overexpression of eIF4A1, eIF2B and eIF4B in lung cancer specimens and recently, eIF4H was found to be overexpressed in NSCLC [116,178].

1.3.1.11.5 eIFs as therapy targets in NSCLC

NSCLC is a frequently diagnosed cancer, and the demand for targeted therapy is high. As described in chapter *1.1.5 - 1.1.8,* targeted therapies are very important for NSCLC patients, and targeting translation initiation machinery is a further approach toward therapy. Enhanced cisplatin sensitivity was reported in NSCLC cell lines after eIF5A2 knockdown [207]. Also a treatment combining mTOR and eIF4E-phosphorylation inhibition was investigated and revealed an increase in apoptosis and enhanced effectiveness of targeted mTOR therapy in NSCLC cell lines [208]. Another study showed that curcumin impacts eIF2α and eIF4E protein expression levels in NSCLC cell lines [209]. After eIF4H knockdown NSCLC cells were more chemo sensitized, which resulted in reduced cell growth and reduced cell migration capacity [116]. In conclusion, new treatment options to interfere with translation are under development, however no drugs targeting this pathway have passed clinical trials yet. Therefore, further studies and preclinical models are urgently needed to drive this targeted therapy approach towards clinical trials.

2 Material and Methods

Most methods described in this section are published in my thesis paper Gantenbein et al. 2018 [81].

2.1 Ethical vote for the use of NSCLC

The study “eukaryotic translation initiation factors in lung cancer” was approved by the Ethics Committee of the Medical University of Graz, Austria, according to the ethical guidelines of the 1975 Declaration of Helsinki (EK 27-240 ex 14/15). Detailed information see *Appendix 8.1* the ethical committee proofed study protocol, patient informed consent and ethical vote. Patients were informed about this study by the thoracic surgeons Prof. Priv.-Doz. Dr.med.univ. Jörg Lindenmann and Dr.^{in} med.univ. Nicole Fink-Neuböck. The informed consent was obtained from all patients, whose fresh frozen tissue for this study was collected.

2.2 Patient survival

Patient survival analysis in the Cancer Genome Atlas (TCGA) and Affymettrix data set was conducted by Martin Pichler. The influence of eukaryotic translation initiation factor expression on NSCLC patient survival was analyzed a publicly available data set generated on Affymetrix platforms as previously described (screening cohort =cohort 1) [210]. This dataset contains whole transcriptome data of over 1900 NSCLC patients. The publicly available visualization software was used to visualize the data with Kaplan-Meier plots [http://kmplot.com/analysis/index.php?p=service&cancer=lung]. The survival data were grouped in two different groups, groups of high and low expression were tested by using a cut-off point determined automatically by the software. Survival was illustrated by Kaplan-Meier curve and differences in survival between dichotomized groups were assessed with the log-rank test. TCGA dataset was analyzed, to validate the results of the Affymetrix database. SQC and ADC of NSCLC cases were analyzed by the same criteria described for cohort.

2.3 Tissue microarray (TMA)

TMAs were constructed at the Institute of Pathology, by the group of Prof. Helmut Popper at the Medical University of Graz, Austria. Formalin-fixed paraffin-embedded samples of lung carcinoma from a total of 414 patients were collected and used for

the generation of 5 TMAs (4 ADC and 1 SQC). Hematoxylin-eosin–stained slides of specimens were reviewed by three experienced, board–certified pathologist (Helmut Popper, Luka Brcic, Johannes Haybäck). The use of the TMAs was approved by the local Ethics Committee. Four independent examiners evaluated the pattern of the IHC (Johannes Haybäck, Ines Anders, Luka Brcic, and Nadine Gantenbein) using light microscopy. Each spot was semi-quantitatively scored, and an intensity score was calculated as follows: 0=no staining, 1=weak staining, 2=moderate staining and 3=strong staining. Additionally, a percentage of stained tumor cells was recorded (0-100%) and grouped in 5 groups, 0=0%, 1=1-≤10%, 2=11-49%, 3=50-79% and 4=≥80%. Intensity score (0-3) was then multiplied by percentage score (0-4), and obtained values were grouped as follows: 0=no staining, 1-4=weak staining, 4-8=moderate staining, 8-12=strong staining, and displayed in stacked plots.

2.4 IHC staining

Immunohistochemistry (IHC) was performed on 3 µm thick sections of each TMA. Primary eIF6 antibody (clone A303-030A, Bethyl) with dilution 1:100 and primary eIF1A (clone ab177939, Abcam) antibody with dilution 1:1000 were stained on a Ventana Immunostainer XT, with Ultra View DAB detection Kit and CC1 as epitope retrieval. Counterstaining with Hematoxylin followed. IHC staining was performed by Margit Gogg-Kammerer.

2.5 Protein isolation from Human tissue

Fresh frozen human lung tissue was cut into small pieces (2-5mm x 2-5mm x 2-5mm) then transferred into a MagnaLyser Tube (Roche) and 200-400 µl of ice-cold final lysis buffer was added. The tissue was homogenized in the MagnaLyser (Roche) by 3 runs with 30 seconds with 6500 rpm, followed by a centrifugation step at 14’000 rpm for 10 minutes at 4°C. The supernatant was transferred into a fresh tube. Protein concentration was determined using Bradford protein assay. The Bradford solution (Bio-Rad) was diluted 1:5 with Aqua dest. 2µl of 1:5 diluted protein lysate was added to 1998µl diluted Bradford solution, followed by vortexing 2-3 seconds. Then protein concentration was measured. Each sample was determined in triplicates to calculate the mean and adjusted to 3µg/µl with Final Lysis Buffer and 4x Laemmli Sample Buffer (Biorad). The samples were stored at -80°C until further usage.

2.6 Protein isolation from cell lines

The harvested cell pellets from A549 and H520 were lysed by adding 20-30 µl of ice cold final Lysis buffer, followed by 20-30 times pipetting up and down with a 100µl pipette. After a centrifugation step at 14'000 rpm for 10 minutes at 4°C, the supernatant was transferred into a fresh tube. Protein concentration was determined using Bradford protein assay. The Bradford solution (Bio-Rad) was diluted 1:5 with Aqua dest. 2µl of 1:5 diluted protein lysate was added to 1998µl diluted Bradford solution, followed by vortexing 2-3 seconds. Then protein concentration was measured and adjusted to 2µg/µl with Final Lysis Buffer and 4x Laemmli Sample Buffer (Biorad). The samples were stored at -80°C until further usage.

2.7 SDS-Page and Western Blot

Total protein lysates were separated with SDS-Page. After samples were heated for 10 minutes at 98°C, a 1-minute centrifugation step with 10.000 rpm at room temperature followed. A total protein amount of 30 µg (for human lung tissue lysates) and 20 µg (for lung cancer cell line lysates) was loaded on an 8% or 12.5% gel and using SDS-PAGE to separate the total protein lysate based on the molecular mass. The electrophoresis was performed for 1.5 h at 120 V in 1x SDS Running Buffer using the Mini-vertical electrophoresis unit (Amersham Biosciences). We used the PageRuler™ Prestained Protein Ladder, 10 to 180 kDa (3 µL) as standard.

Semi Dry Blotting was used to transfer the separated proteins onto a PVDF-membrane (Milipore). The membrane was activated in Methanol for 30 seconds and then transferred into a tray with Towbin buffer (Biorad) for 1-5 minutes until further usage. The sandwich was built in following order: Filter, membrane, gel, filter. The transfer lasted for 1.5 hours with 160 mA. To confirm the protein transfer the membrane was stained with Ponceau Red (Sigma-Aldrich) and then washed with 0.1% TBS-Tween (TBS-T) until no staining was visible anymore. To prevent unspecific binding during the immunoblotting the membrane was blocked with 5% non-fat dried milk powder (AppliChem) solved in 0.1% TBS-T for 1 hour at room temperature. The membrane was washed 3 times with 0.1% TBS-T before incubating the membrane with the primary antibody dissolved in 5% BSA in 0.1% TBS-T at 4°C over night. All wash and incubation steps were performed on a vertical shaker (Heidolph Instruments) with 50 rpm speed. On the next day the primary antibody solution was filled back in a tube and stored at -20 °C for further usage.

The membrane was washed 4 times 5 minutes with 0.1% TBS-T and then incubated with the secondary antibody dissolved in 5% milk powder. The membrane was incubated with ECL Prime or ECL Select Western blotting detection Reagent (GE Healthcare) and exposed in the detection chamber of ImageQuant LAS500 form GE Healthcare. All primary and secondary antibodies used are listed in *Table 13* in the appendix.

2.8 RNA isolation Human tissue

Cells were lysed in 1 ml Trizol® Reagent (Thermo Fischer Scientific Inc.) prior to addition 200 µl of chloroform. After centrifugation at 13'000 rpm for 15 minutes at 4 °C, the aqueous phase was precipitated with 500 µl of isopropanol. A 20 minutes centrifugation step followed at 4 °C and 13'000 rpm. The pellet was washed twice with cold 80% alcohol and dissolved in RNase-free water. RNA concentration in the supernatant was determined via Nanodrop1000 (Thermo Fischer scientific). Detailed protocol see *Appendix 8.4.1*.

2.9 RNA isolation-Cells

Total RNA was isolated from A549 and H520 cells. 1 ml of Trizol was added to the cell pellet. Cells were lysed by pipetting 20-30 times up and down with a 100 µl pipette. RNA was extracted via protocol described above (*chapter 2.9*).

2.10 cDNA transcription and qRT-PCR

1000 ng RNA was reversely transcribed in 20µl end volume with High-Capacity cDNA Reverse Transcription Kit (Applied Biosystems) according to the manufacturer's instructions using the GeneAmp 9700 Thermocycler (Applied Biosystems). 1ng cDNA for human tissue samples and 2ng cDNA from cell culture samples were used for the master mix. SYBR Green PCR Master Mix Kit (Life Technologies), 500 nM of forward and reverse primer was mixed with the cDNA and ddH_2O. Primer sequences are shown in *Appendix Table 10*. qRT-PCR was performed on the Quant Studio 7 Flex (Applied Biosystems). The most stable housekeeping genes (HKG) were determined from 4 different HKGs based on the algorithm implemented in NormFinder Software norm [211]. For ADC tissue samples *succinate dehydrogenase complex, subunit A* (*SDHA*) and *Importin 8* (IPO8) and for SQC tissue samples *β-actin* and *SDHA* were calculated to be most stable HKGs. Fold change values of *eIF6* were normalized to the mean Ct-values

of HKGs. For cell culture (A549, H520) experiments, *β-actin* served as internal control. Fold change levels were analyzed using the $2^{-\Delta\Delta}$CT method [212].

2.11 Transfection

Cell cycle was synchronized by serum starvation for 16h before seeding of $2x10^4$ cells/well of A549 and $8x10^4$ cells/well of H520 on 12 well plates. Transfection was performed with 4µl of Oligofectamine™ (Life Technologies) per 12-well according to manufacturer's instructions Transfection Reagent. Following siRNAs were used: 20 nM siRNA oligonucleotides against *eIF6*: *eIF6_1* (Hs_*ITGB4BP*_5), *eIF6*_2 (HS_*ITGB4BP*_6), scrambled negative control siRNA (Allstar negative control siRNA) and 488-Alexa-labeled scrambled negative control siRNA (Allstars negative control siRNA). The siRNA sequence is listed in *Table 11*. Detailed protocol see *Appendix 8.4.3* (A549) and *8.4.4* (H520).

2.12 FACS apoptosis measurement with Annexin/PI

A549 and H520 cells were transfected as described above (*chapter 2.11*) with *eIF6*-specific or non-targeting siRNAs. The FITC Annexin V Apoptosis Detection Kit (Biolegend) was used according to the manufacturer's suggestion. Three and five days post transfection cells and supernatants and cells were harvested. Supernatants were collected before detachment of adherent cells by either trypsin for A549 or accutase for H520, respectively. Subsequently, cells were washed with cold PBS and incubated with 100 µl of 1x binding buffer (containing 5 µl of Annexin V FITC and 5 µl of PI) for 15 min (25 °C) in the dark [213,214]. Flow cytometric analysis (FACS) was performed using Guava EasyCyte 8 (Millipore) and analyzed with InCyte 3.1 (Millipore). To set up fluorescent compensation and gating for detection of necrosis and early/late apoptosis, unstained and single stained cells were treated with staurosporine (1 µM, 4h, Sigma Aldrich). Detailed protocol see *Appendix 8.4.5*.

2.13 Proliferation Assay

Cells were transfected with siRNA against *eIF6* and negative control as described above (*chapter 2.11*). At day 3 and 5 post transfection, cells were detached with 250 µl of trypsin for A549 or accutase for H520 and 250 µl medium. Then 20 µl of the cell suspension and 180 µl of Guava ViaCount Assay solution (Merck) was mixed and then the cell number was determined on Guava EasyCyte 8 (Millipore).

2.14 Colony Formation Assay

After inducible knockdown of *eIF6* in A549 or H520, 400 cells were collected after 3 days and seeded in 6-well plates. After 4 weeks of cultivation, cells were fixed with 4% paraformaldehyde (Sigma-Aldrich) stained with 1:10 diluted Giemsa solution (1 Giemsa: 9 ddH_2O) for 20 min and rinsed with distilled water.

2.15 Senescence Assay

For detection of senescence-associated β-galactosidase (SA-β-Gal) activity, we followed the protocol described by Dimri et al. [215]. The assay was performed on day 4 post transfection. Untreated, mock and siScr transfected cells were used as controls. Experiments were performed in triplicate.

2.16 ClickIT-Metabolic labelling, click-chemistry and 1 SDS-Page analysis

ClickIT® L–Homo-proparglycerin (HPG) (cat.no. C10186) were used according to the manufacturer's suggestion (Thermo Fischer Scientific Inc.). A549 and H520 cells were seeded out in 12-well plates and were transfected as described prior. Then four days after knockdown of eIF6, methionine starvation followed for 3 hours. Cells were then incubated with 10µM of HPG for 1 h. In control cells translation was inhibited by 350 µM cycloheximid for 30 min prior of HPG incubation. Then cells from six 12-wells were together scraped with 50µl lysis buffer (50 mM Tris/HCl, 1% SDS, pH 8.0) with addition of protease and phosphatase inhibitors and 250U/ml (Benzonase Merck). Cell lysates were further lysed with sonicated, vortexed (5min) followed by centrifugation (18,000g, 5 min, 4°C). 200 µg of protein sample was incubated with ClickIT® Protein Reaction Buffer Kit (cat.no.C10276) containing the fluorophore for protein TAMRA (final conc. 40µM). Further procedure was according to the manufacturer´s suggestion. Samples were then loaded on 1D SDS-Page according to the manufacturer's instructions. Fluorescence was detected via the laser scanner Typhoon 9400 (Amersham Biosciences; excitation 532 nm, emission 580 nm). To ensure the equal loading for the SDS-Gel, Coomassie brilliant Blue staining was performed. The ImageQuant and Image Lab 4.0.1. software was used for quantification of fluorescence and Coomassie intensity. Detailed protocol see *Appendix 8.4.2*.

2.17 Sucrose gradients polysomes fractions

Sucrose density-gradient centrifugation separates polysomes, 80S ribosomes and free 40S and 60S ribosomal subunits. A549 and H520 cells were cultured for 3 days in 100 mm dishes and transfected with siRNA (eIF6_1+2), with mock as a control. 15 min prior to lysis, cells were incubated with 100 µg/ml cycloheximide (CHX) (Sigma-Aldrich) to inhibit translation. Before scraping in lysis buffer (20 mM HEPES pH 7.4, 15 mM $MgCl_2$, 200mM KCl, 1% Triton X-100, 2mM DTT and 100 µg/ml cycloheximide), cells where washed with ice-cold PBS containing 100 µg/ml CHX. After centrifugation (14000 g, 10 min, 4°C), RNA concentration in the supernatant was determined via Nanodrop1000 (Thermo Fischer Scientific Inc., Massachusetts, USA). 3 OD_{260} Units were layered onto 15%-40% sucrose gradients (50 mM NH4Cl, 50 mM Tris-acetate pH 7.0, 12 mM MgCl2, freshly added 100µg/ml cycloheximide and 1mM DTT) and centrifuged in a SW41Ti rotor (Beckman, Villepinte, France) for 150 min at 160000 g, 4°C without breaking. Ribosomal profiles were recorded via an ISCO (Teledyne ISCO) density gradient analyzing unit, which includes a UA-6 detector that measures the absorption at 254nm, allowing for detection of RNA. As the majority of cellular RNAs are contained in ribosomes, this analysis records the ribosomal distribution.

Fractions were collected along the gradients and trichloroacetic acid-precipitated overnight at -20°C to concentrate proteins for gel electrophoresis and subsequent Western Blot analysis. Detailed protocol see *Appendix 8.4.7*.

2.18 Northernblotting

5 µg of RNA per sample was separated on 1.5% MOPS-agarose gels as described in the manual of the RNeasy minikit (QIAGEN). The RNA was transferred overnight onto a Hybond N nylon membrane (GE Health Care) and then cross-linked to the membrane by UV light. Membranes were stained with 0.02% methylene blue, 3% acetic acid to visualize the mature 28S and 18S rRNAs. Hybridization was performed overnight at 37°C in 500 mM NaPO4 buffer, pH 7.2, 7% SDS, 1 mM EDTA using 5′-^{32P}-labeled oligonucleotides with the following sequences: ITS1, 5′-CCTCGCCCTCCGGGCTCCGTTAATGATC -3′; ITS2, 5′-CTGCGAGGGAACCCCCAGCCGCGCA -3′. The membranes were washed three times for 20 min at 37°C in 40 mM NaPO4 buffer, pH 7.2, 1% SDS, and radioactivity

was detected by exposing x-ray films. Membranes were regenerated by washing in 1% SDS. Northern blotting was performed by Valentin Mitterer and Brigitte Pertschy.

Paclitaxel treatment of A549 cell line

$1{,}5x10^6$ cells/well of A549 were seeded out in 6 well plates 24 hours before treatment started. Treatment was performed with five different concentrations (5nM, 10nM, 25nM, 50nM, 100nM) of paclitaxel, which were directly diluted in cell culture medium. Cells were harvested after 24h, 48h and 72h post treatment, cell pellets were stored at -80°C for further analysis. Microscopy pictures for documentation were taken at the three indicated time points. Cell culture medium was changed every 48h. Treatment scheme is displayed in *Appendix 8.4.8*.

2.19 Statistical analysis

For all statistical analyses and graph generation, Graphpad PRISM 5.0 edition software (GraphPad software Inc.) was used. Except of TMA data, all data were analyzed by the statistical software program SPSS (SPSS Inc.). All presented data were analyzed by descriptive statistics and displayed as means ± standard error of means (SEM). Statistical tests according to each data set are mentioned in the figure legends. Each data set was analyzed for Gaussian distribution. Normally distributed data were analyzed by student t-test or one-way ANOVA. Mann-Whitney U or Kruskal-Wallis test were used when data were not normally distributed. For all analyses the alpha was set to 0.05.

3 Hypothesis and Objectives

Protein synthesis is critical for cell live, since it provides the building blocks for fast and effective growth. Eukaryotic translation initiation factors belong to the first regulatory steps, because they assure correct ribosome assembly and thereby translation. For this reason, we hypothesized that:

- eIFs are altered in NSCLC compared to non-neoplastic lung tissue (NNT)
- eIFs represent potential therapeutic targets
- eIFs could serve as biomarkers
- eIF expression affects patient overall survival

To test these hypotheses, the following experimental approaches were used:

I. Characterization of eIF expression levels in human lung carcinoma tissue compared to healthy lung tissue.
II. Identification of promising candidates for prognosis and potential therapy targets.
III. Analysis of the consequences after knockdown of promising eIF candidates on proliferation and ribosome assembly.
IV. Evaluation of eIF expression level on patient overall survival in a public database.

5.1 Basic characterization of eIFs in two NSCLC Cell lines A549 and H1299

In the first experimental approach I have compared protein expression and phosphorylation status of several members of the mTOR pathway. This pathway regulates major cellular functions, eIFs and is known to be dysregulated in cancer. Basic protein expression levels PI3K/AKT/mTOR-pathway members in lung metastasis cell line H1299 and ADC cell line A549 was analyzed to ensure stable protein expression over several passages for later experiments (*Figure 10*). Both cell lines show stable protein expression over different passages. mTOR and PTEN show a lower basal expression level in H1299 cell line than in A549. p70S6K, 4E-BP1, and PTEN were not detected in H1299. Phosphorylation of mTOR, p70S6K, Akt, 4E-BP1, and PTEN is stable over analyzed passages in A549 cell line (*Figure 10*).

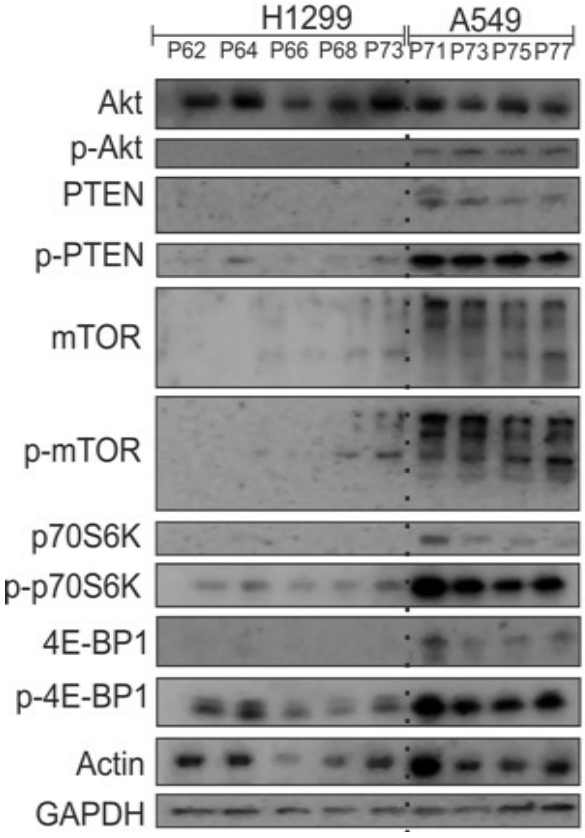

Figure 10 Characterization of PI3K/AKT/mTOR-pathway member protein expression in H1299 and A549 NSCLC cells. 30µg of protein lysates over 4-week of cultivation were analyzed by Western Blot and show stable protein expression of the PI3K/AKT/mTOR-pathway proteins over the cultivation period.

The eIF4F-complex members were also stable expressed in both cell lines over several passages, except for eIF4B in A549, which decreased in life passages (*Figure 11*).

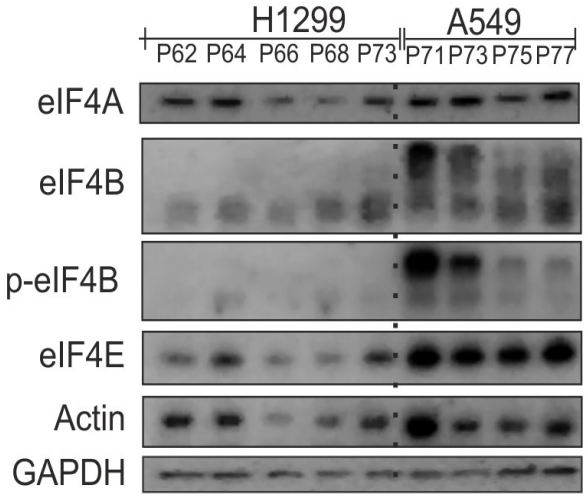

Figure 11 eIF4 complex protein expression in H1299 and A549 cells. 30µg of protein lysates were analyzed by Western Blot over 4-week cultivation and show stable protein expression of the eIF4 complex proteins over the cultivation period, except p-eIF4B and eIF4B expression changes over the passages in A549 cells.

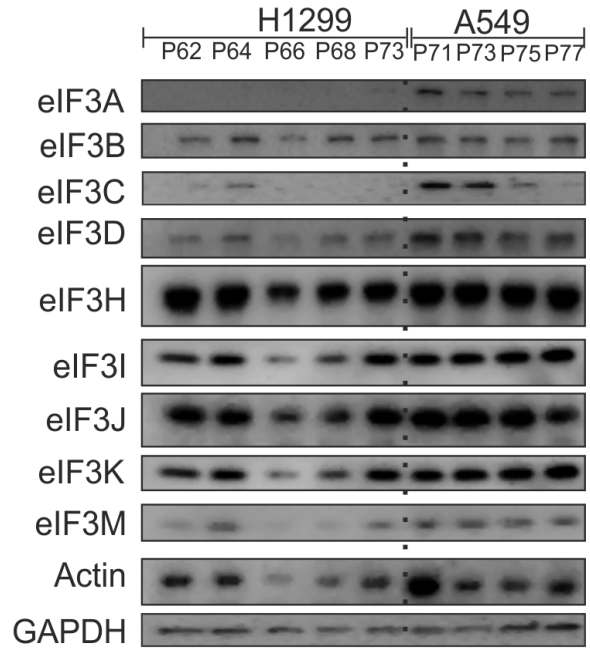

Figure 12 Protein expression of eIF3 complex members in H1299 and A549 cells. 30µg of protein lysates were analyzed by Western Blot over 4- week's cultivation. Protein expression of the eIF3 members is stable over the cultivation period, except in A549 cells eIF3C expression varied.

Expression eIF3 complex members were also studied by on Western blotting. Protein expression of all eIF3 complex members stayed constant over the different passages, except for eIF3C, eIF3I, eIF3K and eIF3M in the H1299 cell line. This

proteins were differentially expressed over the analyzed time period. eIF3A expression was undetectable in H1299 cells. In A549 cells, eIF3C varied depending on expression levels over several passages, the other eIF3 complex members showed the same expression in all 4 passages (*Figure 12*).

Finally, eIF5, eIF2α, and eIF6 protein expression was analyzed in for both cell lines. Phosphorylation of eIF2α varied within the different passages, but eIF5 was stably expressed in both cell lines (*Figure 13*).

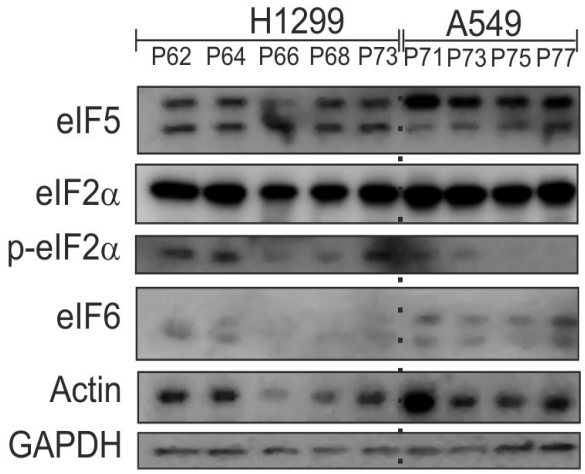

Figure 13 Protein expression analysis of eIF5, eIF2α and eIF6 in H1299 and A549 cells. 30µg of protein lysates were analyzed by Western Blot over 4- week's cultivation. Protein expression of eIF5, eIF2α and eIF6 is stable over the cultivation period.

5.2 Paclitaxel treatment of A549 leads to reduced growth

To test the hypothesis that eIFs are altered upon chemotherapy, A549 cells were treated with paclitaxel. Cells were seeded, and 24h later, cells were treated with five different concentrations of paclitaxel , 10nM is described in the literature as IC_{50} dose for A549 cells [216]. Three time points were analyzed (*Figure 14*).

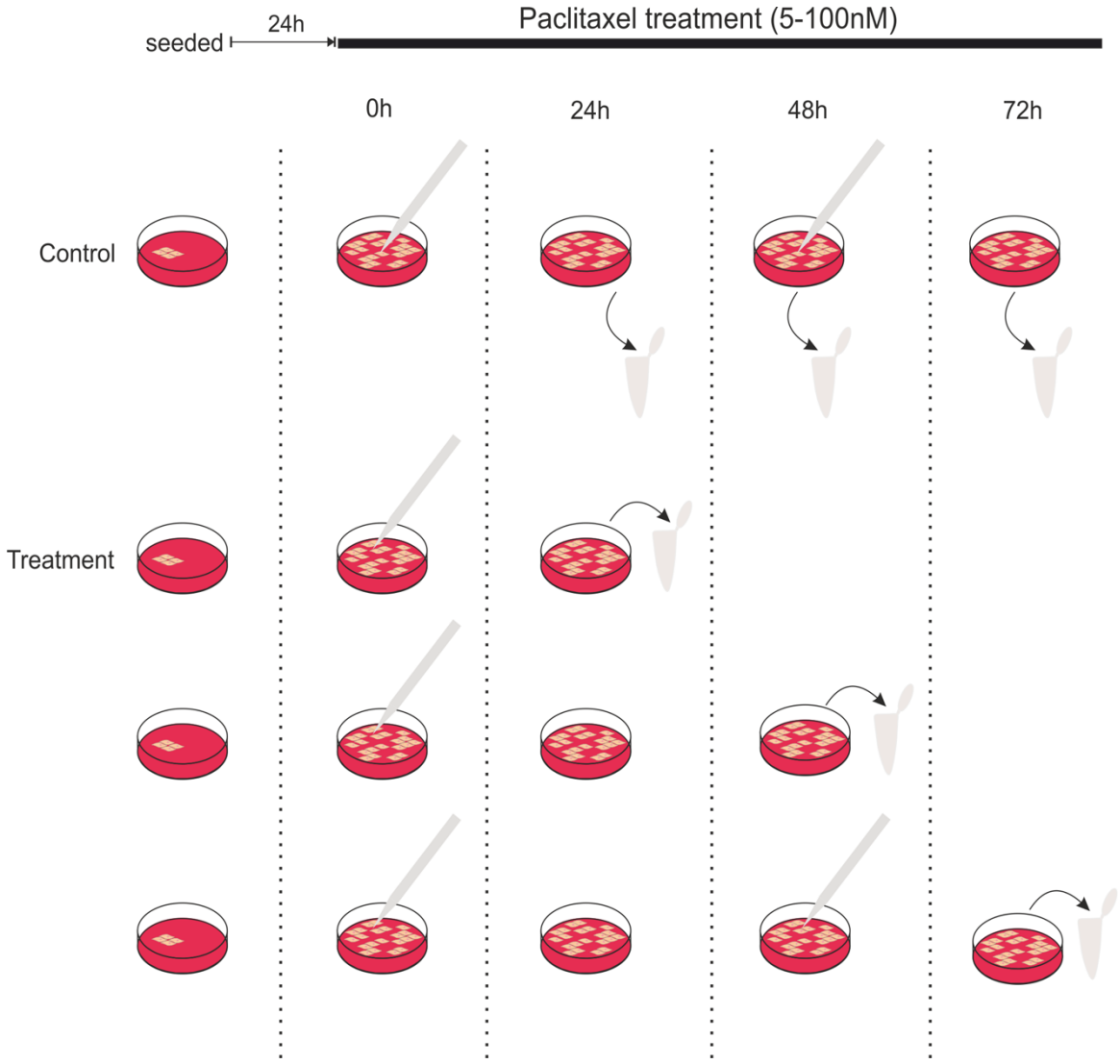

Figure 14 Scheme of chemotherapy treatment of A549 cells with paclitaxel. Cells were seeded and cultivated for 24h before treatment with different concentrations of paclitaxel (5-100nM). Medium containing paclitaxel was changed every 48h. Cells were harvested after three different time points (24h, 48h and 72h) for further analysis.

Microscopy was performed to investigate cell density, morphology and growth upon treatment (*Figure 15*). All used concentrations of paclitaxel revealed in less cells compared to the control condition (EthOH). At the published IC_{50} (10nM) the cell number was decreased by ~50%. Control cells and cells treated with 5nM paclitaxel

were confluent after 48h. For all other treatment concentrations, cells showed reduced growth compared to control condition. After 48h, the IC_{50} concentration showed again ~50% less cells compared to control condition. After 72 hours of paclitaxel treatment, growth defects from the prior time-points remained constant. Over three time-points, no change in cell morphology was observed.

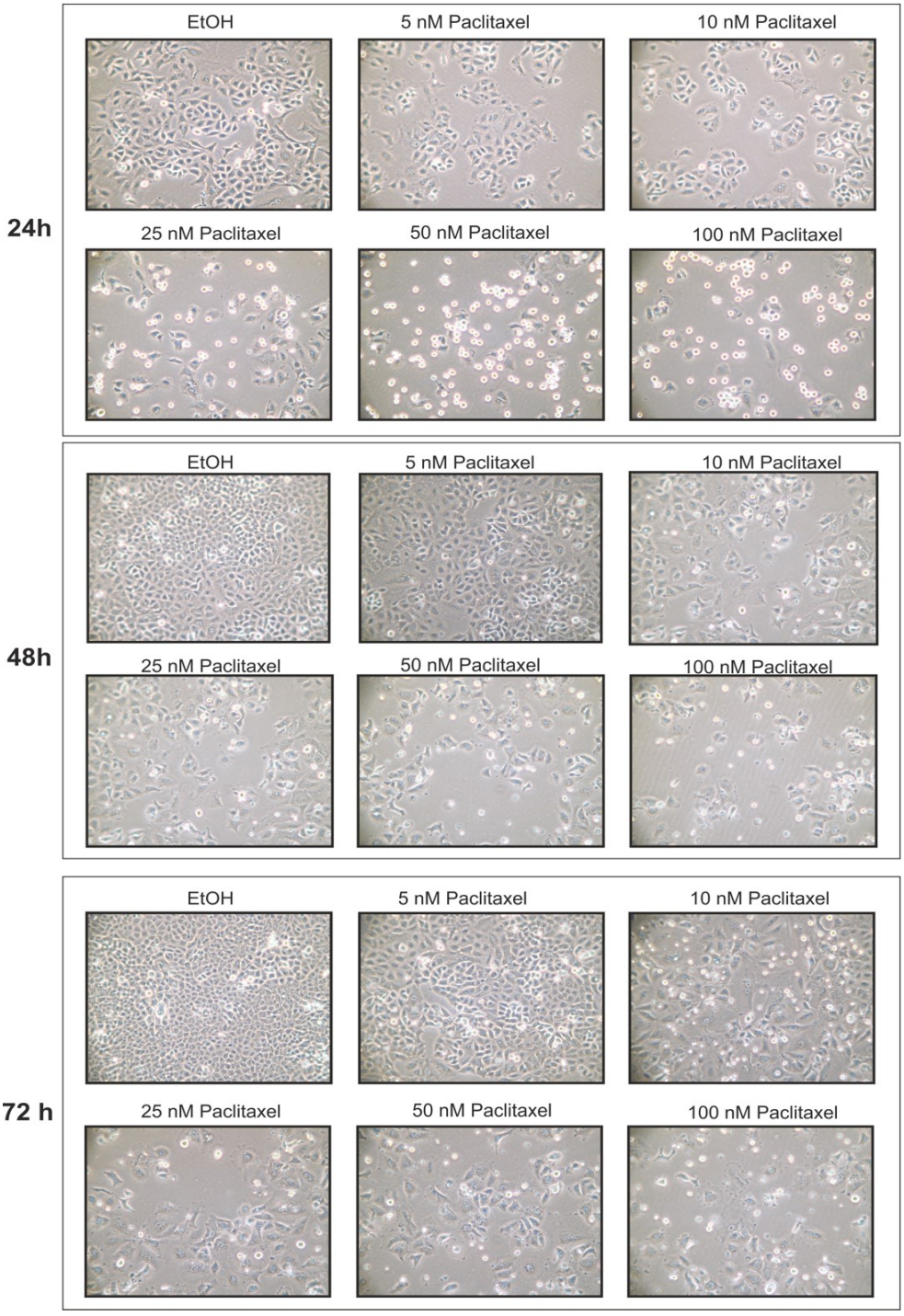

Figure 15 Representative pictures of paclitaxel treated A549 cells at 24h, 48h and 72h. Five different concentrations of Paclitaxel were tested (5, 10, 25, 50 and 100 nM) and analyzed by light microscopy. EtOH served as control condition. The concentrations 5- 100 nm reduced cell growth at the indicated time points.

5.2.1 Western Blot analysis of paclitaxel treated A549 cells

Cells were harvested at the indicated time points, and lysed. Lysates were analyzed by Western Blot for PI3K/AKT/mTOR-pathway members and eIFs.

First, mTOR, p70S6K, Akt, PTEN, and 4EBP-1 were analyzed. At the 24h time point, an increase in mTOR protein expression for 5nM-25nM paclitaxel treatment was observed (*Figure 16*). On day one post treatment, the expression level of Akt stayed constant at low treatment concentrations (5-25 nM), but phosphorylation of Akt was reduced compared to control cells. 48h after treatment, protein expression of mTOR, p70S6K, Akt and PTEN was decreased for 50 nM and 100 nM.

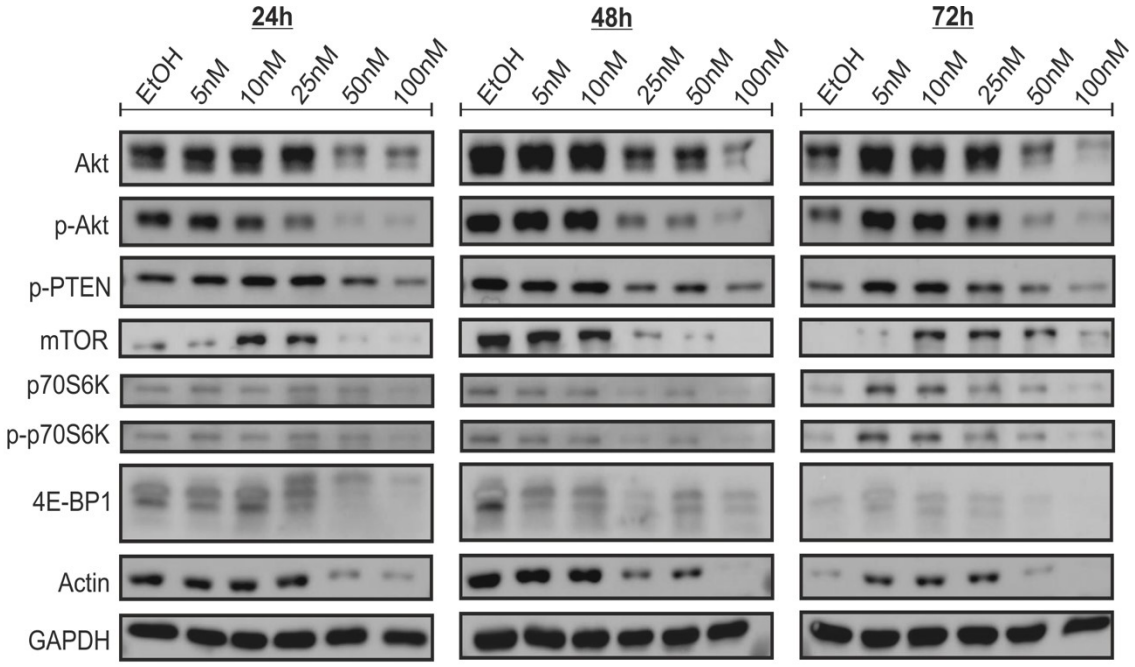

Figure 16 Protein expression of PI3K/AKT/mTOR-pathway members in paclitaxel treated A549 cells. Five different concentrations of Paclitaxel were tested (5, 10, 25, 50 and 100 nM) and 30 µg of protein lysates analyzed by Western Blot at tree time points(24h, 48h and 72h) after paclitaxel treatment. mTOR protein expression is increased compared to control condition (EtOH). Actin and GAPDH served as loading control.

Then the eIF4F complex member were analyzed by Western Blot, analysis is shown in *Figure 17*. Upon paclitaxel treatment, eIF4G showed an increase in protein expression for 24h and 10nM and 25nM. This effect was not observed on day 2, but 72h post treatment, eIF4G expression was increased compared to control cells. eIF4B levels remained at constant levels compared to controls, but for 25nM, 50nM and 100nM paclitaxel after 48 hours, less phosphorylation of eIF4B was detected.

Members of the eIF3 complex remained stable during paclitaxel treatment over the indicated time points, except for eIF3θ and eIF3A. These proteins are upregulated in paclitaxel-treated A549 cells compared to control condition for all indicated time points (*Figure 18*).

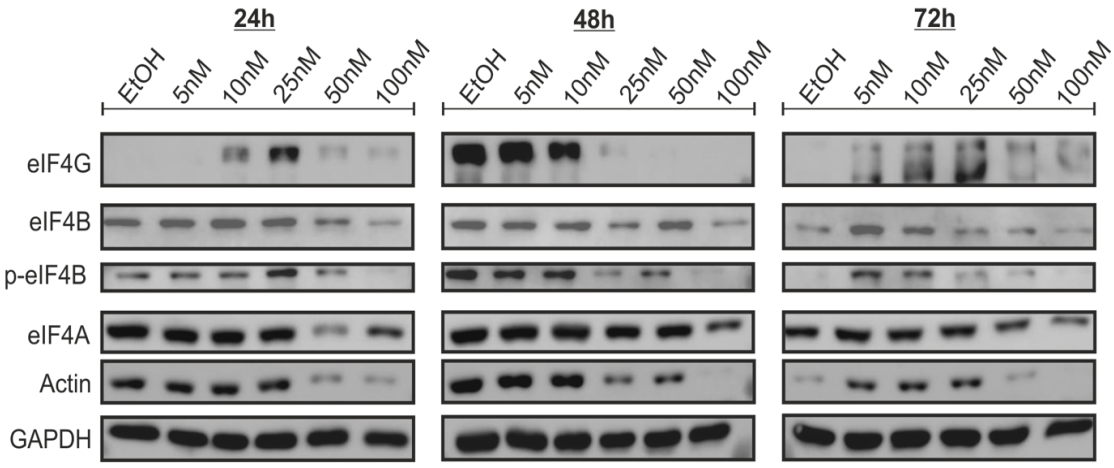

Figure 17 Protein expression of eIF4 members in Paclitaxel-treated A549 cells. Five different concentrations of Paclitaxel were tested (5, 10, 25, 50 and 100 nM) and 30 µg of protein lysates analyzed by Western Blot at tree time points (24h, 48h and 72h) after treatment. eIF4G protein expression is increased compared to control condition (EtOH).

Furthermore, eIFs (eIF2α, eIF1A, eIF6 and eIF5) were analyzed after paclitaxel treatment. For all analyzed time points, a notable change in protein expression was observed for eIF6, which correlated with increasing paclitaxel concentration (*Figure 19*).

Finally, caspase 3 was analyzed to determine if apoptosis is induced by paclitaxel treatment. No changes in caspase 3 levels were detected upon paclitaxel treatment (*Figure 20*).

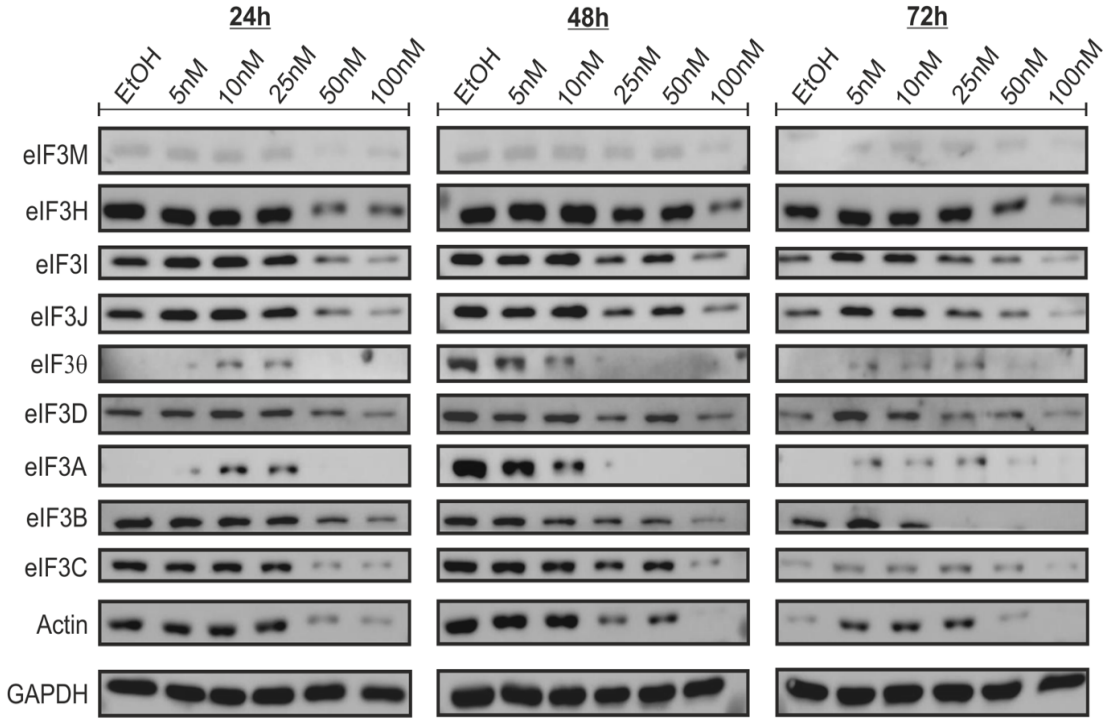

Figure 18 Protein expression of eIF3 members in Paclitaxel treated A549 cells. Five different concentrations of Paclitaxel were tested (5, 10, 25, 50 and 100 nM) and 30 µg of protein lysates analyzed by Western Blot at tree time points (24h, 48h and 72h) after treatment. eIF3A and eIF3θ protein expression is increased compared control condition (EtOH) at all indicated time points.

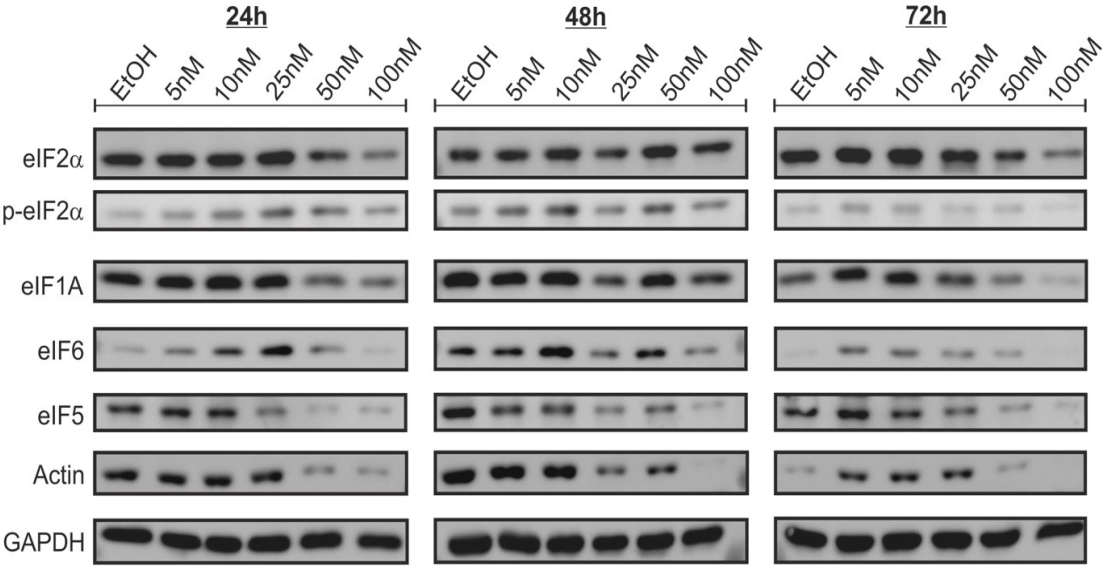

Figure 19 Protein expression of eIF2α, eIF1A, eIF6 and eIF5 in Paclitaxel treated A549 cells. Five different concentrations of Paclitaxel were tested (5, 10, 25, 50 and 100 nM) and 30 µg of protein lysates analyzed by Western Blot at tree time points (24h, 48h and 72h) after treatment. At all indicated time points eIF6 expression and phosphorylation of eIF2α are increased compared to control condition (EtOH).

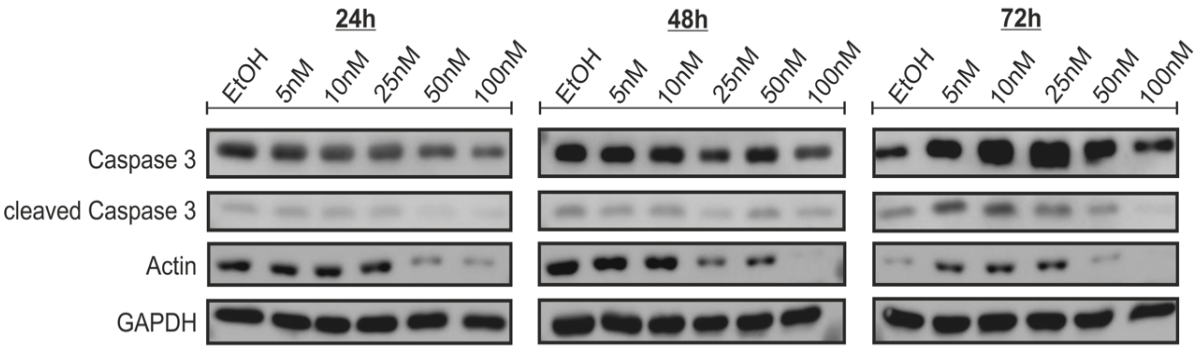

Figure 20 Apoptosis is induced in A549 Paclitaxel treated cells. Five different concentrations of Paclitaxel were tested (5, 10, 25, 50 and 100 nM) and 30 µg of protein lysates analyzed by Western Blot at tree time points (24h, 48h and 72h) after treatment. After 72 h of paclitaxel treatment more cleaved caspase 3 was overserved compared to control condition (EtOH).

5.3 Basic characterization of eIFs in two major histological subtypes of NSCLC, ADC and SQC

Fresh lung tissue material from surgeries, which was immediately frozen and stored for later analyses, was collected mainly form ADC and SQC patients. Lysates of the tissue was generated for protein and mRNA analysis.

In two major histological subtypes (ADC and SQC), the eIF protein expression of fresh frozen NSCLC patient samples was investigated to define the significance of eIFs in NSCLC.

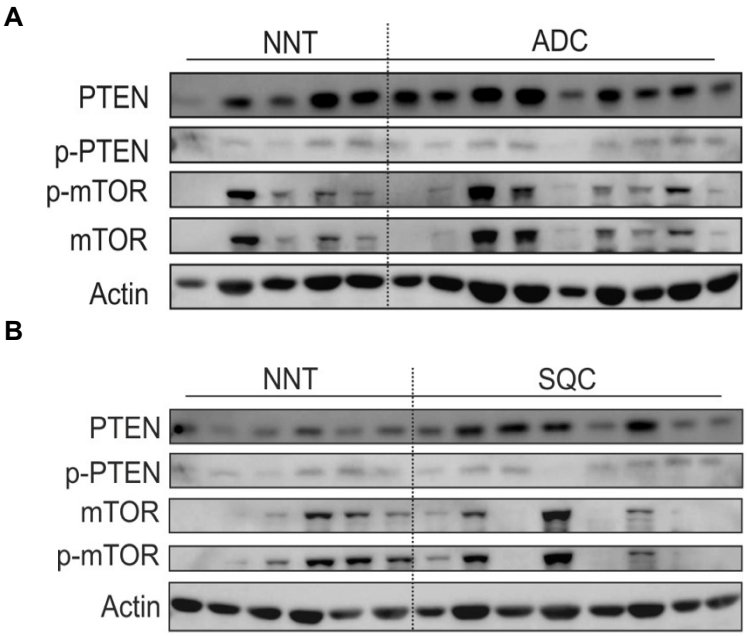

Figure 21 Protein expression of PI3K/AKT/mTOR-pathway members in ADC and SQC patients. (**A**,**B**) 20 µg of protein lysates from ADC (n=9) and SQC (n=8) patients compared to non-neoplastic tissue (NNT, in A n=5, in B n=6) were analyzed by Western Blot. Actin served as loading control. No changes in protein expression and phosphorylation levels of mTOR and PTEN were detected.

Protein expression of PI3K/AKT/mTOR-pathway members and eIFs were investigated in 14 ADC samples with their corresponding tissue. mTOR and PTEN in ADC and SQC samples revealed no different expression compared to NNT. No change in phosphorylation of mTOR and PTEN was observed in the analyzed samples (representative Western Blots see *Figure 21A* and *B*).

After analyzing mTOR pathway members, eIF4G and eIF4A were investigated. eIF4A is upregulated in ADC tissue samples compared to NNT, while eIF4G (*Figure 22A* and *B*).

eIF3 and complex members revealed no change in protein expression between NNT compared to ADC (*Figure 23*).

Additionally, eIF2α, eIF5, eIF6 and eIF1A expression was analyzed in ADC and SQC samples compared to NNT. For eIF2α and eIF5, no changes in protein expression were observed. eIF6 and eIF1A are upregulated in ADC and SQC tissue compared to NNT. Also eIF2α phosphorylation is increased in tumor tissue compared to NNT (*Figure 24*).

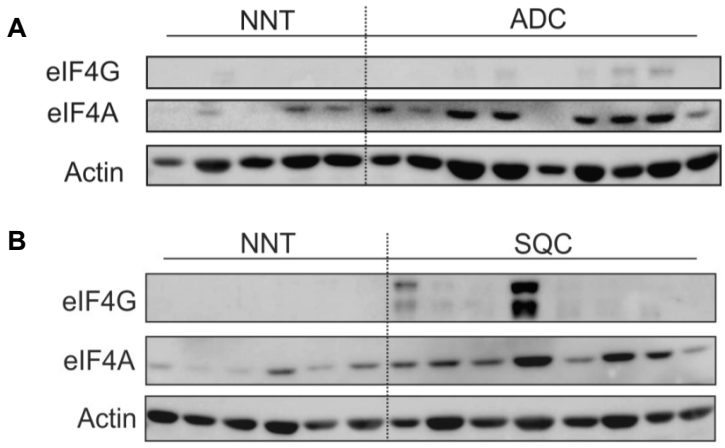

Figure 22 eIF4A is overexpressed in ADC and SQC patients. (**A**,**B**) 20 µg of protein lysates from ADC (n=9) and SQC (n=8) patients compared to non-neoplastic tissue (NNT, in A n=5, in B n=6) were analyzed by Western Blot. Actin served as loading control. eIF4A is overexpressed in ADC and SQC tissue compared to NNT. No changes in protein expression levels of eIF4G for both tissue types were detected.

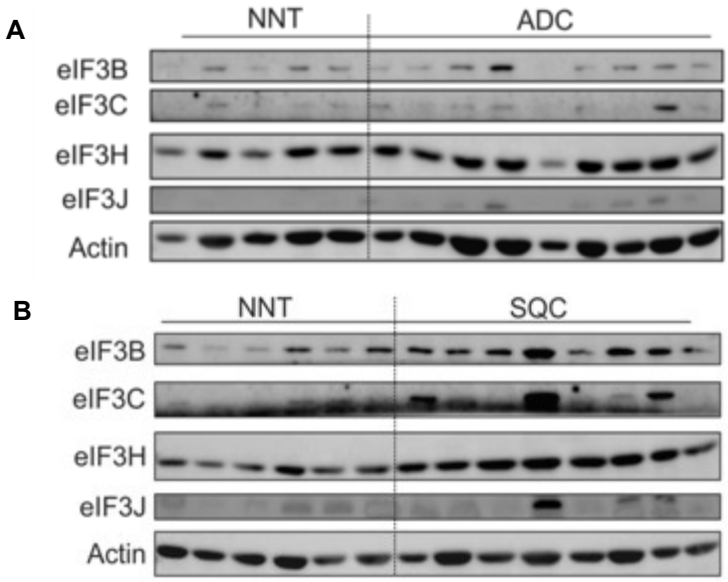

Figure 23 Protein expression eIF3 members in ADC and SQC patients. (**A**,**B**) 20 µg of protein lysates from ADC (n=9) and SQC (n=8) patients compared to non-neoplastic tissue (NNT, in A n=5, in B n=6) were analyzed by Western Blot. Actin served as loading control. No significant changes on protein expression levels of eIF3B, eIF3C, eIF3H and eIF3J for ADC and SQC tumor tissue, compared to NNT, were detected.

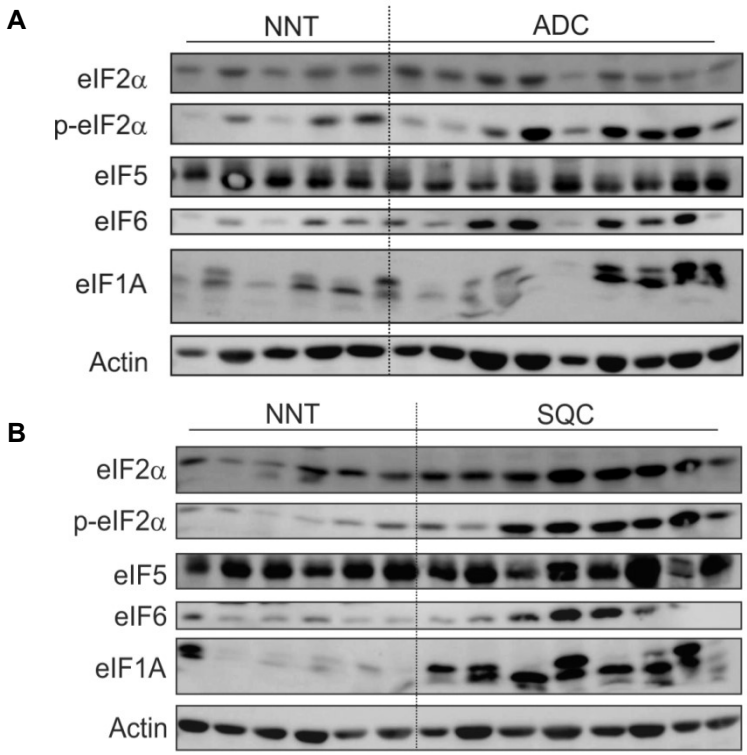

Figure 24 Protein expression eIF2α, eIF5, eIF6 and and eIF1A in ADC and SQC patients. 20 µg of protein lysates from ADC (n=9) and SQC (n=8) patients compared to non-neoplastic tissue (NNT, in A n=5, in B n=6) were analyzed by Western Blot. Actin served as loading control. (**A**) Phosphorylation of eIF2α is increased in ADC tissue compared to NNT. (**B**) No changes were found for eIF2α in SQC tissue samples compared to NNT. (**A**,**B**) eIF6 and eIF1A protein expression is upregulated in ADC and SQC tissue compared to NNT. eIF5 revealed no changes in protein expression levels in ADC and SQC tissue compared to NNT.

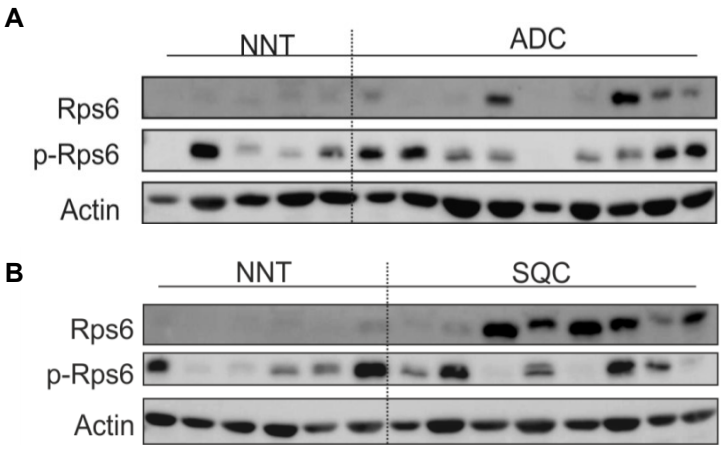

Figure 25 Protein expression Rps6 in ADC and SQC patients. (**A**,**B**) 20 µg of protein lysates from ADC (n=9) and SQC (n=8) patients compared to non-neoplastic tissue (NNT, in A n=5, in B n=6) were analyzed by Western Blot. Actin served as loading control. An overexpression of Rps6 was detected in ADC and SQC compared to their NNT.

5.3.1 Affymetrix survival analysis of eIFs in NSCLC

Not only was protein expression analyzed to determine the basic characteristics of eIFs in NSCLC. Gene expression analysis for eIFs in NSCLC was also performed in a publicly available data set (Affymetrix data base). Therefore, overall survival analysis for *eIF2S1*, *eIF4H*, *eIF3B*, *eIF1AX*, *eIF1AY* and *eIF6* in 1,926 NSCLC patients was performed (*Figure 26*). Overexpression of *eIF2S1* (eIF2α), *eIF3B*, *eIF1AY* and *eIF6* is significantly associated with worse overall survival in NSCLC patients (*Figure 26A-F*). For *eIF4H* expression, no significant correlation with overall survival in NSCLC was observed (*Figure 26B*). The analyses revealed that overexpression of *eIF1AX* is beneficially associated with overall survival in NSCLC (*Figure 26E*). A literature search revealed that details about the contribution of eIF1A and eIF6 in NSCLC are still scarce. Therefore, further investigations into the role of eIF1A and eIF6 in NSCLC were conducted.

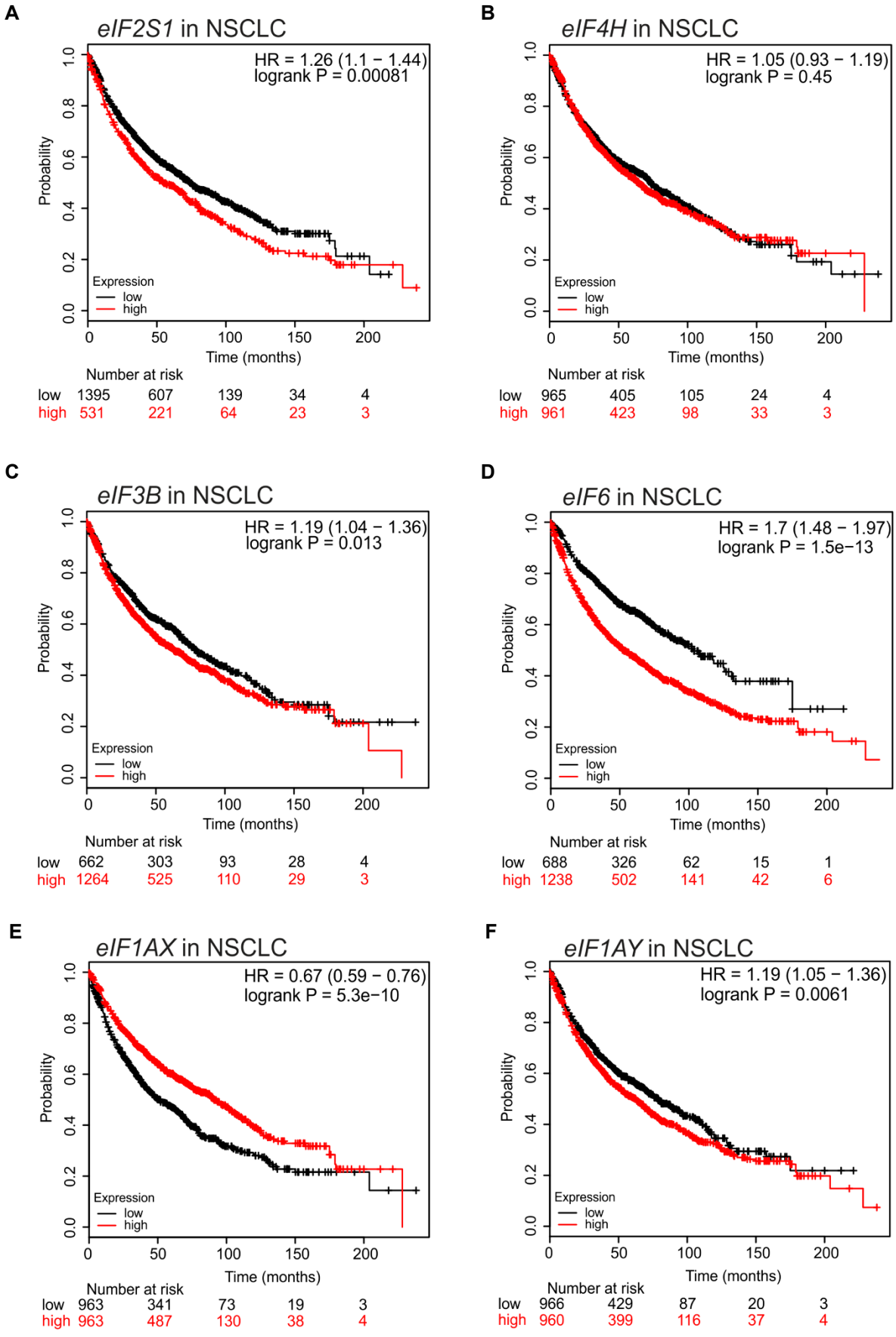
A
eIF2S1 in NSCLC
HR = 1.26 (1.1 − 1.44)
logrank P = 0.00081
Probability
Expression
low
high
Time (months)
Number at risk
low 1395 607 139 34 4
high 531 221 64 23 3
B
eIF4H in NSCLC
HR = 1.05 (0.93 − 1.19)
logrank P = 0.45
Probability
Expression
low
high
Time (months)
Number at risk
low 965 405 105 24 4
high 961 423 98 33 3
C
eIF3B in NSCLC
HR = 1.19 (1.04 − 1.36)
logrank P = 0.013
Probability
Expression
low
high
Time (months)
Number at risk
low 662 303 93 28 4
high 1264 525 110 29 3
D
eIF6 in NSCLC
HR = 1.7 (1.48 − 1.97)
logrank P = 1.5e−13
Probability
Expression
low
high
Time (months)
Number at risk
low 688 326 62 15 1
high 1238 502 141 42 6
E
eIF1AX in NSCLC
HR = 0.67 (0.59 − 0.76)
logrank P = 5.3e−10
Probability
Expression
low
high
Time (months)
Number at risk
low 963 341 73 19 3
high 963 487 130 38 4
F
eIF1AY in NSCLC
HR = 1.19 (1.05 − 1.36)
logrank P = 0.0061
Probability
Expression
low
high
Time (months)
Number at risk
low 966 429 87 20 3
high 960 399 116 37 4

Figure 26 eIF expression is associated with patient overall survival in NSCLC patients. Affymetrix data set on expression data of 1,926 NSCLC patients were plotted in Kaplan-Meier plots comparing overall survival in NSCLC, ADC and SQC patients with different expression levels of eukaryotic translation initiation factors. High expression is highlighted in red and low expression in black. (**A**) Significant worse overall survival is found for patients with high eIF2S1 (p=0.00081), with a median hazard ratio of 1.26 (1.1-1.44) compared to low eIF2S1 expression. (**B**) eIF4H shows no significant impact of eIF4H in NSCLC on overall survival (p=0.45) with a median hazard ratio of 1.05 (0.93-1.19) compared to low eIF4H expression. (**C**) High expression of eIF3B affects NSCLC overall survival (p=0.013) with a median hazard ratio of 1.19 (1.04-1.36) compared to low eIF4H expression. (**D**) High expression levels of eIF6 significantly correlates with shorter overall survival (p=1.5e-13), with a median hazard ratio of 1.7 (1.48-1.97) compared to low eIF6 expression. (**E**) High expression levels of eIF6 are significantly associated with beneficial overall survival (p=5.3e-10), with a median hazard ratio of 0.67 (0.59-0.76) compared to low eIF6 expression. (**F**) High expression levels of eIF6 significantly correlates with shorter overall survival (p=0.0061), with a median hazard ratio of 1.19 (1.05-1.36) compared to low eIF6 expression. Data A-D are published in Gantenbein et al 2018 [81]. Reproduced from [81] with permission of publisher Elsevier.

5.4 eIF1A is overexpressed in NSCLC

eIF1A is not yet well characterized in various cancer types. First the correlation between patient overall survival and *eIF1A* expression level was investigated. In the Affymetrix data set analysis, high *eIF1A* levels significantly correlated with better patient overall survival in ADC patients (*Figure 27A*). In contrast, the TCGA data set showed no correlation between *eIF1A* and patient overall survival (*Figure 28A*). Both data sets revealed no significant correlation between *eIF1A* and SQC (*Figure 27B* and *Figure 28 B*).

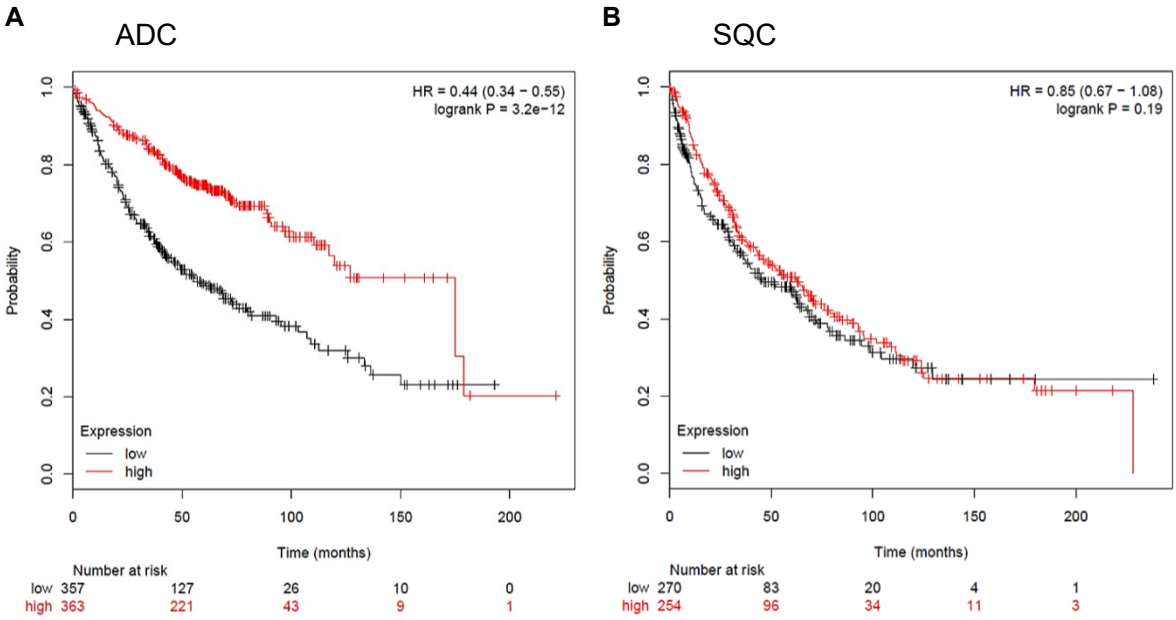

Figure 27 Affymetrix data set analysis of eIF1A expression and patient survival. (**A**) Significantly shorter survival is observed for ADC (n=720) patients with low eIF1A expression (p=3.2e-12) with median hazard ratio of 0.44 (0.34-0.55) (**B**) Patients with squamous cell carcinoma (n=524) show no correlation between eIF1A expression level (p=0.19) and survival, the median hazard ratio is 0.85 (0.67-1.08).

After the survival analysis, immunohistochemistry (IHC) was performed for eIF1A (*Figure 29*). The antibody showed unspecific staining in NSCLC tissue; therefore we decided not to proceed with IHC. The protein expression levels for eIF1A were then analyzed by Western Blot in ADC and SQC tumor tissue and compared with NNT (*Figure 30A* and *C*). The analysis revealed strong overexpression in tumor lung tissue compared to NNT. Also the densitometric analysis showed a significant overexpression of eIF1A in NSCLC (*Figure 30B* and *D*).

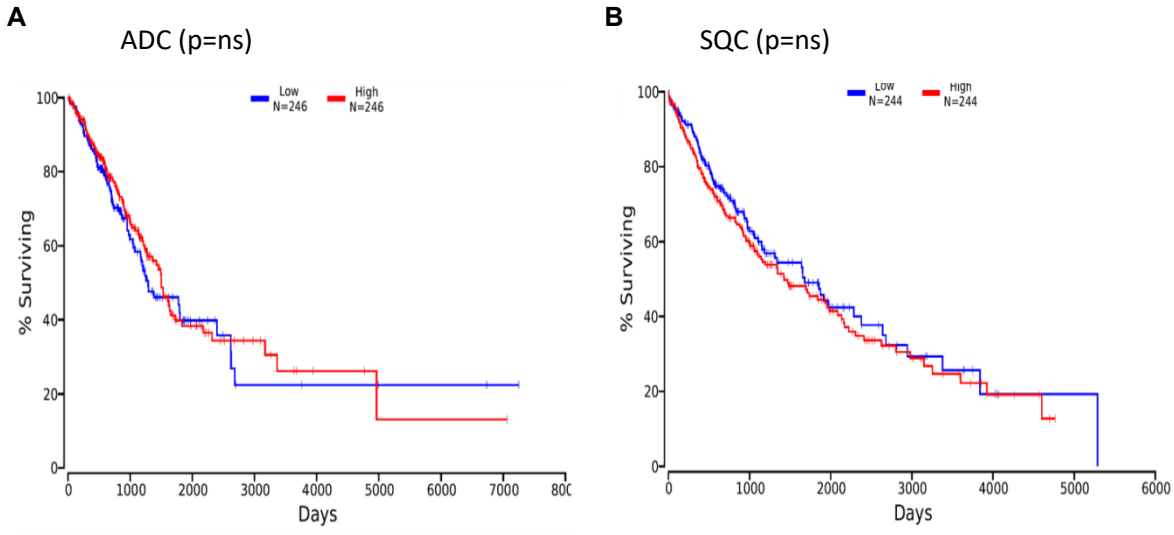

Figure 28 TCGA Analysis of eIF1A expression and patient survival. (**A**) No significantly shorter survival is observed for ADC (n=492) patients with low eIF1A expression (p=ns) (**B**) Patients with squamous cell carcinoma (n=488) show no correlation between eIF1A expression level and survival.

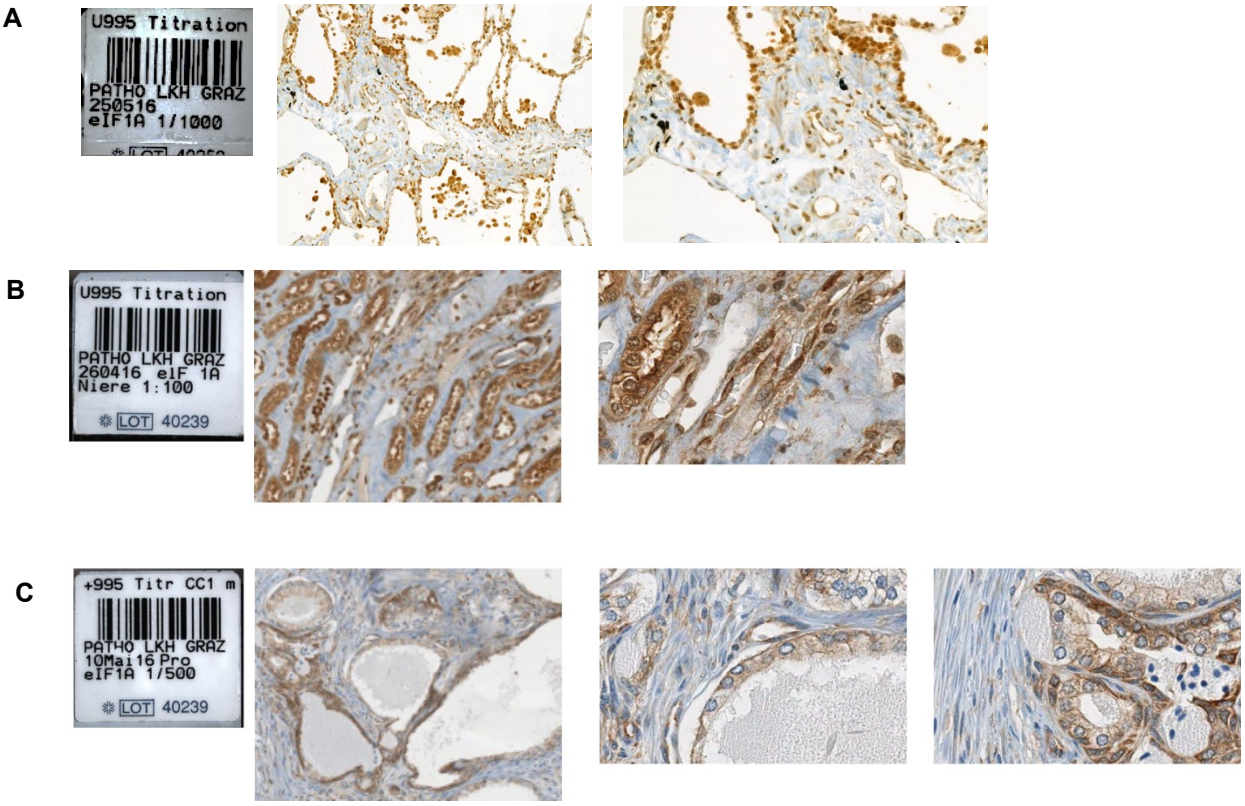

Figure 29 Immunohistochemistry of eIF1A in various tissue. (**A**) 1:1000 eIF1A dilution IHC staining in lung tissue. (**B**) 1:100 eIF1A dilution IHC staining in kidney tissue. (**C**) 1:500 eIF1A dilution IHC staining in prostate tissue.

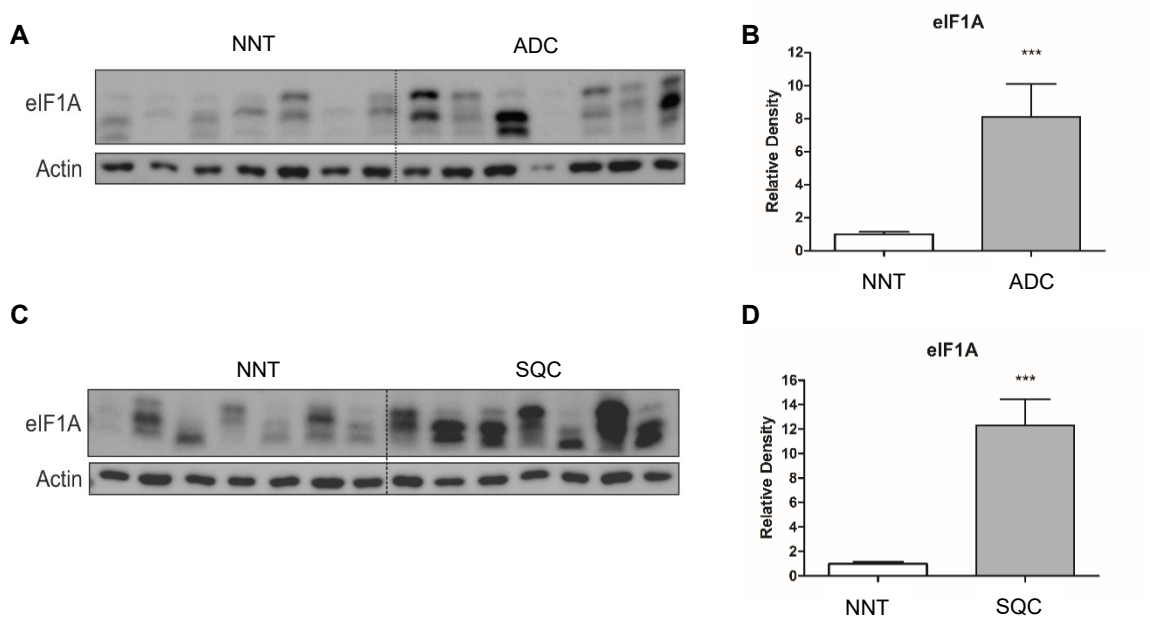

Figure 30 eIF1A is overexpressed in NSCLC tissue. (**A**) Representative Western Blot picture of eIF1A in ADC tissue reveals overexpression compared to NNT tissue (NNT n=14, ADC n=14). (**B**) Quantification of eIF1A Western Blot analysis. eIF1A is significantly upregulated in ADC tissue compared to NNT with an p-values < 0.001. (**C**) Representative Western Blot picture of eIF1A in SQC tissue reveals overexpression compared to NNT tissue (NNT n=14, ADC n=14). (**D**) Quantification of eIF1A Western Blot analysis. eIF1A is significantly upregulated in SQC tissue compared to NNT with an p-values < 0.001.

5.4.1 Characterization of eIF1A knockdown in NSCLC cell lines

To further investigate the role of eIF1A in NSCLC, knockdown of eIF1A in two cell lines was performed (ADC A549 and SQC H520). Cell lysates were analyzed at two different time points, 3 and 5 days after transfection. For the adenocarcinoma cell line A549, a 60% knockdown could be achieved at day 3. On day 5, maximum silencing efficacy ranged between 40 and 50% (*Figure 31A* and *B*). The knockdown of eIF1A was also tried twice in the H520 SQC cell line. The knockdown efficacy was 40-50% on day 3. On day 5, only silencing with siRNA_2 revealed a relevant knockdown (*Figure 31C* and *D*).

Three and five days after transfection, cells number were counted with FACS VIA Count. The A549 cell line showed a tendency toward reduced proliferation upon knockdown. We noted a significant reduction in cell numbers at day 5 post transfection for both silencing constructs (*Figure 31E*). There were no significant changes in proliferation after eIF1A knockdown in H520 cell line at the two time points tested (*Figure 31F*).

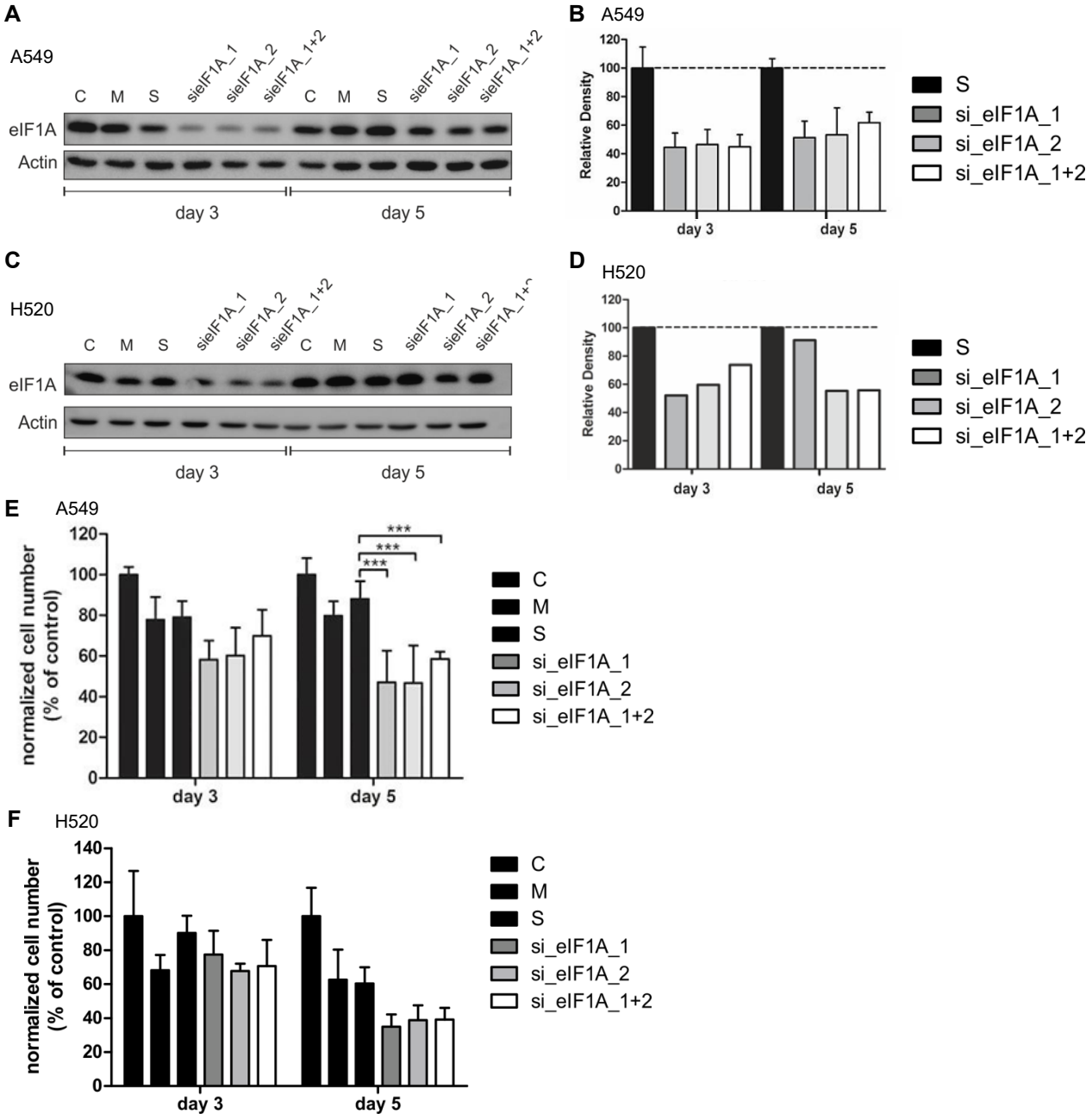

Figure 31 Knockdown of eIF1A in A549 and H520 cells. (**A**) Representative Western Blot of eIF1A knockdown in A549 cell line. (**B**) Quantification of Western Blot images 3 and 5 days after knockdown. (**C**) Representative Western Blot of eIF1A knockdown in H520 cell line. (**D**) Quantification of Western Blot images 3 and 5 days after knockdown. Proliferation after eIF1A knockdown in H520 (**E**) and H520 (**F**) cell line. Cell numbers were counted 3 and 5 days post transfection. Data were normalized to scrambled (S) Results shown represent mean ± SEM (one-way ANOVA). (*p<0.05; **p<0.001; ***p<0.0001 ns=not significant). C=control, M=mock, S=scrambled, si... =targeted construct.

5.4.2 Apoptosis is not a consequence of eIF1A knockdown in NSCLC cell lines

To evaluate whether reduced cell proliferation is coupled to apoptosis I analyzed Cap-3 and PARP activation. However, these analyses revealed that both, pro-Casp-3 and PARP levels remained unaffected by RNAi (*Figure 32*).

5.4.3 Knockdown of eIF1A does affect ribosomal profiles in ADC cell line

The impact of the knockdown in ADC cell line A549 on ribosome biogenesis by ribosomal profiling on day 3 after *eIF1A* siRNA transfection was investigated. Harvested cells were lysed, and 5 units were loaded on sucrose density gradients, followed by ultra-centrifugation of ribosomes and subsequent immunoblotting of the fractions. The elution profiles (254nm) were overlaid and mock was compared to si_eIF1A_1+2 transfected A549 cells (*Figure 33A*). No major change was visible on the profiles, although a slightly content of more free of more free 60S and 80S particles was detected. The immunoblot pictures display less eIF1A in knockdown cells compared to mock control. Two ribosomal markers were used to identify 40S (Rps6) and 60S (Rpl35) particle. The original elution profiles are displayed in *Figure 33C* and *D*.

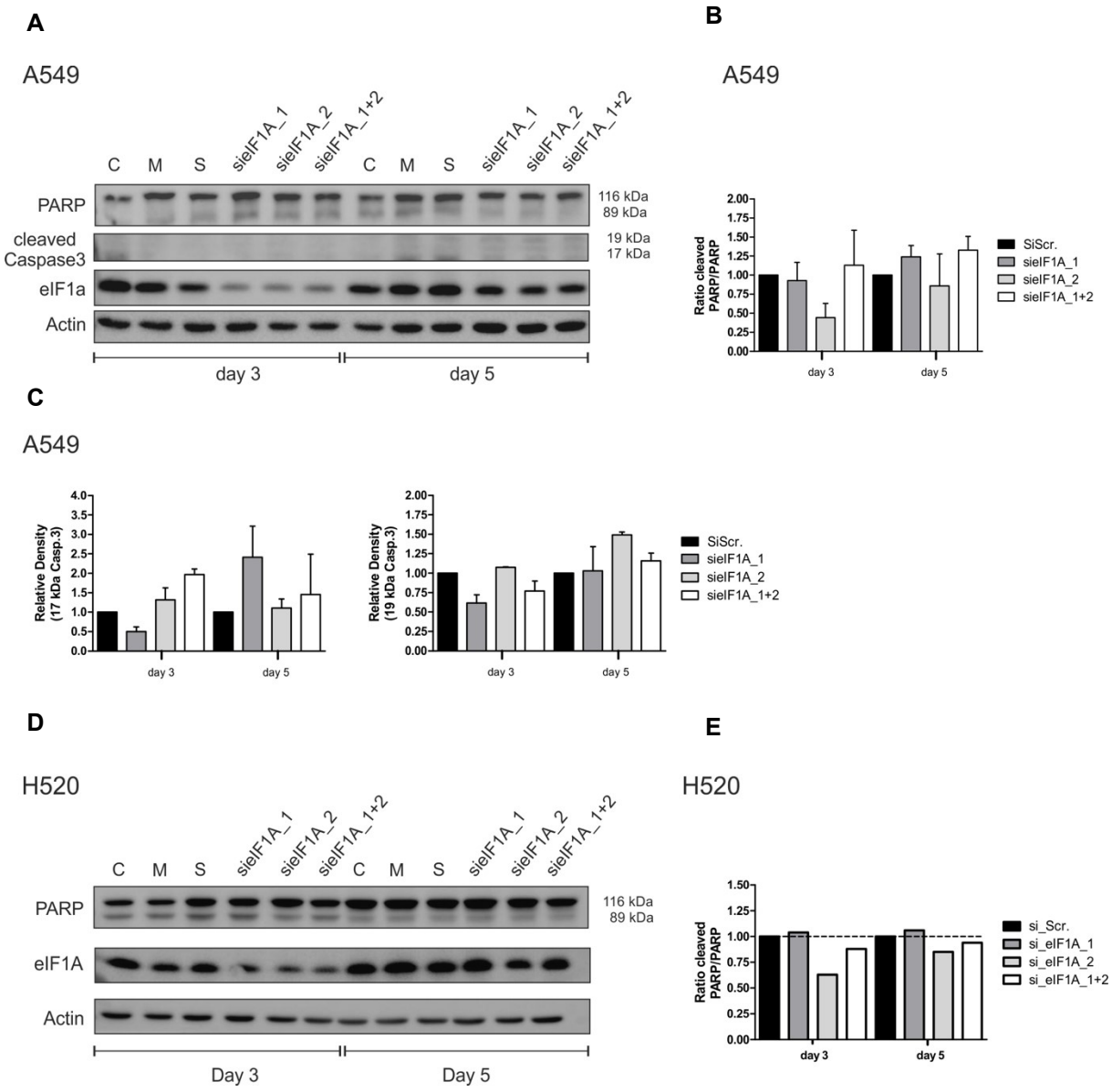

Figure 32 No changes in apoptotic markers were observed upon knockdown of eIF1A. (**A**) Representative Immunoblots of PARP and Casp 3 processing in response to eIF1A-silencing in A549 cells. β-Actin served as loading control. (**B,C**) Densitometric evaluation of cleaved Casp 3 (17 kDa and 19 kDa) and cleaved PARP in A549. (**D**) Representative Immunoblots of PARP processing in response to eIF1A-silencing in H520 cells. β-Actin served as loading control. (**E**) Densitometric evaluation of cleaved PARP in H520. C=control, M=mock, S=scrambled

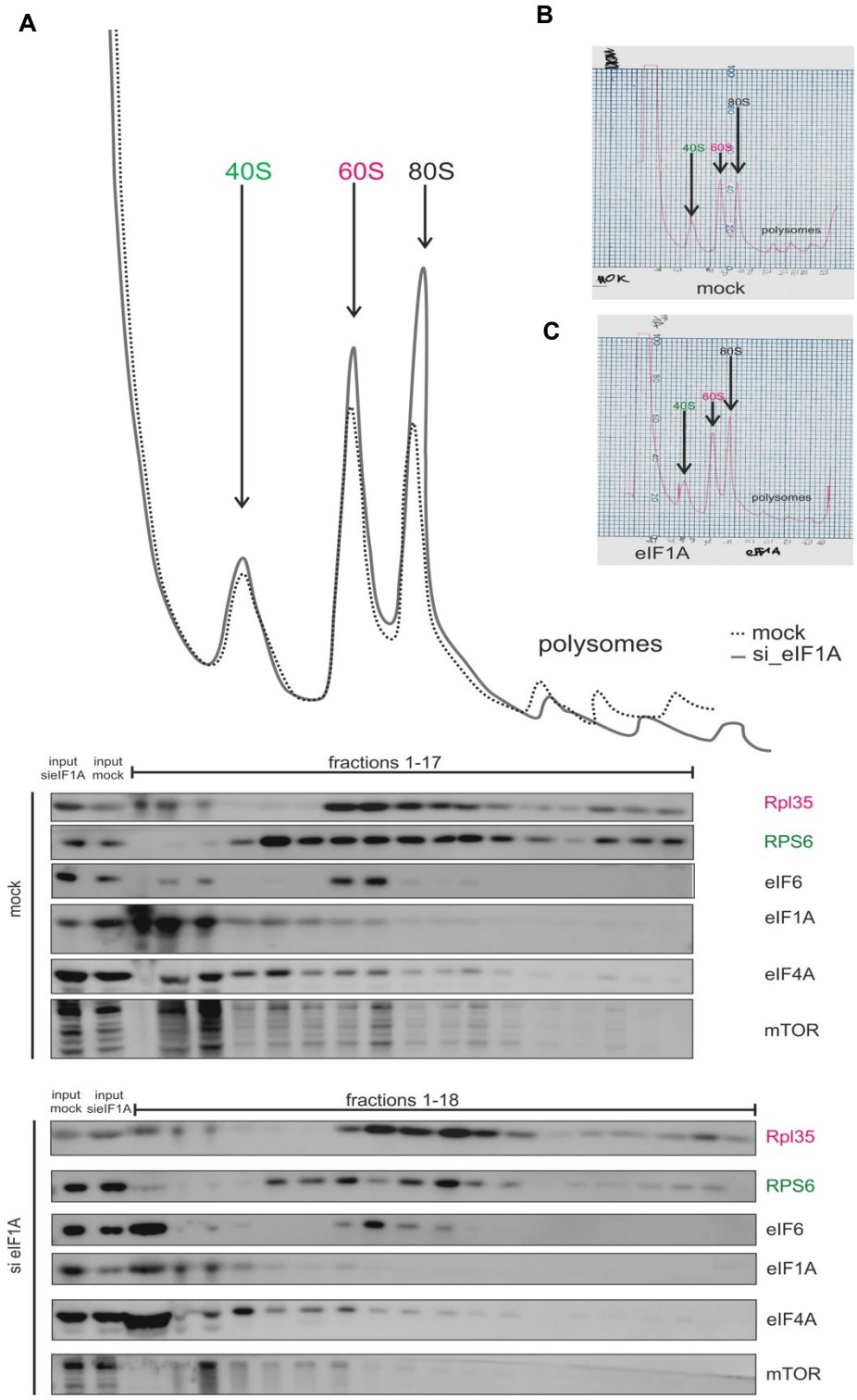

Figure 33 Ribosomal profiles 3 days after eIF1A knockdown. (**A**) Sucrose density gradient profiles of sieIF1A_1+2 and mock transfected A549 cells are shown. Rpl35 antibody was used as marker for the 60S subunit and Rps3 for the 40S subunit. Representative Western Blots of eIF1A, mTOR, eIF4A and eIF6 (**B,C**) Original elution profiles at 254nm.

5.5 Eukaryotic Translation Initiation Factor 6 impacts NSCLC

To investigate the correlation between the expression of eukaryotic translation initiation factors and patient overall survival rate, the Affymetrix and TCGA data set on NSCLC was analyzed and tested for statistical significance with the log rank test (performed by Martin Pichler).

The Affymetrix data set comprises 1.926 NSCLC patient data collected over 15 years. Higher expression of eIF6 in NSCLC shows a significant association with poor OS compared to low expression of *eIF6* (p=1.5e-13) (*Figure 34A*). Therefore, we further investigated *eIF6* expression and its correlation with survival on the two largest subtypes of NSCLC, ADC and SQC. *eIF6* expression significantly correlated with patient OS in ADC patients (p=3.8e-13) (*Figure 34B*) with a hazard ratio of 2.4 while OS did not correlate with *eIF6* expression in SQC patients (*Figure 34C*). TCGA data sets revealed similar results. eIF6 expression is significantly associated with worse patient overall survival in ADC patients, but not in SQC patients (*Figure 35*).

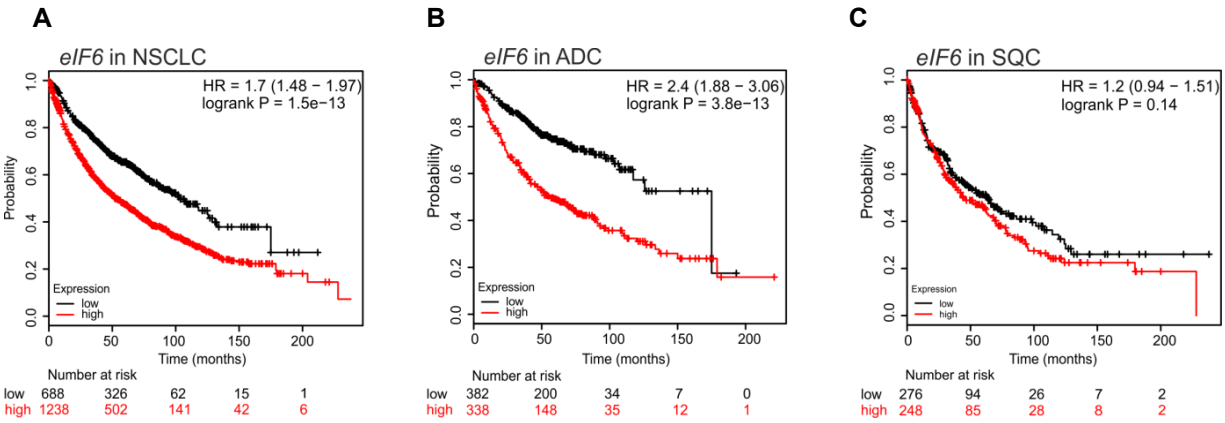

Figure 34 Patient overall survival analysis of Affymetrix data set for eIF6 expression in NSCLC. (**A**) Shorter survival for 1,926 NSCLC patients with high eIF6 expression (p=1.5e-13), with a median hazard ratio of 1.7 (1.48-1.97) compared to low eIF6 expression. (**B**) Significantly shorter survival is observed for ADC (n=720) patients with high eIF6 expression (p=3.8e-13) with median hazard ratio of 2.4. (1.88-3.06) (**C**) Patients with squamous cell carcinoma (n=524) show no correlation between eIF6 expression level (p=0.14) and survival, the median hazard ratio is 1.2 (0.98-1.51). Data presented are published in Gantenbein et al 2018 [81]. Reproduced from [81] with permission of publisher Elsevier.

To confirm to these results on protein level, over 400 NSCLC FFPE patient samples were investigated for eIF6 protein levels with IHC. The two major histological subtypes, adenocarcinoma and squamous cell carcinoma, were stained and scored

from 0-3. Representative images for the scoring scale are displayed in *Figure 36*. Image for no staining (score=0) shows brown positive staining only for lung macrophages, which were not considered for evaluating eIF6 staining in the ADC and SQC cohort. 306 ADC patients on tissue microarray sections (TMA) were stained with an anti-eIF6 antibody and compared to 152 NNT samples, which served as control (*Figure 37A*). Clinical data of patients are listed in *Table 5*. Cytoplasmic staining of eIF6 was mainly observed, in the cytoplasm. Of note, the tissue score was significantly higher ($p<0.0001$) in ADC tissue compared to NNT controls (*Figure 37B*). Then the differences between grades (G1-G3) in ADC were statistically analyzed for the tissue score. This analysis revealed significant differences in eIF6 expression within the different grades ($p=0.04$). Staining increases significantly with higher grades for G1 vs. G2 ($p=0.014$) and G1 vs G3 ($p=0.047$) (*Figure 37C*). After statistical analysis no significant change was observed for G2 vs. G3 (*Figure 37C*).

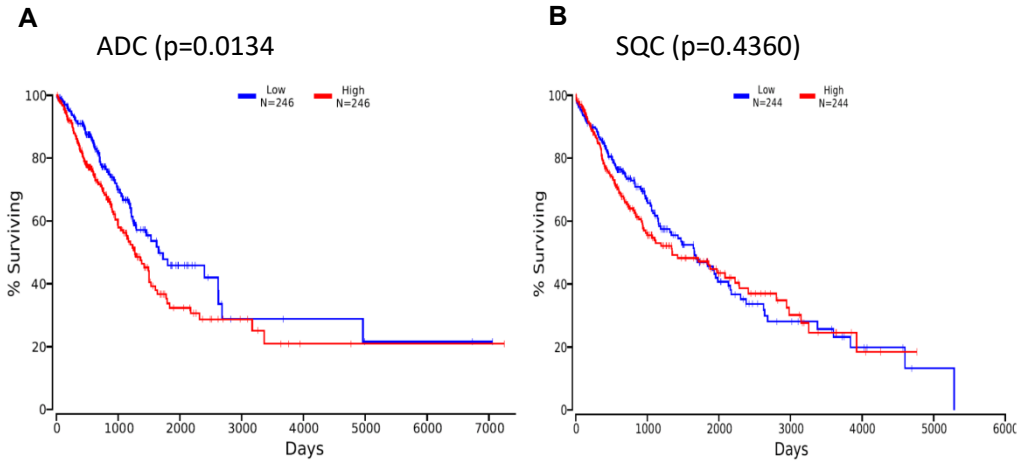

Figure 35 *eIF6* expression levels correlates with patient overall survival in TCGA data set. (**A,B**) Kaplan-Meier plots comparing median patient survival in the TCGA data set for NSLCL, ADC and SQC in eIF6 high and low conditions. High expression is shown in red and low expression in blue. Data presented are published in Gantenbein et al 2018 [81]. Reproduced from [81] with permission of publisher Elsevier.

62 squamous cell carcinoma samples in TMA were stained for eIF6. SQC-stained tissue showed mainly cytoplasmic staining (*Figure 38A*). Statistical analysis revealed a significantly higher score for SQC samples compared to NNT controls ($p<0.0001$) (*Figure 38B*). As described above, the different grades were analyzed for statistically significant differences in eIF6 staining between grades, but no significance was observed (*Figure 38C*).

Fresh frozen non-neoplastic lung- and tumor-tissue from 28 NSCLC patients (14 ADC, 14 SQC) was analyzed with Western Blot analysis for eIF6 expression (Clinic pathological data is listed in *Table 6*). All samples were analyzed with the NGS cancer panel. Mutation status is listed in *Table 6*. eIF6 is significantly upregulated in ADC and SQC patients (*Figure 39A-C*). Additionally, in these samples, mRNA levels of eIF6 were analyzed with qRT-PCR. For both subtypes, eIF6 mRNA is significantly higher in tumor tissue compared to NNT (*Figure 39D*).

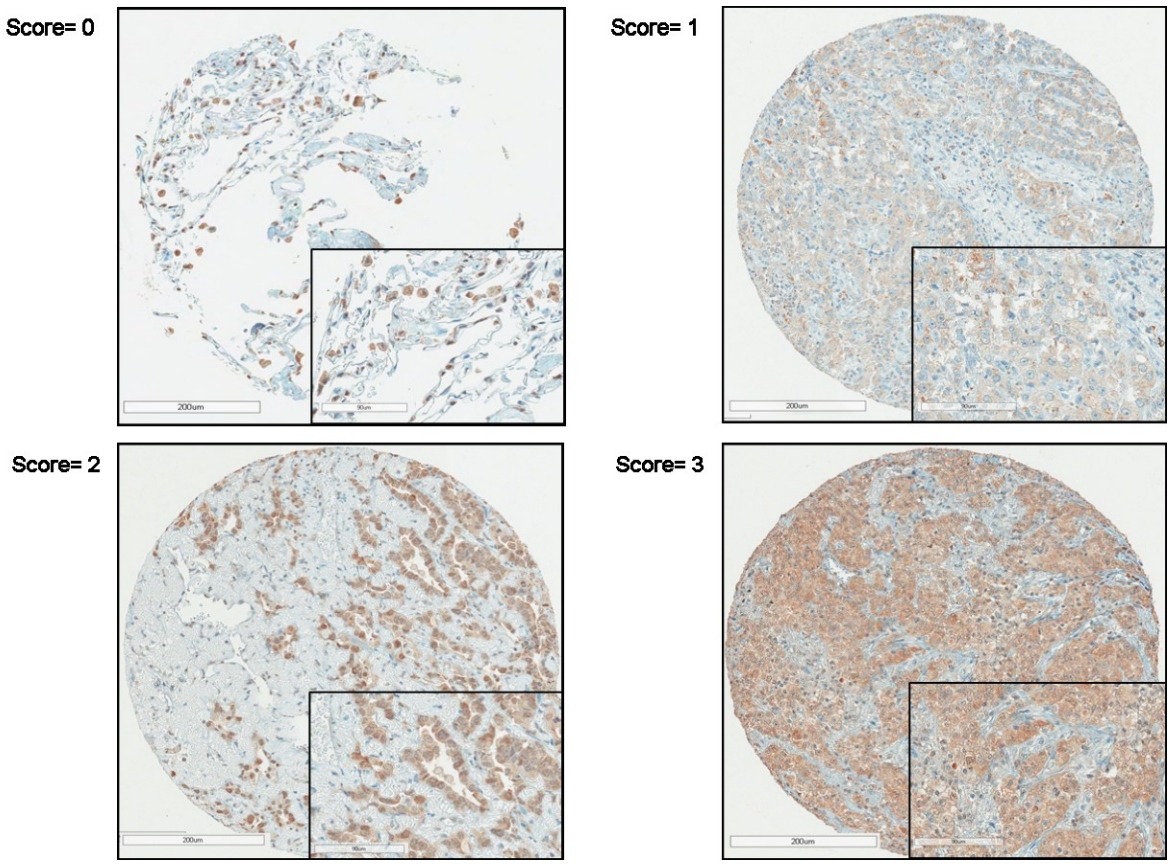

Figure 36 Scoring scale for eIF6 IHC staining in NSCLC. Staining intensity,0=no staining, 1=weak staining, 2=moderate staining, 3=strong staining is displayed for eIF6 Bethyl antibody (1:500).

Table 5 Clinic pathological characteristics of patients assed by TMA tissue specimens [81]**.** Reproduced from [81] with permission of publisher Elsevier.

Adenocarcinoma		**n=306**	**%**
Gender	Female	120	39.2
	Male	186	60.8
Grade	G1	67	21.9
	G2	125	40.8
	G3	114	37.3
Intensity	0	35	11.4
	1	186	60.8
	2	81	26.5
	3	4	1.3
Density	0%	35	11.4
	0-10%	30	9.8
	11-49%	60	19.6
	50-79%	95	31.0
	80-100%	86	28.1
Non-neoplastic tissue		**n=152**	**%**
Gender	Female	58	43.9
	Male	74	56.1
Squamous Cell Carcinoma		**n=62**	**%**
Gender	Female	10	16.1
	Male	52	83.9
Grade	G1	3	4.8
	G2	37	59.7
	G3	22	35.5
Intensity	0	7	11.3
	1	31	50.0
	2	21	33.9
	3	3	4.8
Density	0%	7	11.3
	0-10%	4	6.5
	11-49%	10	16.1
	50-79%	20	32.3
	80-100%	21	33.9
Smoking status	Smoker	13	21.0
	Non-Smoker	2	3.2
	unknown status	49	79.0
Non-neoplastic tissue		**n=31**	**%**
Gender	Female	6	19.4
	Male	25	80.6

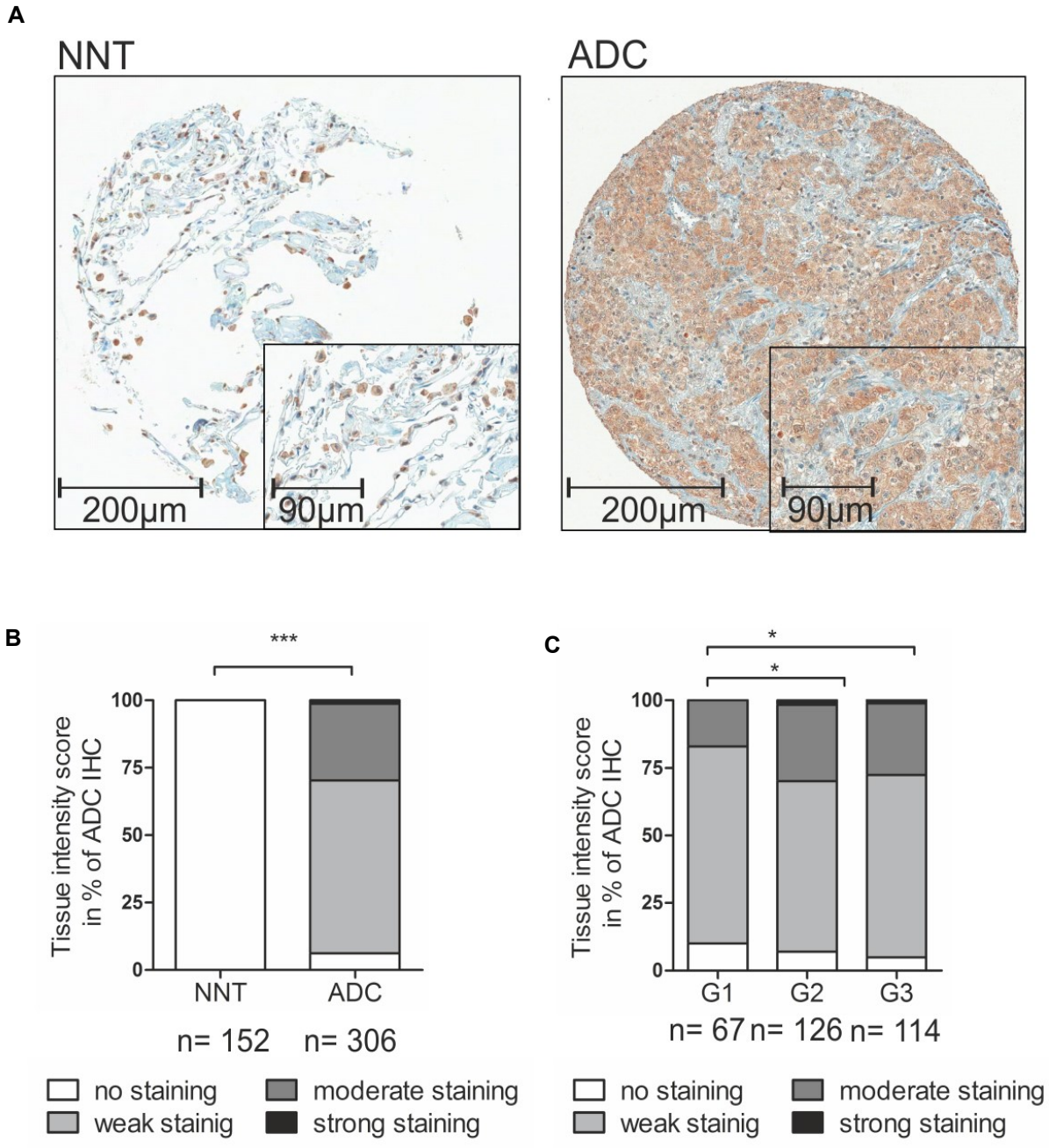

Figure 37 eIF6 is over-represented in ADC tissue. (**A**) Representative micrographs of eIF6- stained non-neoplastic tissue (NNT) and ADC tissue. eIF6 is evident in both the nucleus, and cytoplasm of tumor cells. (**B**) Analysis of tissue intensity score by Mann-Whitney U test revealed significantly stronger staining intensity of eIF6 in ADC patients compared to NNT ($p<0.0001$). (**C**) Kruskal Walis test ensured significant differences between NNT and ADC or SQC. For analyzing G1 vs. G2 ($p=0.014$) and G1 vs. G3 ($p=0.047$) in ADC, the Mann- Whitney U test was performed, comparing unstained vs. stained samples. Data presented are published in Gantenbein et al 2018 [81]. Reproduced from [81] with permission of publisher Elsevier.

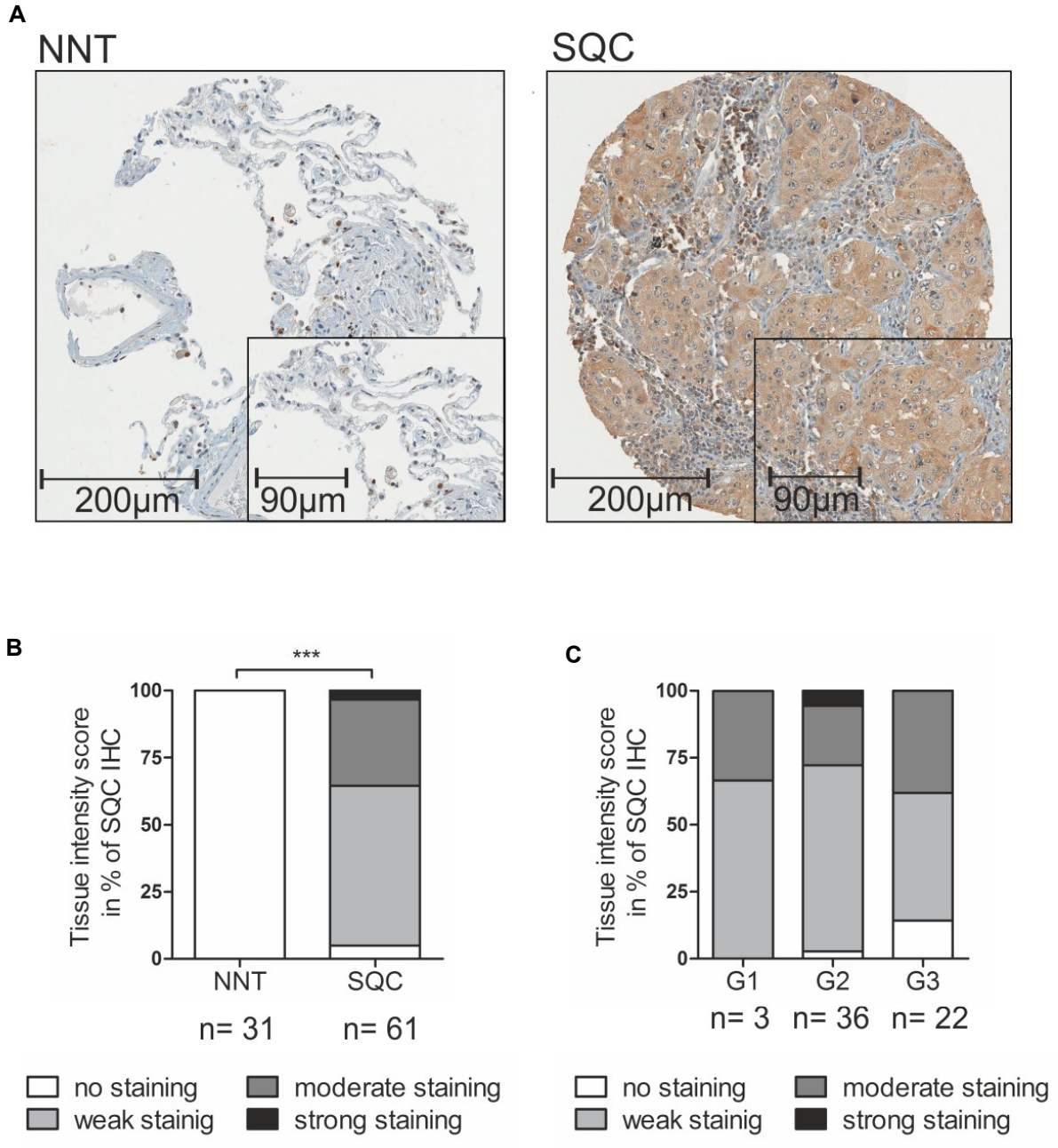

Figure 38 eIF6 is overexpressed in SQC tissue compared to NNT. (A) Representative IHC pictures of eIF6- stained non-neoplastic tissue (NNT) and SQC tissue. eIF6 is mainly stained in the cytoplasm but also evident in the nucleus. (B) 61 SQC patients compared to 31 NNT samples, have significant overexpression of eIF6 in the cytoplasm ($P<0.0001$). Mann- Whitney U test was performed comparing unstained vs. stained samples. (C) Tissue intensity score analysis of different SQC tumor grades is not significant. Data presented are published in Gantenbein et al 2018 [81]. Reproduced from [81] with permission of publisher Elsevier.

Table 6 Clinic pathological characteristics of cryo samples of 28 patients [81]**.**
Reproduced from [81] with permission of publisher Elsevier.

Adenocarcinoma		**n=14**	**%**
Gender	Female	11	78.6
	Male	3	21.4
Median age		69	
Grade	G1	1	7.1
	G2	5	35.7
	G3	10	71.4
Stage*	I A2	3	21.4
	I B	4	28.6
	II B	5	35.7
	III A	2	14.3
Smoking status	Smoker	6	42.9
	Non-Smoker	9	64.3
Mutation status	*EGFR*	5	35.7
	KRAS	5	35.7
	BRAF	0	0.0
	TP53	8	57.1
Squamous Cell Carcinoma		**n=14**	**%**
Gender	Female	2	14.3
	Male	12	85.7
Median age		71	
Grade	G1	2	14.3
	G2	4	28.6
	G3	8	57.1
Stage*	I A	1	7.1
	I B	4	28.6
	II A	2	14.3
	II B	6	42.9
	III A	1	7.1
Smoking status	Smoker	13	92.9
	Non-Smoker	1	7.1
Mutation status	*EGFR*	0	0.0
	KRAS	0	0.0
	BRAF	0	0.0
	TP53	11	78.6

Italic font is used for gene symbols
* IASLC (International Association for the Study of Lung Cancer) 8th Edition of TNM Classification for Lung Cancer

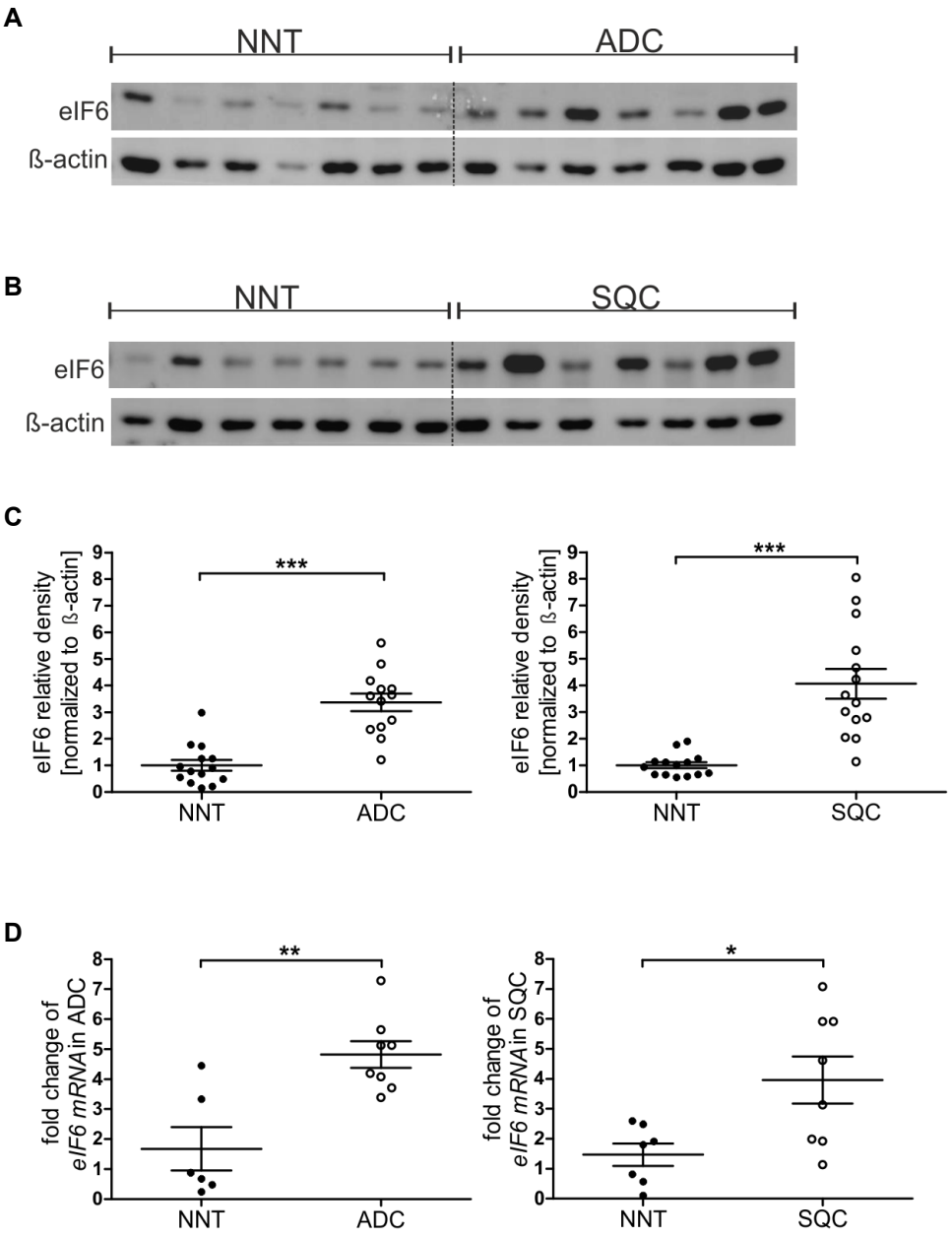

Figure 39 eIF6 is overexpressed in NSCLC fresh frozen tissue. Representative Western Blot picture of eIF6 protein expression in ADC (**A**) and SQC (**B**) compared to NNT. (**C**) Densitometric analysis of eIF6 Western Blot bands normalized to β-actin. (**C,** left panel) 14 ADC patient samples show significant overexpression of eIF6 compared to NNT. (**C,** right panel) 14 SQC patient samples show significant overexpression of eIF6 compared to NNT. (**D,** left paned) qRT-PCR of 9 ADC patient samples show significant overexpression of eIF6 mRNA compared to 7 NNT samples. The fold change was normalized to ACTB and IPO8. (**D,** right paned) qRT-PCR of 9 SQC patient samples show significant overexpression of eIF6 mRNA compared to 7 NNT samples. The fold change values were normalized to SDHA and IPO8.Results shown represent mean ± SEM. Mann-Whitney U test was used for ADC data and Student t-test was performed after ensuring Gaussian distribution on SQC data. (*p<0.05; **p<0.001; ***p<0.0001). Data presented are published in Gantenbein et al 2018 [81]. Reproduced from [81] with permission of publisher Elsevier.

5.5.1 Knockdown of eIF6

According to the overexpression of eIF6 in human NSCLC tissue, the consequences of reduced eIF6 levels can be of great interest in the fight against NSCLC. Therefore, two cell lines A549 and H520 were transfected with siRNA targeting *eIF6*. Two time points, day 3 and day 5 post transfection, were investigated. Protein lysates of siRNA-transfected A549 cells were analyzed for eIF6 levels with immunoblot and compared with control, mock and scrambled setting **(***Figure 40A*). Quantification of immunoblots revealed a significant knockdown of eIF6 in si_eIF6 transfected cells up to 80-90% compared to untreated cells, mock or scrambled transfected cells at both time points (*Figure 40B*). mRNA levels in these samples were investigated after knockdown. qRT-PCR revealed a significant eIF6 knockdown for all construct combinations at day 3. On day 5 post-transfection, eIF6 mRNA was still 40-50% were downregulated (*Figure 40C*).

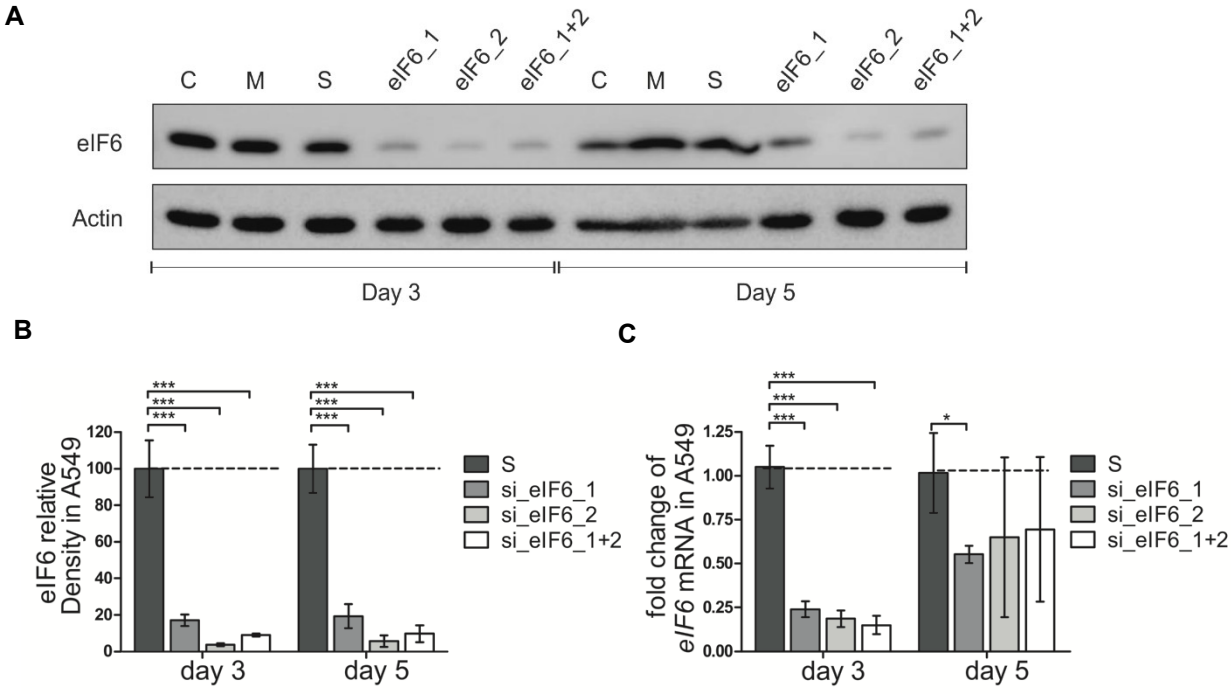

Figure 40 *eIF6* knockdown in A549 ADC cell line. (**A**) Representative Western Blot of eIF6 knockdown in A549 cells 3 and 5 days after transfection in A549 cell line. (**B**) Densitometric analyses of eIF6 bands normalized to ß-actin, which served as loading control. In A549 cells eIF6 protein levels are significantly decreased, compared to scrambled siRNA transfected conditions. (**C**) mRNA levels of *eIF6* of transfected H520 measured by qRT-PCR and normalized to *SDHA*. Results shown represent mean ± SEM of three independent experiments (one-way ANOVA*).* (*p<0.05; **p<0.001; ***p<0.0001) C=control, M=mock, S=scrambled). Data presented are published in Gantenbein et al 2018 [81]. Reproduced from [81] with permission of publisher Elsevier.

The efficacy of siRNA transfection in A549 cells was investigated with Alexa-488 labeled non-targeting siRNA with subsequent FACS analysis. FACS analysis of Alexa-488 positive cells was performed 0h, 6h and 24h post transfection. Over 98% of transfected cells were Alexa-488-positive and confirmed successful transfection *(Figure 41*).

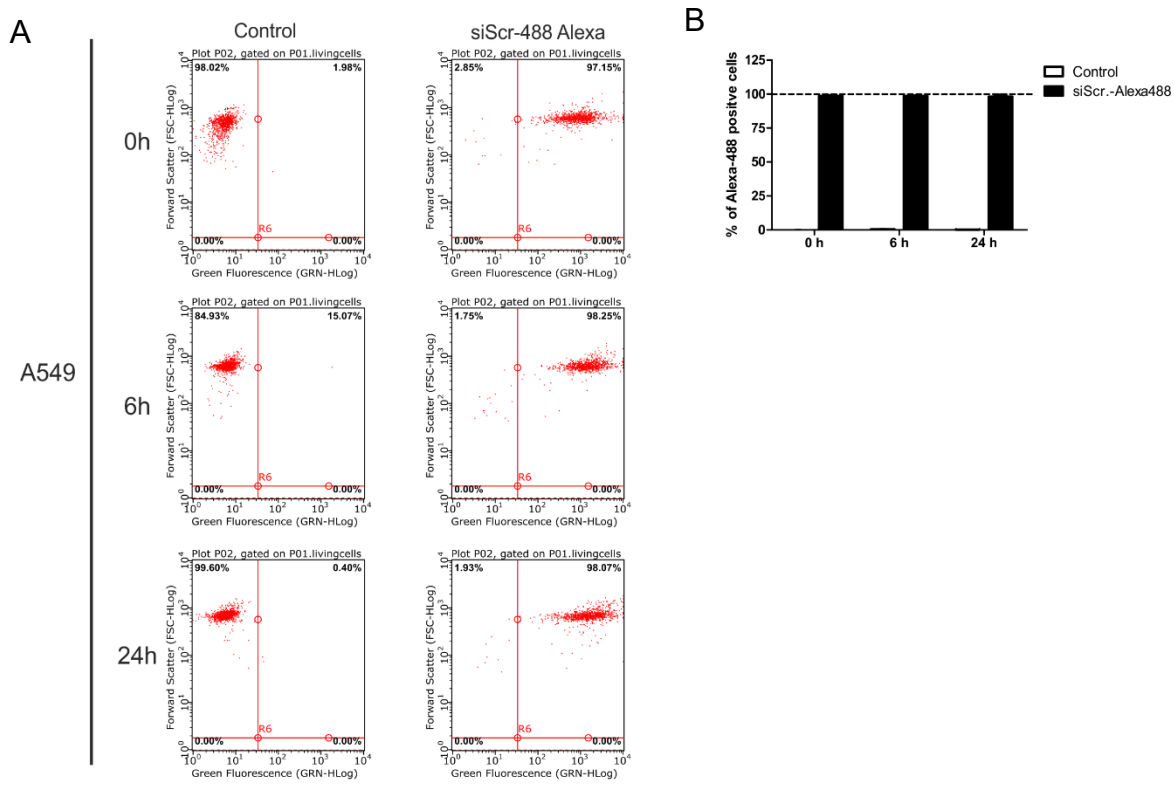

Figure 41 Transfection efficacy in A549 cells is >98%. (**A**) FACS scatter plots of A549 cells transfected with Alexa-488 labeled scrambled siRNA at three different time points (0h, 6h and 24h). (**B**) Quantification of Alexa-488 positive A549 cells represented with mean ± SEM. Data presented are published in Gantenbein et al 2018 [81]. Reproduced from [81] with permission of publisher Elsevier.

Furthermore, *eIF6* knockdown in H520 SQC cell line was performed and analyzed 3 and 5 days after transfection. Immunoblot and its quantification of eIF6 levels showed successful knockdown of eIF6 in H520 cells at both time points (*Figure 42A,B*). qRT- PCR of eIF6 mRNA confirmed downregulation at both time points indicated. Significance could only be reached at day 3 when compared to scrambled control (*Figure 42C*). Knockdown of eIF6 in H520 cell line was not as effective as in A549. Therefore, Alexa-488-labeled scrambled siRNA was transfected in H520 cells to see if the siRNA is successfully transfected. The transfected cell line was then measured for Alexa-488-positive cells with FACS. The analysis revealed over 90%

Alexa-488-positive cells. Therefore, the transfection method should be appropriate (*Figure 43*).

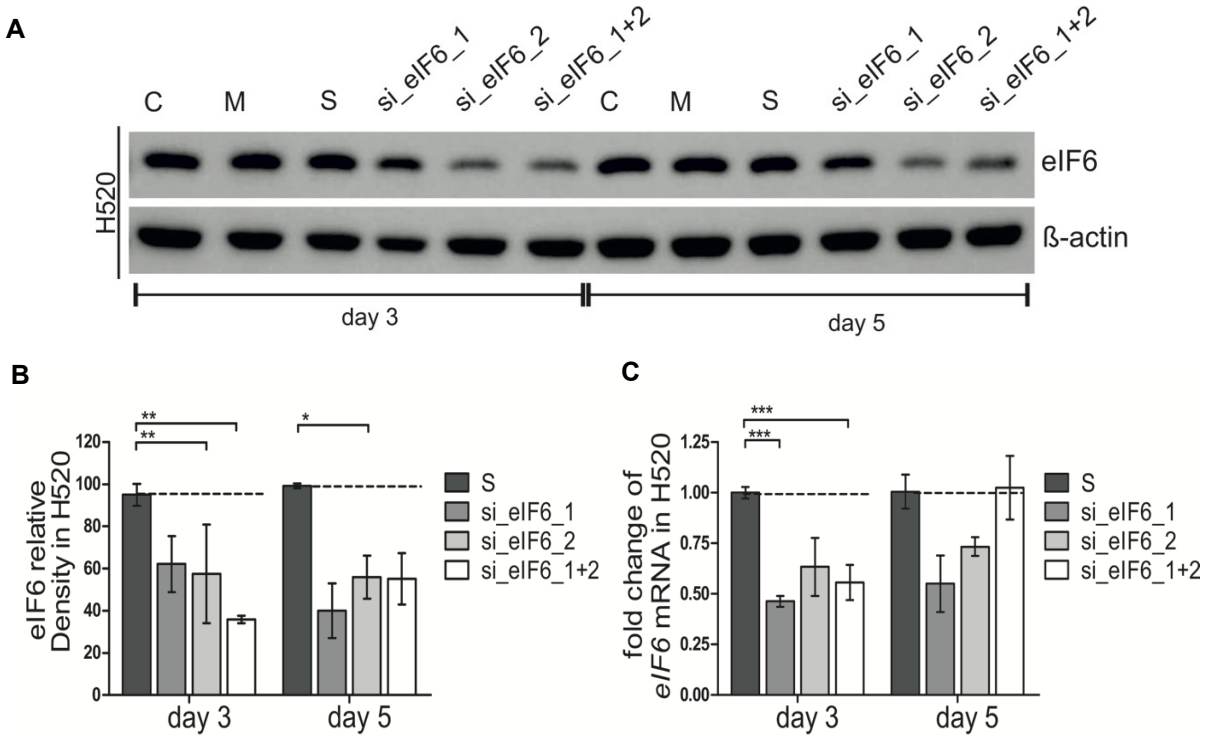

Figure 42 Analysis of knockdown *eIF6* efficacy in H520 SQC cell line. (**A**) Representative Western Blot of eIF6 knockdown in A549 cells 3 and 5 days after transfection in A549 cell line. (**B**) Densitometric analyses of eIF6 bands normalized to ß-actin. In A549 cells eIF6 protein levels are significantly decreased, compared to scrambled siRNA transfected conditions. (**C**) mRNA levels of *eIF6* of transfected H520 measured by qRT-PCR and normalized to *SDHA*. Results shown represent mean ± SEM of three independent experiments (one-way ANOVA). (*p<0.05; **p<0.001; ***p<0.0001). C=control, M=mock, S=scrambled. Data presented are published in Gantenbein et al 2018 [81]. Reproduced from [81] with permission of publisher Elsevier.

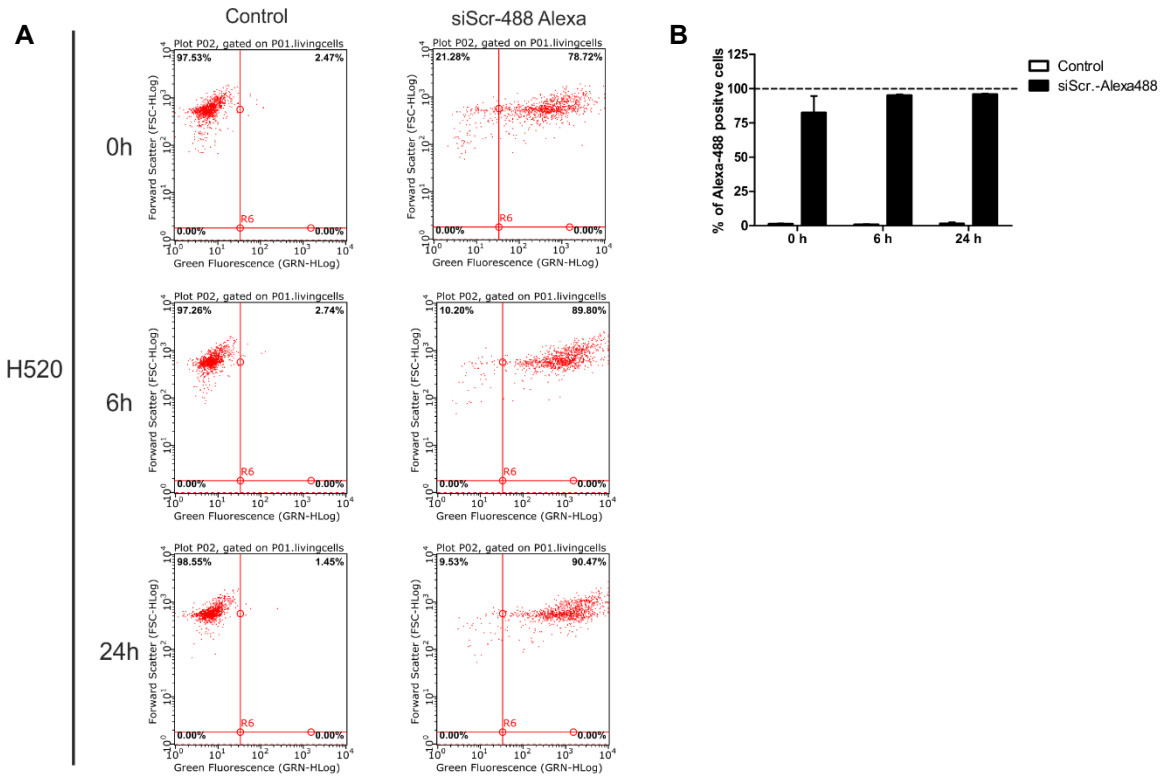

Figure 43 Transfection efficacy in H520 SQC cells is > 90%. (**A**) FACS scatter plots of A549 cells transfected with Alexa-488 labeled scrambled siRNA at three different time points (0h, 6h and 24h). (**B**) Quantification of Alexa-488 positive H520 cells represented with mean ± SEM. Data presented are published in Gantenbein et al 2018 [81]. Reproduced from [81] with permission of publisher Elsevier.

5.5.2 Knockdown of eIF6 reduces proliferation of A549 and H520 cells

After confirming successful knockdown in both cell lines, the phenotypic outcome of eIF6 silencing was investigated. Most adherent cancer cell lines have the capability to form colonies, with the colony formation assay not only the colony formation but also the growth can be easily visualized. For A549 cells less colonies were observed for transfected cells compared to control conditions (*Figure 44A*). Also, for H520 cell line, the colony formation after transfection was investigated. Control, mock and scrambled conditions do have more colonies 4 weeks after cultivation compared to sieIF6-transfected cells (*Figure 44B*).

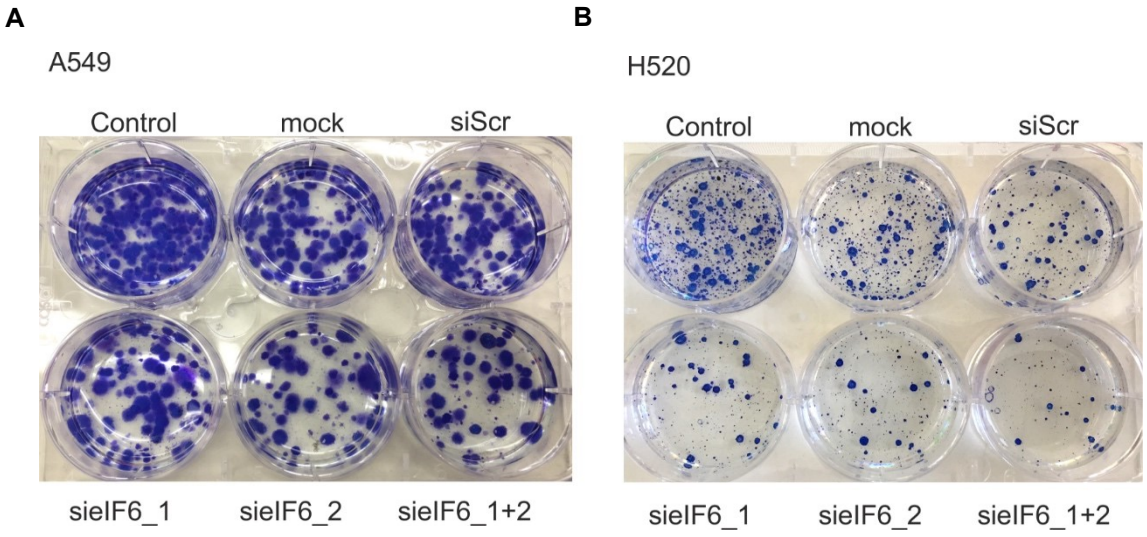

Figure 44 Colony formation Assay is affected by eIF6 knockdown in A549 and H520 cell line. 3 days post transfection 400 cells for each condition (control, mock, siScr., sieIF6_1, sieIF6_2 and sieIF6_1+2) were seeded into 6 well plates and cultured for 4 weeks, followed by Giemsa staining. (**A**) Representative picture of Giemsa stained A549 cells. sieIF6, sieIF6_2 and the combination of both constructs show less colonies compared to all three control conditions. (**B**) Representative picture of Giemsa stained H520 cells. sieIF6, sieIF6_2 and the combination of both constructs show less colonies compared to all three control conditions. Data presented are published in Gantenbein et al 2018 [81]. Reproduced from [81] with permission of publisher Elsevier.

Furthermore, cells were counted with FACS for each condition before harvesting cells for further analysis. Cells were counted using Guava ViaCount Reagent, which stains living and dead cells. Three days post transfection, the cell number was significantly reduced for si_eIF6_1+2 condition. At day 5 post transfection, the cell number was reduced for si_eIF6_1, si_eIF6_2 and si_eIF6_1+2 conditions in A549 cell line (*Figure 45A*). Cells were also counted with FACS for the H520 cell line. Three days post transfection, a tendency toward reduction in cell number was

visible, but at day 5 after transfection, the cell number in the H520 cell line was reduced significantly (*Figure 45B*).

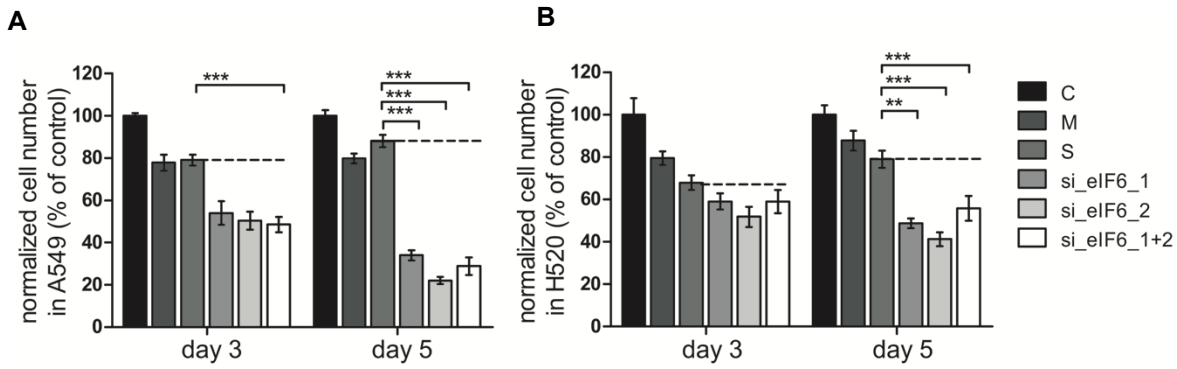

Figure 45 *eIF6* knockdown in A549 (A) and H520 (B) results in reduced proliferation. FACS cell counting for A549 cells at the two indicated time points. Data were normalized to siScr. Results shown represent mean ± SEM of three independent experiments (one-way ANOVA). (*p<0.05; **p<0.001; ***p<0.0001). C=control, M=mock, S=scrambled. Data presented are published in Gantenbein et al 2018 [81]. Reproduced from [81] with permission of publisher Elsevier.

5.5.3 *eIF6* knockdown induces apoptosis in A549 ADC cell line

To investigate whether reduced proliferation is coupled to apoptosis or necrosis, Annexin V/PI staining followed by FACS analysis was performed. A549 and H520 cells were stained and counted 3 and 5 days post transfection. Three days after transfection, A549 cells showed no apoptosis upon control conditions (C,M,Scr.), the Annexin V-positive population amounted to around 1-2%. A percentage below 1% was PI-positive (*Figure 46A*). For siRNA-transfected probes, a tendency toward an increase in apoptosis was visible. The Annexin V-positive population ranged between 2-3%, and over 1% was PI positive at day 3 (*Figure 46A*). 5 days after transfection with siRNA against *eIF6*, A549 cells showed a significant increase in apoptosis. The Annexin V-positive population was over 20% compared to control conditions, only 5% of which were Annexin V-positive. Around 3% of the siRNA transfected cells were PI-positive compared to below 1% positive control conditions (*Figure 46C,D*).

Reduced proliferation was not so prominent in H520 cell line after targeting eIF6. Nevertheless, in the colony formation assay and at day 5, cell count revealed reduced cell growth after transfection. Therefore, apoptosis was also investigated with FACS analysis. Again, Annexin V and PI staining was performed 3 and 5 days post transfection. At day 3 post transfection, over 12% of analyzed cells were

Annexin V-positive under control conditions. PI-positive cells were less than 1%. The probes in which eIF6 was knocked down had an Annexin V-positive population of 12-16%, and less than 1% were positive for PI at day 3 (*Figure 47A,B*). Day 5 revealed results similar to those of day 3 after transfection. After eIF6 knockdown, 12-15% of analyzed cells were Annexin V and 1-2% PI positive. Under control conditions, 8-12% of analyzed cells were Annexin V and 1% PI positive (*Figure 47C,D*).

Several pathways are known to induce apoptosis. To gain further insights into the question which pathway is induced, Caspase 3 (Casp 3) and PARP were analyzed via Western Blot (*Figure 48*). A549 cell lysates of all conditions and both time points were analyzed via immunoblot and revealed increased PARP and Casp 3 cleavage after siRNA knockdown compared to controlled conditions (*Figure 48A*). Densitometric analyses were statistically tested and revealed a significantly higher number of cleavages for Casp 3 in siRNA_eIF6-transfected cells than in control cells, on both days (*Figure 48B*). Also for H520 the cell line, the Casp 3 and PARP cleavage upon transfection was analyzed. No change in Casp 3 and PARP cleavage was observed at both indicated time points (*Figure 48C,D*).

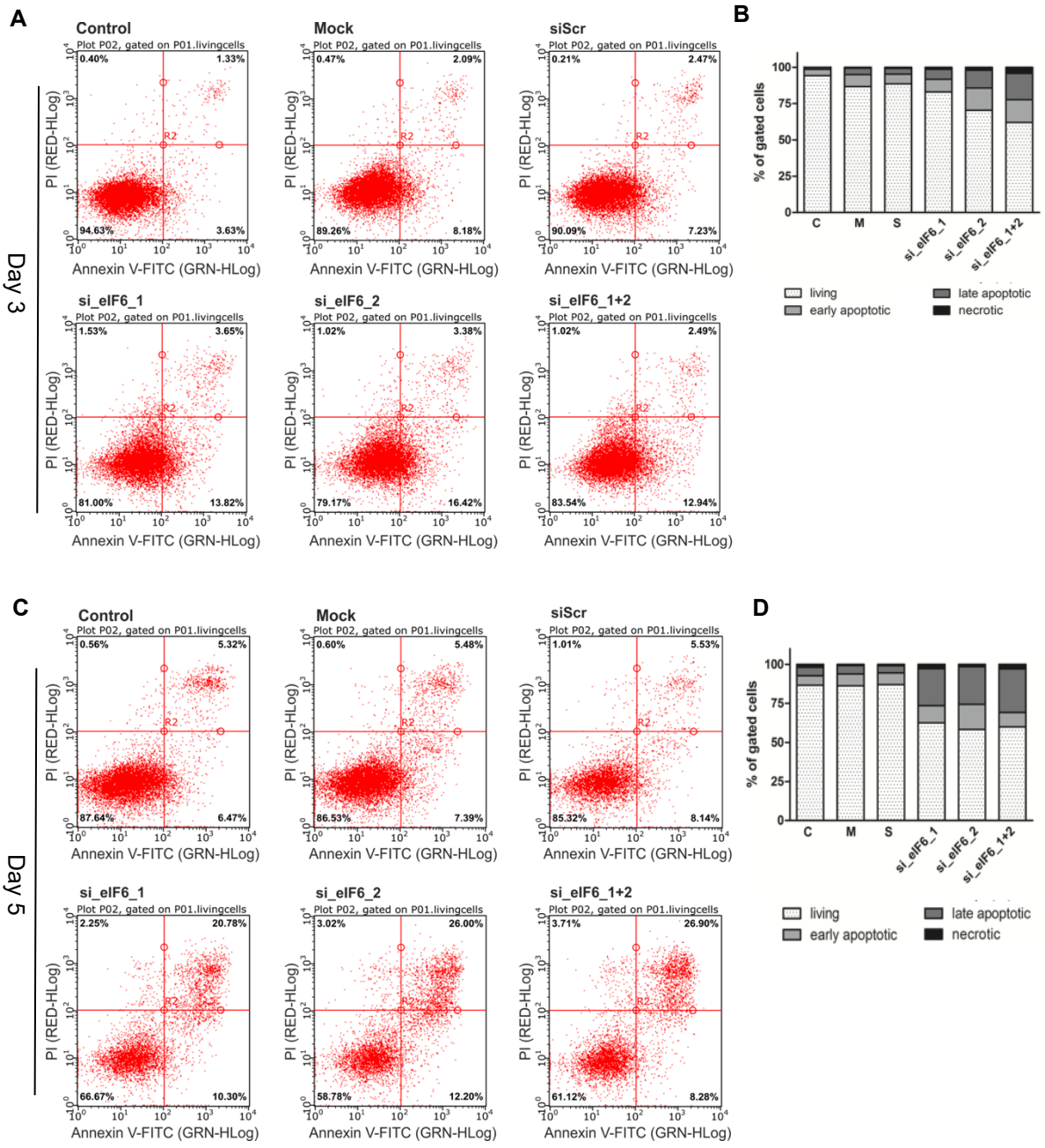

Figure 46 Increase of Annexin V and PI positive cells after eIF6 knockdown in A549 cell line. Representative FACS plots determining Annexin V / PI positive cells 3 (**A**) and 5 (**C**) days post transfections. (**B**) Stacked bar blots of three independent experiments at day 3, displaying ratio of living, early- and late-apoptotic cells as well as necrotic cells. (**D**) Stacked bar blots of three independent experiments at day 5, displaying ratio of living, early- and late-apoptotic cells as well as necrotic cells. Results shown represent mean of three independent experiments (one-way ANOVA, p-values are listed in *Table 9 in appendix 8.3*.C=control, M=mock, S=scrambled. Data presented are published in Gantenbein et al 2018 [81]. Reproduced from [81] with permission of publisher Elsevier.

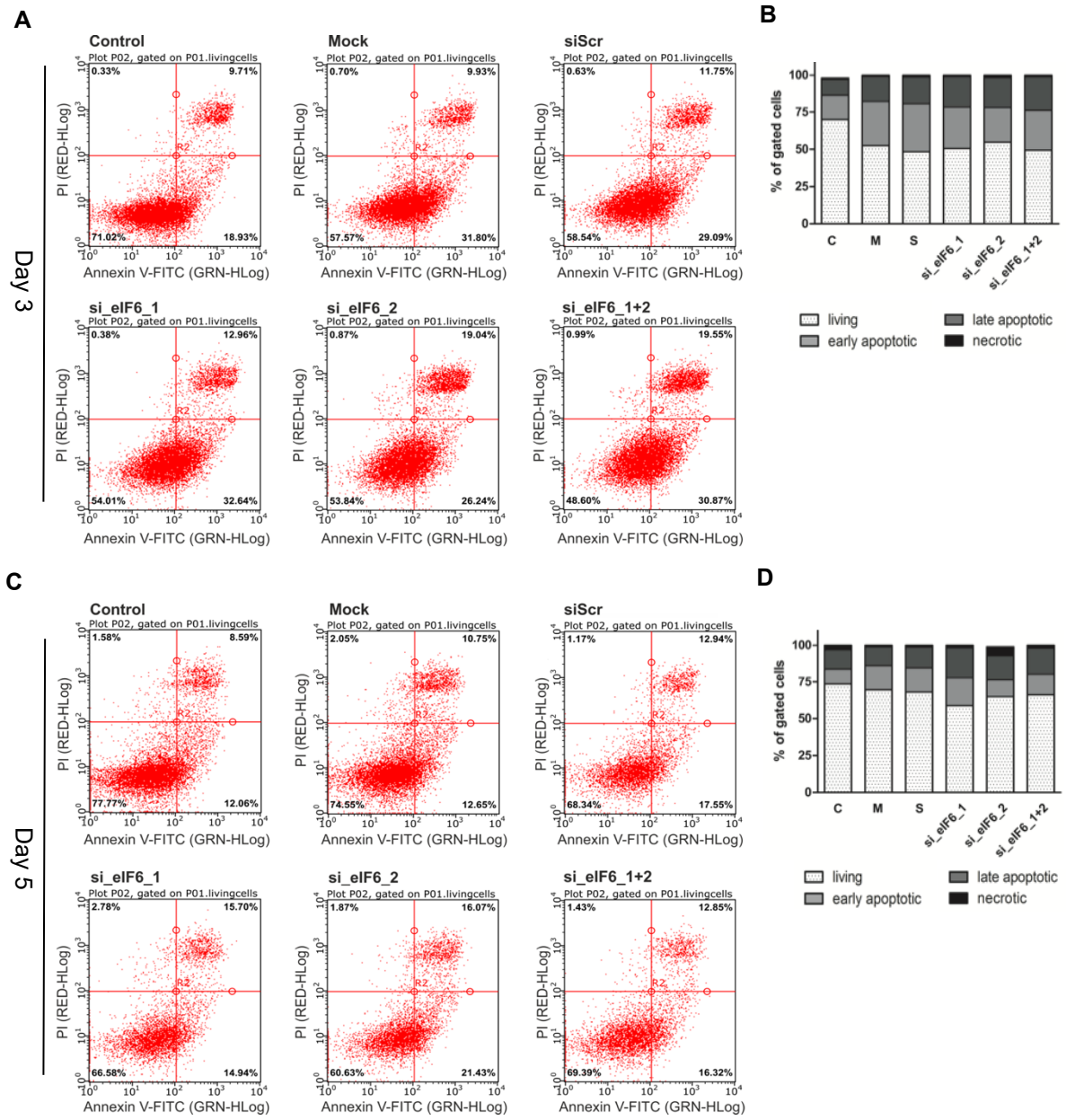

Figure 47 Annexin V/ PI stain of eIF6 knockdown H520 cell line. Representative FACS plots determining Annexin V / PI positive cells 3 (**A**) and 5 (**C**) days post transfections. (**B**) Stacked bar blots of three independent experiments at day 3, displaying ratio of living, early- and late-apoptotic cells as well as necrotic cells. (**D**) Stacked bar blots of three independent experiments at day 5, displaying ratio of living, early- and late-apoptotic cells as well as necrotic cells. Results shown represent mean of three independent experiments (one-way ANOVA, p-values are listed in *Table 9 in appendix 8.3*.C=control, M=mock, S=scrambled. Data presented are published in Gantenbein et al 2018 [81]. Reproduced from [81] with permission of publisher Elsevier.

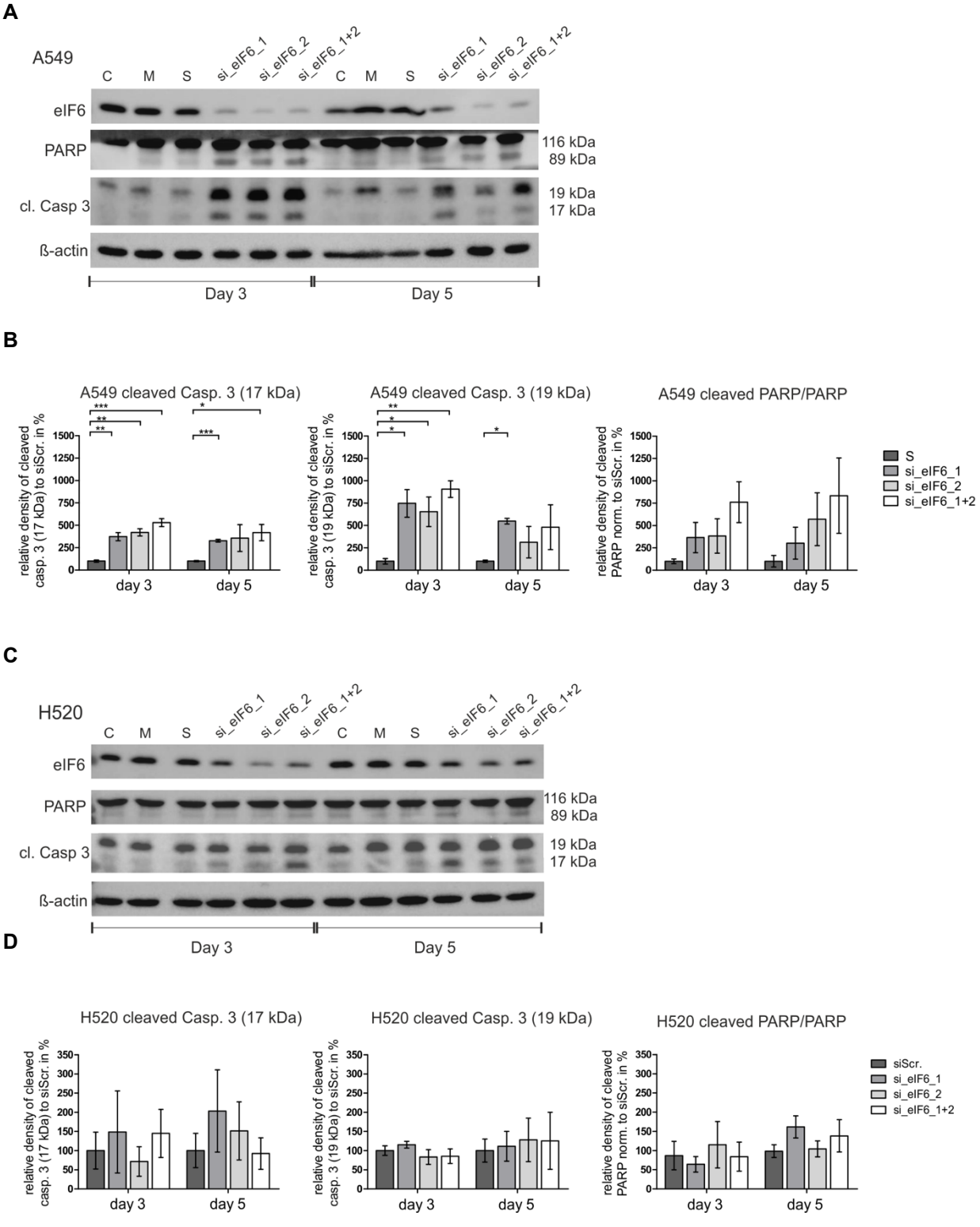

Figure 48 *In vitro* knockdown of *eIF6* in A549 cell line induces caspase 3 apoptotic pathway. Representative Western Blots for Caspase 3 and PARP 3 and 5 days post transfection in A549 (**A**) and H520 (**C**) cell line. Quantification of cleaved caspase 3 and cleaved PARP/PARP ratio in (**B**) A549 (Results shown represent mean ± SEM of three independent experiments, *p<0.05; **p<0.001; ***p<0.0001), and (**C**) H20 cell line. C=control, M=mock, S=scrambled Data presented are published in Gantenbein et al 2018 [81]. Reproduced from [81] with permission of publisher Elsevier.

5.5.4 Senescence is not induced by eIF6 knockdown in A549 and H520 cell line

Not only apoptosis can be responsible for reduced cell growth after targeting a factor, but also senescence can play a role. Therefore, induction of senescence-associated β-galactosidase activity was analyzed. In this assay cells undergoing senescence turn blue and expand in size, a process that can be visualized by light microscopy. For A549 cells, some blue cells are visible, but there was no increase in the number of senescent cells upon reduced eIF6 levels (*Figure 49A*). P21 is associated with senescence, it is upregulated when cells undergo senescence and was therefore analyzed with Western Blot. The analysis showed similar results. p21 is not increased on day 3, but showed an increase at day 5 (*Figure 49B*).

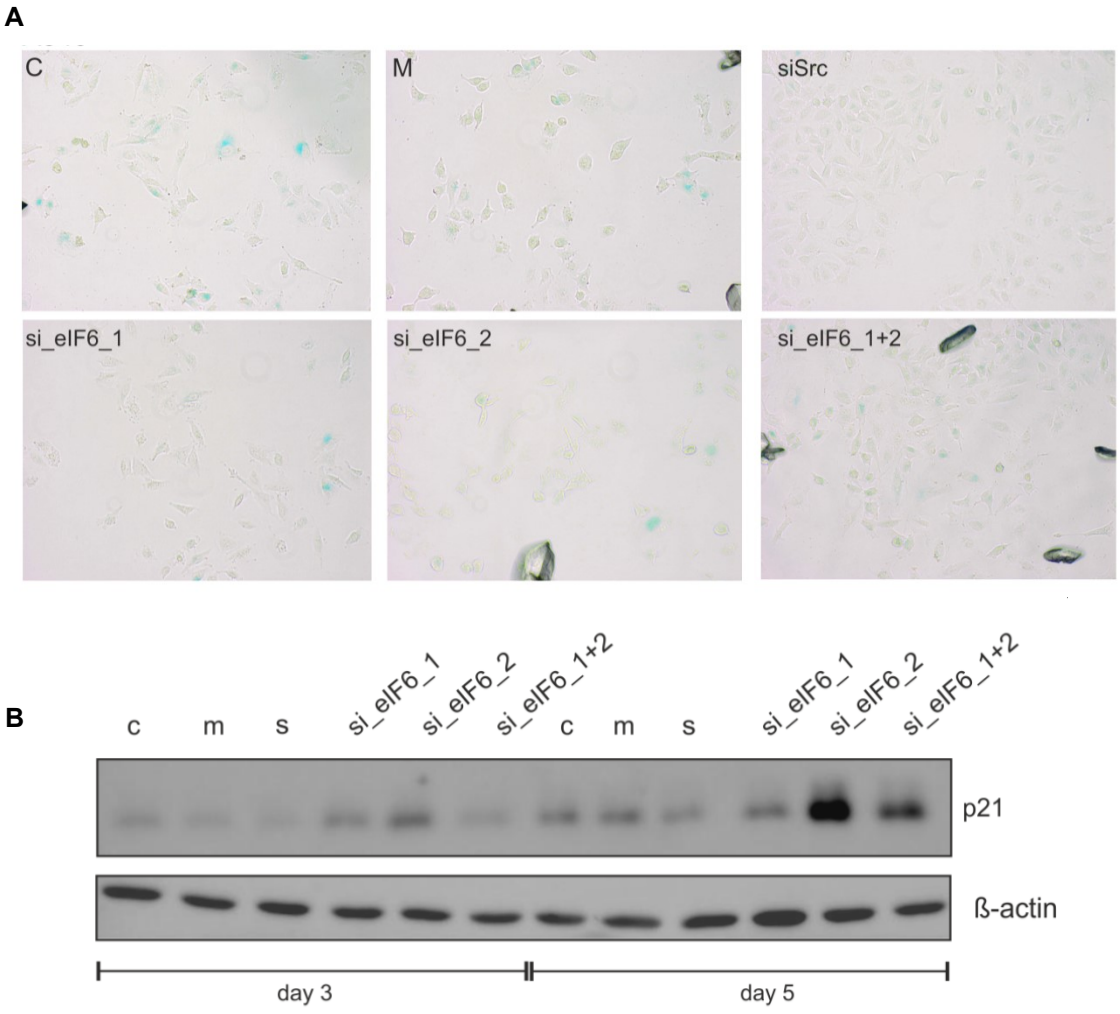

Figure 49 Senescence is not increased after eIF6 knockdown in A549. (**A**) Representative microscopy pictures of senescence-associated ß-galactosidase activity assay in A549 cell line. (**B**) p21 Western Blot picture of 3 and 5 post transfection, in A549 cell line. C=control, M=mock, S=scrambled. Data presented are published in Gantenbein et al 2018 [81]. Reproduced from [81] with permission of publisher Elsevier.

No changes in apoptosis were visible for transfected H520 cell line. Therefore, senescence might be responsible for the reduction in cell growth after eIF6 knockdown. The senescence-associated β-galactosidase activity assay was performed at day 3 post transfection and revealed no increase in senescent cells compared to controlled conditions (*Figure 50A*). The p21 protein levels were investigated to confirm the results of the β-galactosidase activity assay and revealed no change in p21 levels for all conditions and both time points (*Figure 50B*).

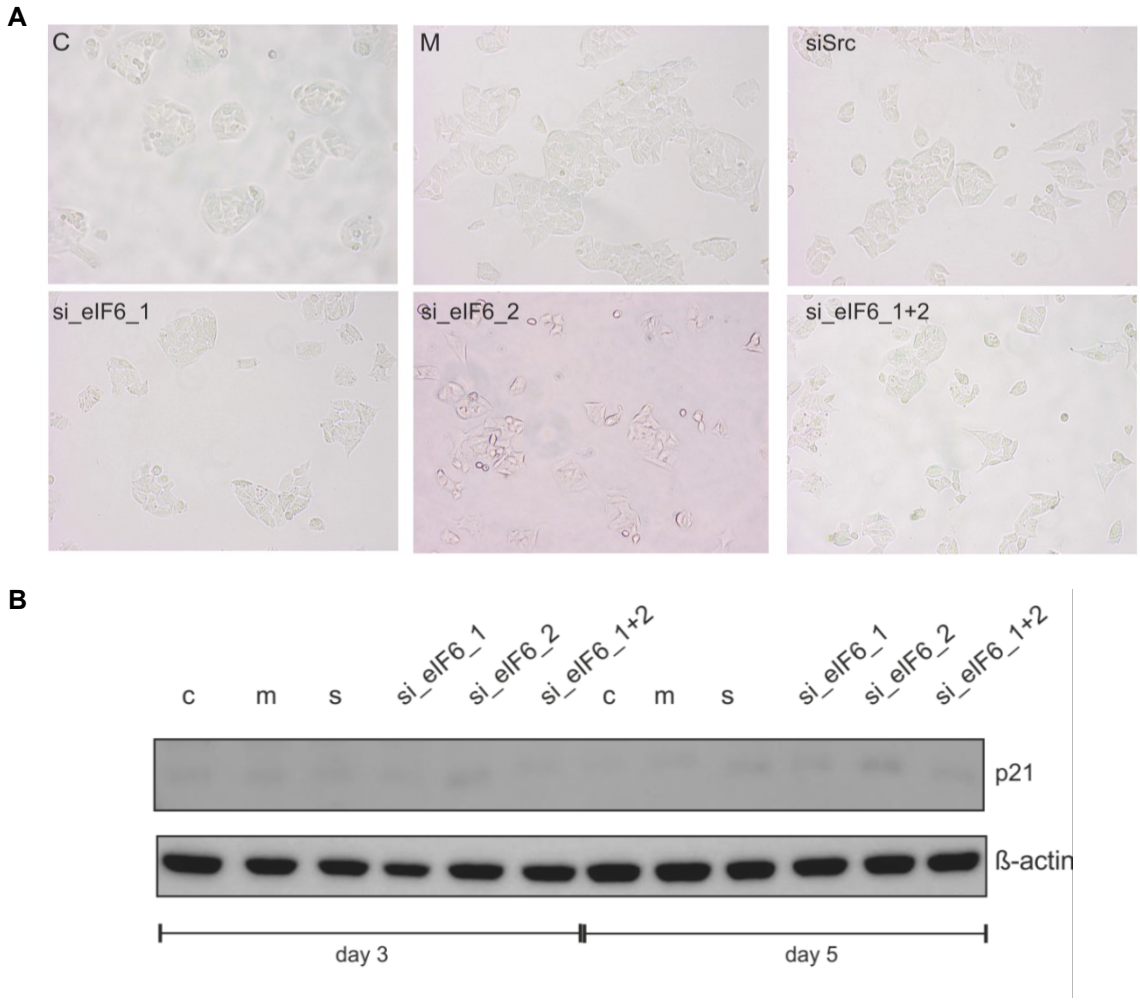

Figure 50 Senescence is not induced after *eIF6* knockdown in H520 cell line. (**A**) Representative microscopy pictures of senescence-associated ß-galactosidase activity assay in H520 cell line. (**B**) p21 Western Blot picture of 3 and 5 post transfection, in H520 cell line. C=control, M=mock, S=scrambled. Data presented are published in Gantenbein et al 2018 [81]. Reproduced from [81] with permission of publisher Elsevier.

5.5.5 Reduced eIF6 levels in A549 and H520 cell line have only little effect on translation

eIF6 is a translation initiation factor and key player in ensuring the correct assembly of 60S and 40S ribosomal subunits. The role and impact of eIF6 on translation in human cell lines are still not fully understood.

Click reaction was used for investigating the human NSCLC cell line for the influence of reduced eIF6 levels on translation. In this assay an alkyne labeled methionine is incorporated into the newly synthesized protein pool. Detection is then performed by the chemoreactive reaction of azide labeled TAMRA through the formation of an 1.2.3-triazole. Artificial amino acids, such as azidohomoalanine (AHA) or homopropargylglycine (HPG), which both compete with Methionine, are added to a sample and are incorporated into newly made proteins when a cell is anabolically active (*Figure 51*).

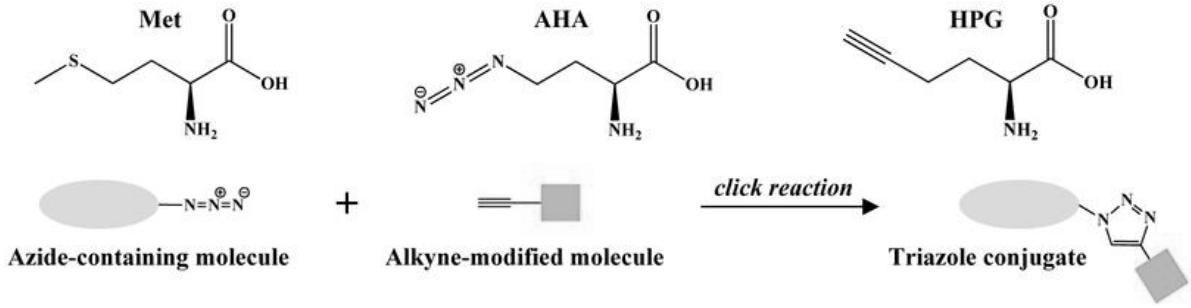

Figure 51 Scheme visualizing the click reaction. Structure of L-methionine (Met) and L-azidohomoalanine (AHA) and L-homopropargylglycine (HPG), which both compete with Methionine during translation [217]. Reproduced from [217] with permission of publisher Springer Nature.

Cycloheximide (+CycHx) is a strong translation inhibitor and served as a positive control. The “click” reaction was followed by a SDS-PAGE of whole protein lysates. The gel was then scanned with a Typhoon laser scanner. The positive control (+CycHx) showed less intense bands compared to control cells, indicating less translational activity. Scrambled condition revealed an intensity similar to that of the control condition. siRNA_eIF6_1+2 lane was slightly less intense than under controlled conditions (*Figure 52A*). The fluorescence signal was correlated with the Coomassie-stained lanes that served as loading control (*Figure 52B*) for quantification. Surprisingly A549 cells treated with CycHx reduced protein synthesis by only 10% in comparison to control conditions. Transfection with siRNA against *eIF6* led to a 5% reduction in translational activity of A549 cells (*Figure 52C*).

Furthermore, H520 cells were also analyzed for translational activity with reduced eIF6 levels. Control and scrambled samples showed the same fluorescence intensity of Alexa-488. By adding Cycloheximide to the H520 cell line before the “click” reaction, the fluorescent signal was reduced by over 20%, and targeting *eIF6* with siRNA reduced the fluorescence signal by approx. 10% (*Figure 52D*). Then the SDS gel was Coomassie (*Figure 52E*) stained, and the fluorescence signal was correlated with it for quantification (*Figure 52F*).

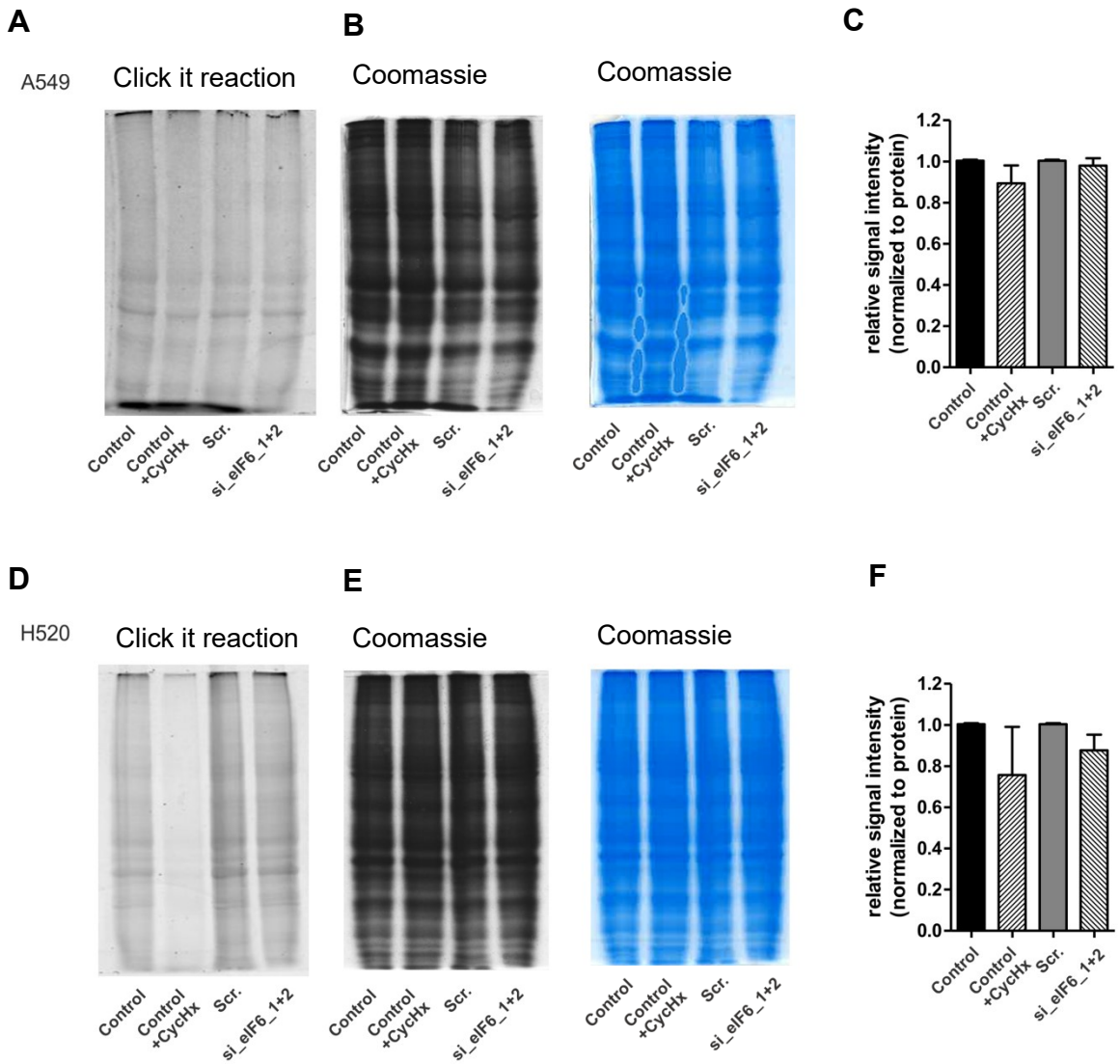

Figure 52 *In vitro* translation is not significantly influenced by low eIF6 levels in A549 (A-C) and H520 (D-E) cell lines. Measurement of protein synthesis of newly produced methionine via Click it chemistry in eIF6-transfected cell lines. Cycloheximide (CycHx)-treated cell lines served as control for inhibited translation. (**A,D**) Alexa-488 fluorescence-scanned gel with whole protein lysates. (**B,E**) Representative Coomassie-stained gel (grey- and color scale) served as loading control. (**C,F**) Quantification of 3 independent experiments for both cell lines. Scr= Scrambled siRNA.

5.5.6 eIF6 knockdown induces aberrant large ribosomal subunit assembly

eIF6 plays a role in in the pre-60S ribosomal subunit maturation and accompanies the 60S subunit to the 40S subunit for assembly of a translational competent ribosome. Therefore, the distribution of the 40S, 60S and 80S ribosomal particles was investigated by ribosomal profiling, and the collected fractions were analyzed via immunoblot. Cells were harvested with siRNA against *eIF6* at day 3 post transfection. Ribosomal fractions were separated using density gradient centrifugation and subsequent immunoblotting of the fractions.

Less free 60S fraction was found after eIF6 knockdown in A549 cells compared to mock control, suggesting a 60S processing defect (*Figure 53A*). No notable changes were observed for free 40S and 80S fractions. Western Blot analysis of the gradient fraction was performed for marker proteins RPS6 (small 40S subunit) and RPL35 (large 60S subunit) (*Figure 53B*). eIF6 was also analyzed to confirm knockdown and to identify the ribosome fraction in which eIF6 is located. As expected, eIF6 is in the early free 60S fraction, and knockdown for eIF6 in A549 was confirmed. mTOR and eIF4A were also studied to reveal potential effects of eIF6 silencing on these proteins (*Figure 53A*).

The consequences of eIF6 knockdown in H520 cell line on ribosomal fraction distribution was also studied as described above for A549 cells (*Figure 53*). Compared to Mock control, there were no changes for eIF6 knockdown in the distribution of ribosomal fractions . The collected fractions are in accordance with UV-profiles (*Figure 54A,B),* confirmed by immunoblotting using RPS6 as a marker for small ribosomal subunit 40S and RPL35 as a marker for large ribosomal subunit 60S. eIF6 is located within the early 60S fraction. Knockdown could be confirmed, and compared to Mock control, less eIF6 was detected in siRNA, transfected samples (*Figure 54A*).

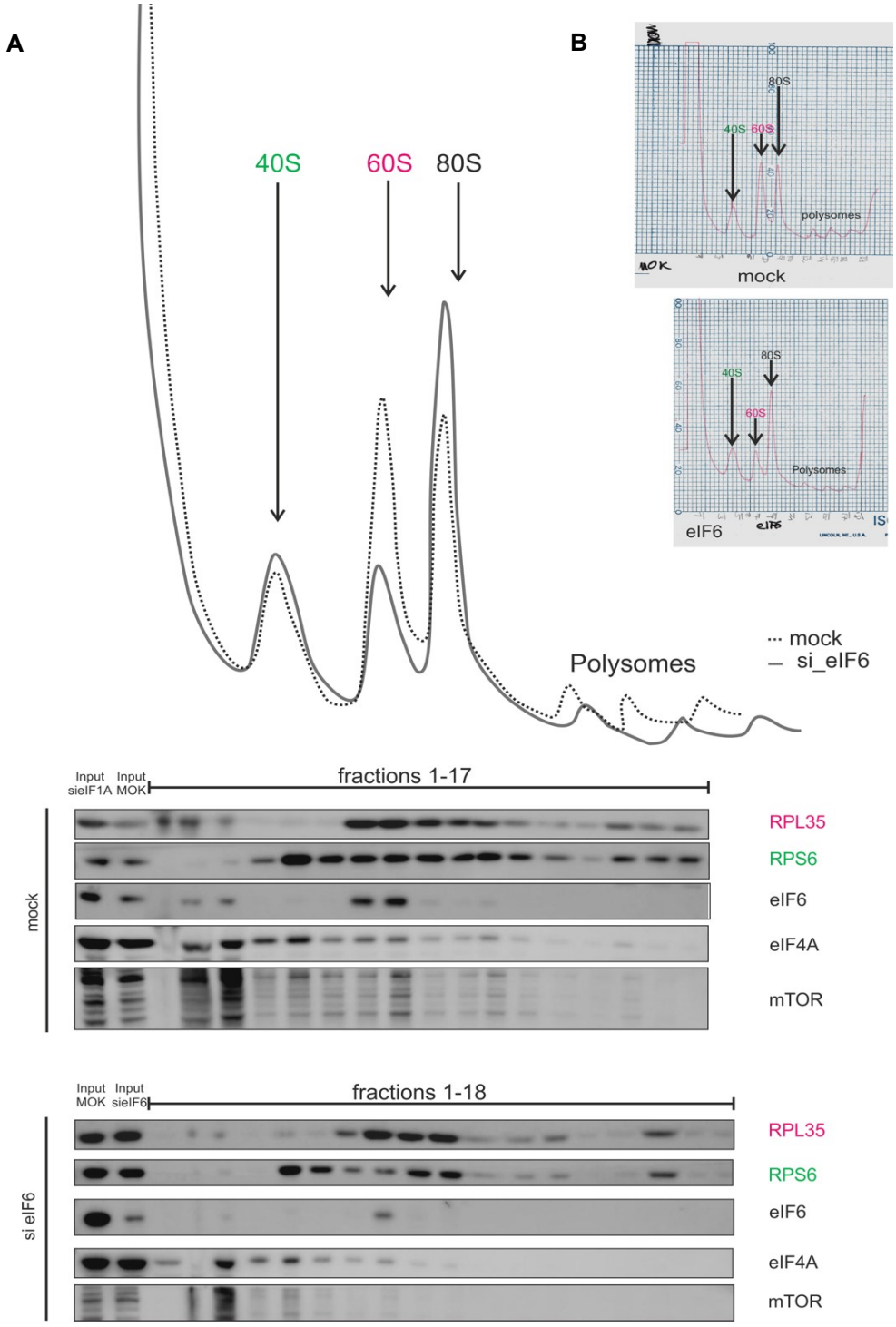

Figure 53 Reduced levels of eIF6 leads to less free 60S particles. (**A**) Sucrose density gradient profiles of 3 days post transfected A549 cells are shown. Rpl35 antibody was used as marker for the 60S subunit and Rps3 for the 40S subunit. mTOR, eIF4A and eIF6 were detected to see influence of eIF6 knockdown on distribution upon ribosomal particles. (**B**) Original elution profiles (detection at 254 nm). Data presented are published in Gantenbein et al 2018 [81]. Reproduced from [81] with permission of publisher Elsevier.

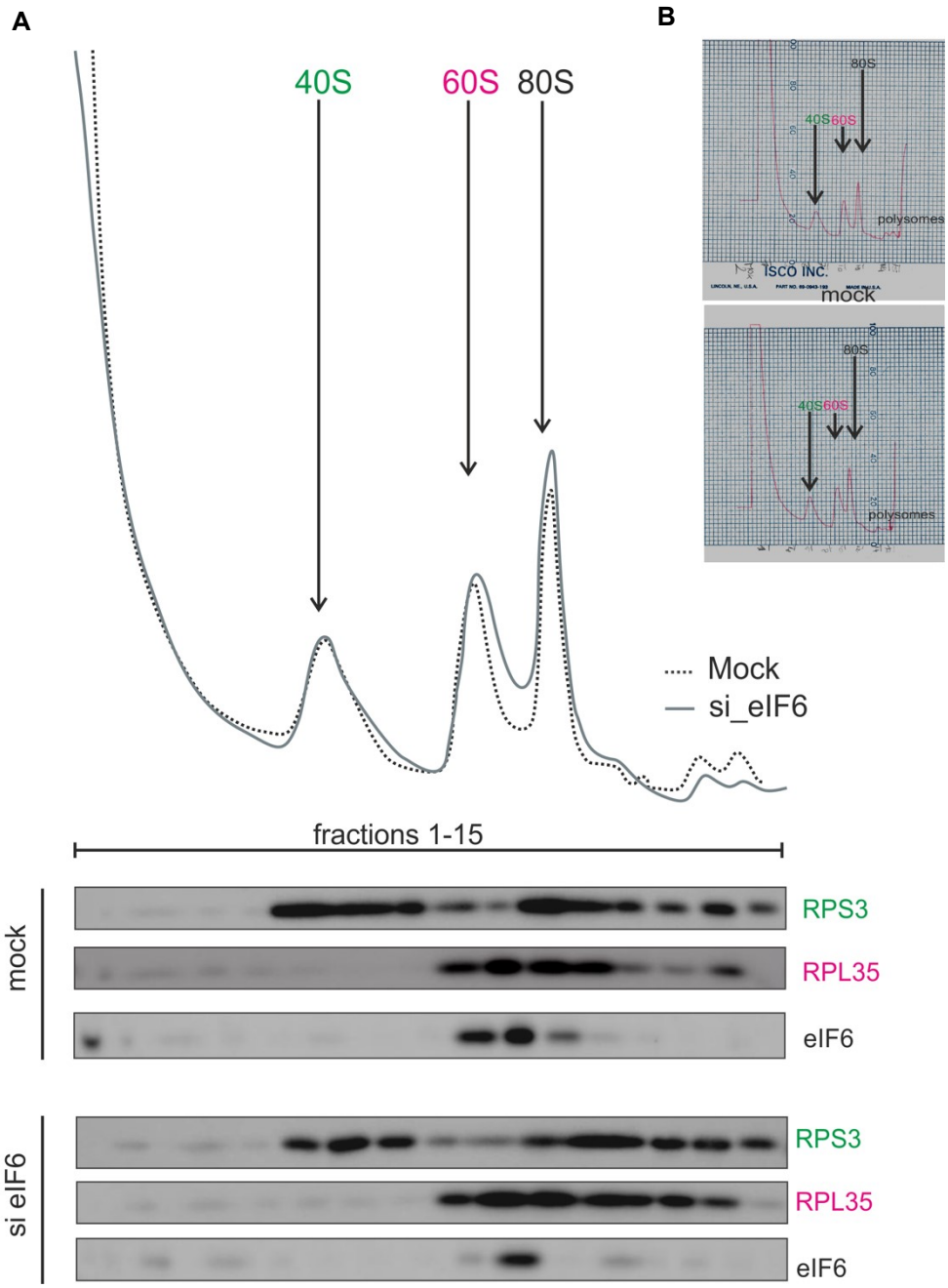

Figure 54 Reduced levels of eIF6 have no influence on ribosomal particle distribution in H520 cell line. (**A**) Sucrose density gradient profiles of 3 days post transfected H520 cells are shown. Rpl35 antibody was used as marker for the 60S subunit and Rps3 for the 40S subunit. eIF6 was detected to confirm eIF6 knockdown and location within the fractions. (**B**) Original elution profiles (detection at 254 nm). Data presented are published in Gantenbein et al 2018 [81]. Reproduced from [81] with permission of publisher Elsevier.

5.5.7 Ribosomal RNA processing of 60S subunit is defective in response to eIF6 knockdown

To gain insight into the underlying mechanism that is responsible for aberrant 60S assembly in response to eIF6 silencing we performed Northernblot analysis, 3 days post transfection with siRNA against eIF6 or Mock control of both NSCLC cell lines. Methylen-blue staining of the membrane was used to detect 28S and 18S precursor rRNA (pre-rRNA) and also served as loading control. No notable changes for both cell lines were found for 28S and 18S per-rRNA, when comparing Mock to knockdown samples (*Figure 55 B, lower part*). Complementary probes to the 5´-internal transcribed spacer 1 (ITS1) and internal transcribed spacer 2 (ITS2) were hybridized to a range of pre-rRNA intermediates of both ribosomal subunits. With this method, most processing intermediates were detected (*Figure 55A*, bold font pre-RNAs). A scheme of RNA processing for 40S (green) and 60S (pink) particles is displayed in *Figure 55A*. For both cell lines, reduced levels of a variety of precursors were detected upon eIF6 knockdown. For A549, a reduction of 30S (component of 40S subunit) and its successors was observed after eIF6 knock-down compared to mock control. The most prominent effect was detected for 12S pre-rRNA, which is the ancestor of the 5.8S rRNA (*Figure 55B*). 5.8S rRNA is processed and a compound of the 60S subunit. Reduced 12S pre-rRNA indicated a processing defect or inhibition of its direct precursor 32S rRNA, which is then processed to 12S rRNA (*Figure 55B*).

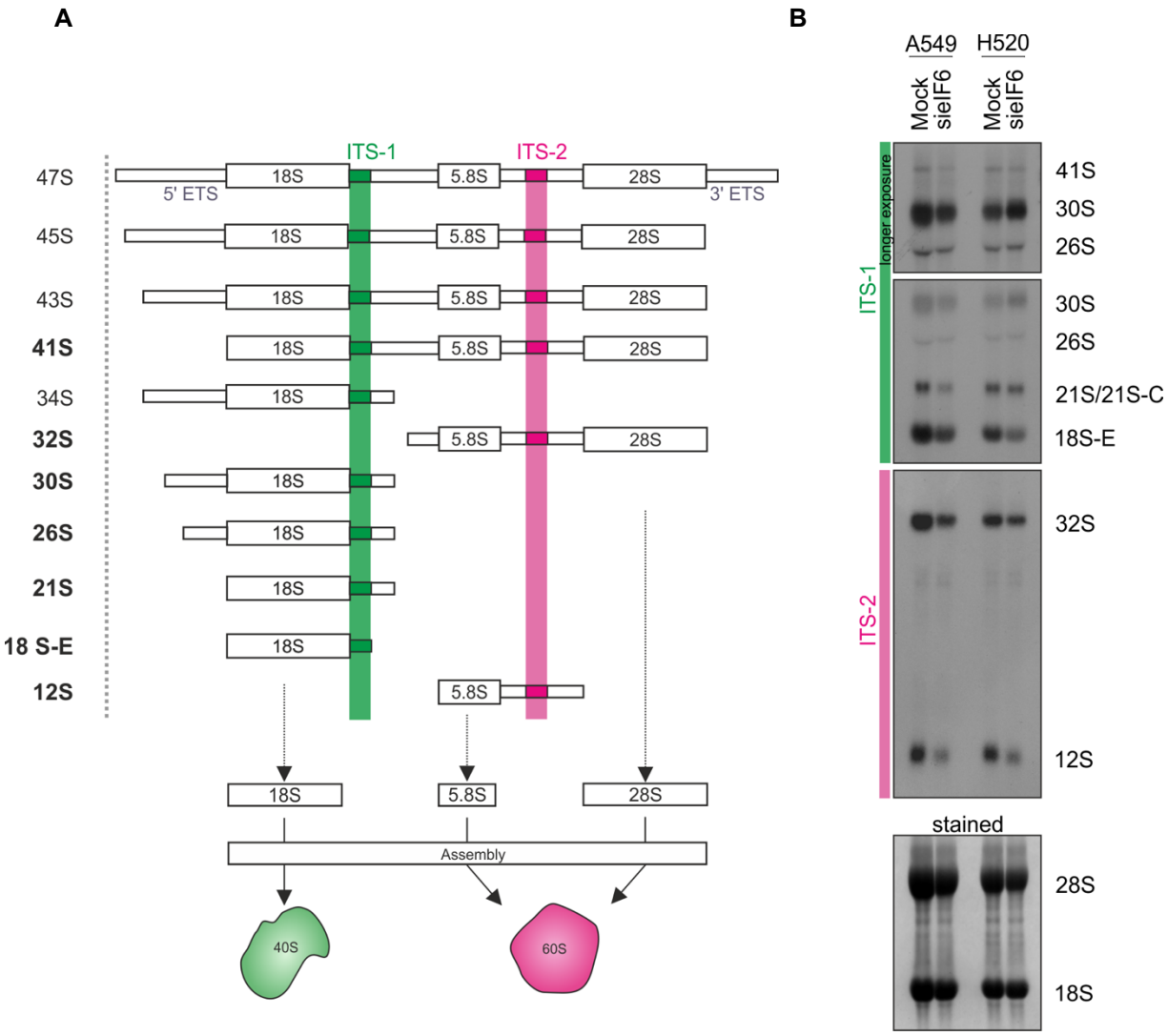

Figure 55 *eIF6* knockdown down in A459 has influence on rRNA processing of the ITS-2. (**A**) Scheme of human rRNA processing. Binding site for the ITS-1 probe detects 40S precursors and is marked in green. The ITS-2 binding site, detects 60S precursors and is highlighted in pink. Precursors which could be detected with probes used in this study are bold type (left site). (**B**) Representative northern blot picture of eIF6 knockdown down in A549 and H520 cell line. Upper panel shows representative blots and lower part methylene blue stained membrane, which served as loading control. Data presented are published in Gantenbein et al 2018 [81]. Reproduced from [81] with permission of publisher Elsevier.

6 Discussion

Parts of this discussion section resemble the discussion section in Gantenbein et al 2018 [81].

Lung cancer is one of the leading causes of death worldwide. A better understanding of this disease is required to further improve patient care. Lung cancer research focuses on NSCLC and targeted therapy such as PD-1 immunotherapy. We hypothesize that eIFs contribute to lung cancer development and progression, and might serve as potential biomarker. eIFs are responsible for the formation of a mature ribosome and ensure translation in each cell. Currently, the eIF4F [118,178,218] and eIF3 [174–176] complex, as well as eIF2α [206,209] and eIF5A [207,219], are being investigated in NSCLC. The aim of this PhD project was to define the role of eIFs in NSCLC. We analyzed eIFs in NSCLC cell lines, fresh frozen human tissue, FFPE patient samples and a publicly available gene expression data set. The major findings of this analysis are as follows:

- eIFs are over expressed in NSCLC compared to NNT
- eIFs are associated with OS outcome of NSCLC patients
- Silencing of eIF1A in NSCLC cells reduces proliferation by unknown mechanisms
- Knockdown of eIF6 in NSCLC cells reduces proliferation, induces apoptosis and leads to pre-rRNA processing and ribosomal 60S maturation defects

To get an impression about basal protein expression patterns of eIFs and mTOR pathway members I performed Western Blot analyses of tissue lysates obtained from my patient cohorts. In the ADC cohort, eIF4A, eIF1A, eIF2α and eIF6 are overexpressed in tumor tissue compared to NNT. The SQC cohort showed protein overexpression of eIF3B, eIF2α, eIF1A and eIF6 compared to NNT. These findings confirm results demonstrating eIF4A and eIF2α overexpression in NSCLC [178,206,209]. The role of eIF3B, eIF1A and eIF6 in NSCLC progression is currently unclear. However, eIF6 [134,193,194,220] and eIF3B [99,169–171] overexpression was demonstrated in other cancer entities.

Additionally, gene expression analysis of eIFs in NSCLC in a publicly available data sets (TCGA and Affymetrix) was conducted for eIF2α, eIF4H, eIF3B, eIF6 and

eIF1A. Kaplan Maier survival analyses revealed that high expression of eIF2α, eIF3B, eIF6 and eIF1AY (Y-chromosome coded eIF1A) is significantly associated with worse overall survival for NSCLC patients compared to the low expression levels of these factors. Regarding eIF1AX (X-chromosome coded eIF1A), overexpression is beneficial for patient overall survival in NSCLC. At present, only little is known about gene expression in eIFs and their association with OS in NSCLC.

Before starting cell culture experiments, I analyzed basal and stable eIF and mTOR pathway member protein expression by cultivating NSCLC cell lines over a period of several weeks. These data demonstrated stable protein expression over 4 weeks of cultivation in H1299 and A549 cells, except for eIF4B and eIF3C, whose expression time-dependently changed in A549 cells.

Currently, the definite or side targets of many chemotherapeutics are not known. Therefore, I tried to answer the question whether eIFs or their upstream pathway could be a target of paclitaxel treatment on A549 cell. Paclitaxel is a chemotherapeutic drug used in several types of cancer, including lung cancer. It is a cytotoxic microtubule-stabilizing agent thereby preventing cell division [221,222]. Paclitaxel has been reported to activate the PI3K/Akt signaling pathway, which is upstream of the mTOR and eIF pathway [223,224]. In 2011, Sun et al reported an IC_{50} for paclitaxel treatment of A549 cells [225]. During the present study I treated A549 cells with paclitaxel and analyzed the effects at three time points by light microscopy and Western Blot. Light microscopy analysis of A549 treated cells in this PhD study showed a cell density of approximately 50% compared to control conditions, which is in line with the study of Sun et al., where an IC_{50} of 10nM was reported for A549 cells [225].

Protein lysates of the treated cells, as well as control lysates, were analyzed by Western Blot. Actin and GAPDH served as loading control. It is noteworthy, however, that in contrast to other reports [223,225] actin levels were highly variable during my first set of experiments therefore I decided to normalize on GAPDH During these analyses I observed changes in protein levels for Akt, P70S6k, mTOR, eIF4G and eIF6 in paclitaxel-treated as compared to untreated A549 cells. All these proteins were upregulated upon paclitaxel treatment compared to control conditions. The results for Akt, p70S6K and mTOR are in agreement with an earlier study

reporting activation of PI3K/Akt signaling pathway by paclitaxel? [224]. The underlying mechanisms that induce upregulation of eIF4G and eIF6 in paclitaxel-treated cells are currently unclear. In the literature, an association with 4EBP-1 and paclitaxel is discussed [223]. 4EBP-1, which binds eIF4E, is a member of the eIF4F complex, like eIF4G. Although 4EBP-1 is hyperphosphorylated during paclitaxel treatment, eIF4E levels are not affected by paclitaxel. There might be a correlation with paclitaxel affecting eIF4E and thus also with eIF4G, but that has yet to be proven. Paclitaxel is a drug targeting microtubules, which are a component of the cytoskeleton. Furthermore, eIF6 is also known as integrin beta 4 binding protein, a functional component of hemidesmosomes, which connect the basal lamina and the intermediate filament of the cytoskeleton [132,226]. Thus, there might be a connection between paclitaxel targeting the cytoskeleton via microtubules and eIF6 levels in a treated cell.

Based on eIF characterization in NSCLC performed during the present PhD thesis and the current literature on eIFs in NSCLC, my further experiments focused on the role of eIF1A and eIF6. A search in PubMed revealed that a study characterizing eIF1A in cancer tissue has not yet been conducted. Compared to NNT, eIF1A is overexpressed in fresh patient samples of ACD and SQC. One problem with eIF1A is that this protein is encoded on the X-Chromosome and on the Y-Chromosome. These two isoforms are 99% (eIF1AX blasted against eIF1AY-1) and 88% (eIF1AX blasted against eIF1AY-2) identical. Therefore, every available antibody against eIF1A detects both forms in male tissue, and a specific primer to separately analyze eIF1A in male and female samples is not available. Companies sell specific antibodies irrespective of the form, but the binding site of the antibody is not in the region where those isoforms are different. We decided to base our results on eIF1A and did not differentiate between eIF1AX and eIF1AY. To understand the role of eIF1A in NSCLC, I established siRNA mediated eIF1A knockdown in NSCLC cell lines. To mimic the two major NSCLC subtypes characterized previously, I performed the knockdown in an ADC cell line, A549, and in H520 cell, an SQC cell line. Knockdown of eIF1A resulted in significantly reduced proliferation of A549 cells and a tendency towards reduced proliferation in H520 cells. This data is in concordance other studies [226-228], reporting that eIF1A is an essential protein in yeast and in experiments with rabbit reticulocytes [227–229]. To answer the

question if apoptosis is responsible for reduced cell growth after eIF1A knockdown, PARP and Casp 3 cleavage was analyzed by Western Blot, but no effects on PARP and Casp 3 cleavage were detected. Currently, there are no other studies investigating PARP and Casp 3 cleavage in human cell lines after eIF1A knockdown. As an alternative pathway we studied whether eIF1A silencing induces senescence. However, the SA-ß-Gal assay failed to show more senescent cells in eIF1A silencing samples compared to control conditions.
Additionally, after eIF1A knockdown, the ribosomal profiles were analyzed to get an impression about eIF1A-mediated effects on ribosome assembly. There were polysome profiles stably expressing eIF1A or eIF1A mutant HEK293 cells. Changes in polysome complex formation between the wildtype eIF1A or the mutant were not observed. These results are similar to our polysomal profiles in A549 cells, and no difference was detected between mock control profiles and silenced eIF1A profiles. To sum up, interesting results concerning eIF1A were collected, but further analysis is clearly needed to define the role of eIF1A in NSCLC.

I then went on to investigate the role of eIF6 that is overexpressed in ADC and SQC. Gene expression analysis revealed that eIF6 overexpression is associated with worse OS in ADC but not in SQC patients. Silencing of eIF6 with siRNA reduced proliferation and induced Casp-3 mediated apoptosis. Downstream analysis of eIF6 knockdown revealed defects in rRNA-processing, resulting in reduction of free 60S in A549 cells.
Changes in eIF6 levels were reported for various cancer entities, such as mesothelioma, colorectal carcinoma (CRC), ovarian serous adenocarcinoma and head and neck cancer [99,132,134,188,194]. One study on eIF6 in mesothelioma showed that compared to NNT, eIF6 is overexpressed and hyperphosphorylated in mesothelioma tissue [134]. However, compared to NNT, eIF6 was reported to be overexpressed in tumor tissue not only in mesothelioma but also in CRC [99]. In both studies, overexpression of eIF6 was detected by IHC staining and analyzed by Western Blot in fresh frozen tissue [99,134]. To answer the question if eIF6 is overexpressed in NSCLC tumor cells, IHC staining of ADC and SQC FFPE tissue was performed. Indeed, eIF6 is significantly overexpressed in tumor tissue of ADC and SQC but not in NNT. After grouping the TMA cohort in tumor grades for ADC and SQC, eIF6 staining was analyzed for changes in ascending grades. In the SQC

cohort, staining intensity of eIF6 did not correlate with different tumor grades. However, in the ADC TMA cohort, a significant difference within increasing tumor grades was observed. A cytoplasmic overexpression of eIF6 was also reported for other cancer entities. IHC staining of eIF6 in FFPE human tissue specimens for CRC, ovarian serous adenocarcinoma and pleural mesothelioma revealed a cytoplasmic overexpression of eIF6 compared to NNT [99,134,194]. Additionally, fresh frozen ADC and SQC tissue was analyzed by Western Blot and qRT-PCR. Both analyses revealed significant eIF6 overexpression in tumor samples compared to NNT (protein and mRNA levels). . Results of eIF6 analysis in NSCLC match the findings reported for eIF6 in mesothelioma and CRC [99,134].

In principal, a significant association of *eIF6* with worse overall survival was found. ADC and SQC are different pathological types of lung cancer, have a different mutational pattern and receive different therapies. Therefore, by distinguishing ADC from SQC, we separately analyzed the cohort for *eIF6* expression and overall survival [10,26]. Affymetrix data analysis revealed that high levels of *eIF6* are significantly associated with overall survival in ADC but not in SQC. The association of overexpressed *eIF6* and worse OS in ADC was confirmed by analyzing an independent TCGA data set. Also, in this second data set, no significant association between *eIF6* expression and OS was found in SQC, which suggests that *eIF6* might play different roles in ADC compared to SQC development and progression. For CRC, a significant association of eIF6 with OS was reported in the TCGA data set [99].

Due to the lethal phenotype of a total knockout of *eIF6* in a mouse model of myc-induced lymphomagenesis in which $eIF6^{-/-}$ littermate mice were not viable, we decided to perform siRNA mediated silencing for further experiments, because $eIF6^{+/-}$ mice are viable [133]. First, eIF6 knockdown efficacy in A549 and H520 cells was tested. 488 Alexa labeled siRNA was transfected, and fluorescent analysis of the cells revealed >98% and >90% transfection efficacy for A549 and H520, respectively. Then, knockdown of eIF6 was analyzed on protein and mRNA level, revealing > 80% reduction of eIF6 in A549 cells, which is similar to eIF6 siRNA knockdown in CRC cell line HTC116 [99]. In H520 cells, eIF6 knockdown was >50%. Proliferation was reduced in A549 and H520 cell line after eIF6 knockdown. Also, in $eIF6^{+/-}$ mice, reduced eIF6 levels impaired G1/S progression in hepatic and adipose cells [159]. For $eIF6^{+/-}$ heterozygous knockout in mice, tumor-free survival was

prolonged, suggesting a rate-limiting role of eIF6 in tumor progression [133]. In Saccharomyces cerevisiae, reduced cell proliferation and viability were reported for depletion of *TIF6*, the yeast homologue of eIF6 [142]. Also, in the CRC cell line HTC116 cell viability was reduced 72h after eIF6 knockdown [99].

Reduced cell proliferation and colony formation after eIF6 silencing might be a result of apoptosis induction. In HTC116, a tendency towards increased apoptosis was reported 24h post transfection, but not at later time points [99]. In REN cells, apoptosis was also unaffected 72h post transfection [134]. In the present study we found that eIF6 depletion in H520 cells did not induce apoptosis, nor did it affect Casp 3 or PARP processing. However, in A549 cells 3 and 5 days after eIF6 silencing, we observed a clear increase in apoptotic cells and an induction of Casp 3 dependent apoptosis.

Additionally, induction of cellular senescence pathways was analyzed by β-Gal activity assay, as well as by p21 Western Blot in A549 and H520 cell line [230]. Both β-Gal activity and p21 levels were elevated in response to eIF6 silencing, indicating an induction of cellular senescence in eIF6 depleted cells. No evidence for apoptosis or senescence could be found in H520 cells. The mechanism for reduced cell growth and colony formation in this cell line is still unknown. However, it has to be considered that knockdown efficacy of eIF6 was lower in these cells, possibly explaining the less pronounced phenotypes.

Translation was analyzed in A549 and H520 cells using ‘click-chemistry’. This analysis revealed no major effects after eIF6 depletion in the two cell lines. However, it has to be considered that cycloheximide, a general translation inhibitor, only scarcely affected A549 cells. This indicates that the experimental setup probably needs further optimization, as the positive control did not work properly. For H520 cells cycloheximide did inhibit translation but no effect on protein synthesis was seen in response to eIF6 depletion.

Ribosomal profiling after eIF6 silencing revealed major 60S ribosomal subunit synthesis defects in A549 but not in H520 cells. eIF6-dependent reduction of free 60S particles was demonstrated in yeast, *C.elegans*, pleural mesothelioma, HeLa, ovarian carcinoma cells and mouse liver extracts [134–138].

Furthermore, pulse chase studies in yeast demonstrated that *TIF6* depleted cells have pre-rRNA processing defects. Accumulation of 27S (the analog of human 32S) and a rapid decrease in 7S pre-rRNA, which corresponds to the human 12S

precursor led to a reduction of free 60S particles [142]. Northern blot analysis of a pulse chase experiment revealed that depletion of *TIF6* leads to an accumulation of 27S (yeast homologue to 32S) and 7S (yeast homologue to 12S) pre-rRNA at early time points [142]. Northern blot analyses suggested that reduction of the 7S pre-rRNA triggers aberrant processing of downstream pre-rRNAs [142]. In this study, pre-RNA analysis by Northern blot analysis in eIF6 silenced HTC116 cell line showed pre-RNA processing defects similar to A549 cells [77]. Data from our Northern blot analysis are reminiscent of results in the yeast system at later time points when also secondary effects evolve [142]. These data suggest that in the human system, eIF6 acts at a similar stage of ribosome biogenesis as does Tif6 in yeast, i.e. at the conversion of the human 32S pre-rRNA (27S in yeast) into the corresponding downstream products.

In conclusion, the findings of the present thesis demonstrate that eIFs are altered in NSCLC compared to NNT, and some eIFs are associated with worse OS in NSCLC. We have provided evidence that eIFs undergo changes during paclitaxel treatment. The results regarding eIF1A in this study provide a deeper insight into the role of eIF1A in human cancer. eIF1A is overexpressed in NSCLC, and high levels of eIF1AY are associated with shorter OS in NSCLC. Knockdown of eIF1A reduces proliferation but the mechanism that is responsible for reduced cell growth is still unknown.

Furthermore I could show that eIF6 is overexpressed in NSCLC and associated with shorter OS in ADC. Knockdown of eIF6 reduces proliferation and induces apoptosis. This study gives mechanistic insights into the consequences of eIF6 depletion by discovering defects in rRNA processing. eIF6 has the potential of a biomarker for OS in ADC, and targeting its functionality could lead to the development of new therapeutic approaches in NSCLC. Results regarding eIF6 function in NSCLC are graphically summarized in *Figure 56*.

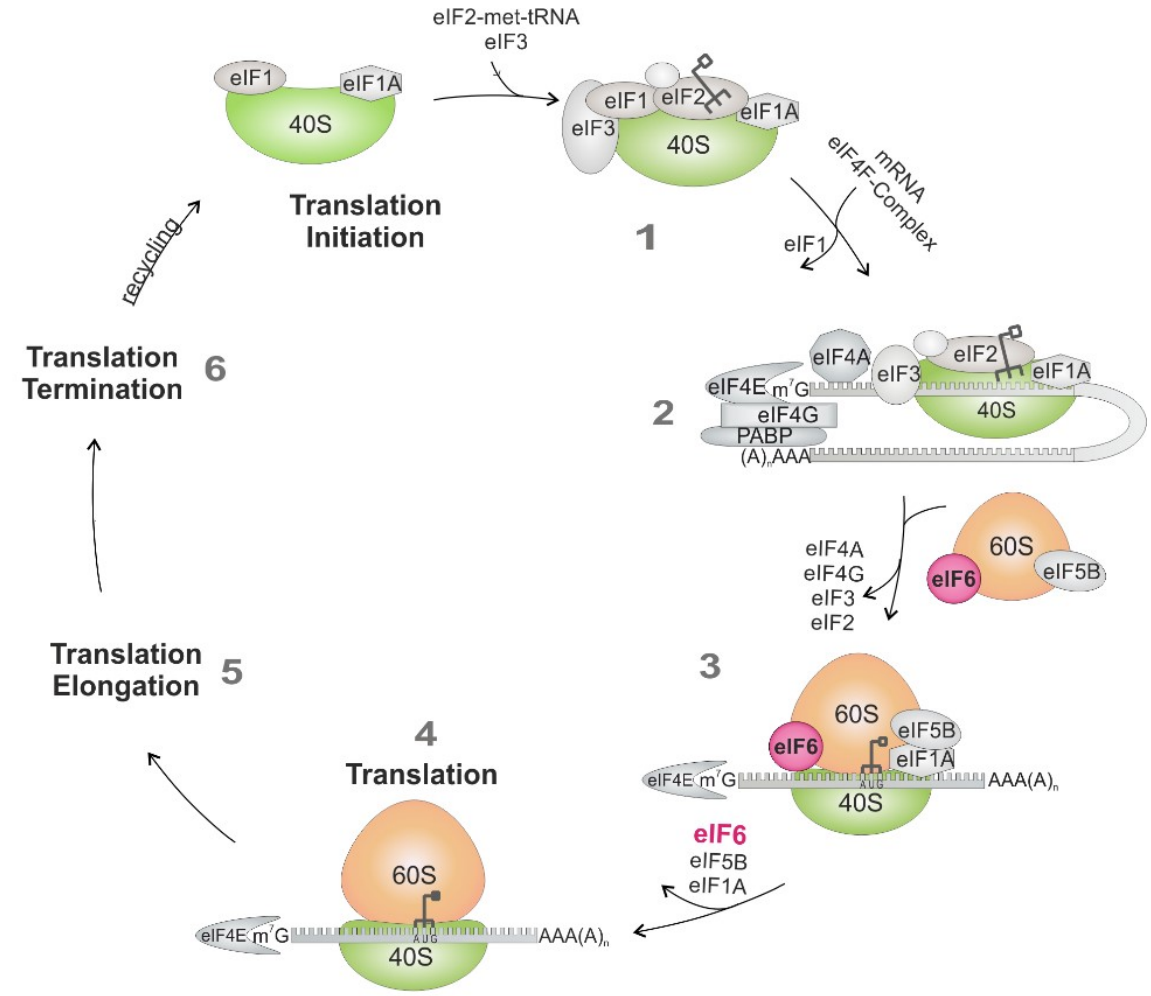

role of eIF6 in NSCLC

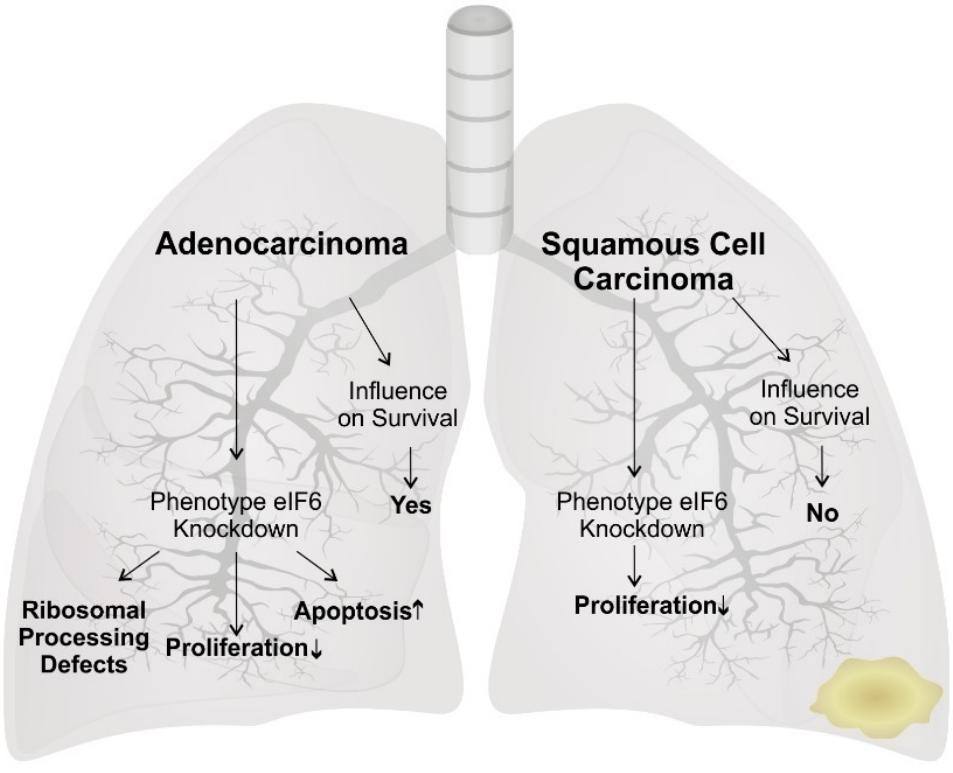

Figure 56 Model describing the role of eIF6 in NSCLC. The eukaryotic translation initiation starts with the assembly of the 43S-initiation complex (1), in which the 40S ribosomal subunit binds to eIFs (eIF1, eIF1A, eIF3 and eIF2-$_{met}$tRNAi). Subsequently, the eIF4F complex (eIF4A, eIF4G and eIF4E) accompanies the mRNA to the 43S complex and builds the pre-48S initiation complex (2). After scanning for the start codon AUG, the large ribosomal subunit 60S accompanied by eIF6 and eIF5B binds to the 48S-initiation complex (3). After the formation of a translational competent 80S ribosome, translation is initiated (4), followed by elongation (5), termination (6) and ribosomal recycling. eIF6 is overexpressed in NSCLC and is associated with patient OS in ADC. After eIF6 knockdown in the ADC cell line decreased proliferation, increased apoptosis and ribosomal processing defects were observed. For SQC, no influence of eIF6 on patient OS was found. The phenotype of the eIF6 knockdown in SQC cell line showed decreased proliferation. NSCLC, non-small cell lung cancer; ADC, adenocarcinoma; OS, overall survival; SQC, squamous cell carcinoma. [81]. Reproduced from [81] with permission of publisher Elsevier.

7 Bibliography

[1] Klitschko W, Bilen S. Challenge Management : Was Sie als Manager vom Spitzensportler lernen können. 1. Auflage. Campus Verlag; 2017.

[2] Gridelli C, Rossi A, Carbone DP, Guarize J, Karachaliou N, Mok T, et al. Non-small-cell lung cancer. Nat Rev Dis Prim 2015;1:15009. doi:10.1038/nrdp.2015.9.

[3] Ferlay J, Soerjomataram I, Dikshit R, Eser S, Mathers C, Rebelo M, et al. Cancer incidence and mortality worldwide: sources, methods and major patterns in GLOBOCAN 2012. Int J Cancer 2015;136:E359-86. doi:10.1002/ijc.29210.

[4] Bray F, Ren J-S, Masuyer E, Ferlay J. Global estimates of cancer prevalence for 27 sites in the adult population in 2008. Int J Cancer 2013;132:1133–45. doi:10.1002/ijc.27711.

[5] Siegel RL, Miller KD, Jemal A. Cancer statistics, 2016. CA Cancer J Clin 2016;66:7–30. doi:10.3322/caac.21332.

[6] Howlader N, Noone A, Krapcho M, Miller D, Bishop K, Kosary C, et al. SEER Cancer Statistics Review, 1975-2014. Natl Cancer Institute Bethesda, MD 2017.

[7] Travis WD, Brambilla E, Riely GJ. New pathologic classification of lung cancer: Relevance for clinical practice and clinical trials. J Clin Oncol 2013;31:992–1001. doi:10.1200/JCO.2012.46.9270.

[8] Travis WD, Brambilla E, Nicholson AG, Yatabe Y, Austin JHM, Beasley MB, et al. The 2015 World Health Organization Classification of Lung Tumors: Impact of Genetic, Clinical and Radiologic Advances since the 2004 Classification. J Thorac Oncol 2015;10:1243–60. doi:10.1097/JTO.0000000000000630.

[9] Reck M, Rabe KF. Precision Diagnosis and Treatment for Advanced Non–Small-Cell Lung Cancer. N Engl J Med 2017;377:849–61. doi:10.1056/NEJMra1703413.

[10] Chen Z, Fillmore CM, Hammerman PS, Kim CF, Wong K-K. Non-small-cell lung cancers: a heterogeneous set of diseases. Nat Rev Cancer 2014;14:535–46. doi:10.1038/nrc3775.

[11] Howlader N, Noone A, Krapcho M, Miller D, Bishop K, Kosary C, et al. SEER

Cancer Statistics. Natl Cancer Institute Bethesda, MD 2017. https://seer.cancer.gov/csr/1975_2014/%0Ahttps://seer.cancer.gov/archive/csr/1975_2008/%0Ahttp://seer.cancer.gov/archive/csr/1975_2010/.

[12] Socinski MA, Evans T, Gettinger S, Hensing TA, Van Dam Sequist L, Ireland B, et al. Treatment of stage IV non-small cell lung cancer: Diagnosis and management of lung cancer, 3rd ed: American college of chest physicians evidence-based clinical practice guidelines. Chest 2013;143:e341S–e368S. doi:10.1378/chest.12-2361.

[13] Alberg AJ, Brock M V., Ford JG, Samet JM, Spivack SD. Epidemiology of lung cancer: Diagnosis and management of lung cancer, 3rd ed: American college of chest physicians evidence-based clinical practice guidelines. Chest 2013;143:e1S–e29S. doi:10.1378/chest.12-2345.

[14] Sun S, Schiller JH, Gazdar AF. Lung cancer in never smokers - A different disease. Nat Rev Cancer 2007;7:778–90. doi:10.1038/nrc2190.

[15] Detterbeck FC, Boffa DJ, Kim AW, Tanoue LT. The Eighth Edition Lung Cancer Stage Classification. Chest 2017;151:193–203. doi:10.1016/j.chest.2016.10.010.

[16] Silvestri GA, Gonzalez A V, Jantz MA, Margolis ML, Gould MK, Tanoue LT, et al. Methods for Staging Non-small Cell Lung Cancer. Chest 2013;143:e211S–e250S. doi:10.1378/chest.12-2355.

[17] Rami-Porta R, Bolejack V, Giroux DJ, Chansky K, Crowley J, Asamura H, et al. The IASLC lung cancer staging project: The new database to inform the eighth edition of the TNM classification of lung cancer. J Thorac Oncol 2014;9:1618–24. doi:10.1097/JTO.0000000000000334.

[18] Rami-Porta R, Ball D, Crowley J, Giroux DJ, Jett J, Travis WD, et al. The IASLC lung cancer staging project: Proposals for the revision of the T descriptors in the forthcoming (seventh) edition of the TNM classification for lung cancer. J Thorac Oncol 2007;2:593–602. doi:10.1097/JTO.0b013e31807a2f81.

[19] Eberhardt WEE, Mitchell A, Crowley J, Kondo H, Kim YT, Turrisi A, et al. The IASLC Lung Cancer Staging Project: Proposals for the Revision of the M Descriptors in the Forthcoming Eighth Edition of the TNM Classification of Lung Cancer. J Thorac Oncol 2015;10:1515–22. doi:10.1097/JTO.0000000000000673.

[20] Eberhardt WEE, Mitchell A, Crowley J, Kondo H, Kim YT, Turrisi A, et al. The IASLC Lung Cancer Staging Project. J Thorac Oncol 2015;10:1515–22. doi:10.1097/JTO.0000000000000673.

[21] Goldstraw P, Chansky K, Crowley J, Rami-Porta R, Asamura H, Eberhardt WEEEE, et al. The IASLC Lung Cancer Staging Project: Proposals for Revision of the TNM Stage Groupings in the Forthcoming (Eighth) Edition of the TNM Classification for Lung Cancer. J Thorac Oncol 2016;11:39–51. doi:10.1016/j.jtho.2015.09.009.

[22] Nicholson AG, Chansky K, Crowley J, Beyruti R, Kubota K, Turrisi A, et al. The International Association for the Study of Lung Cancer Lung Cancer Staging Project: Proposals for the Revision of the Clinical and Pathologic Staging of Small Cell Lung Cancer in the Forthcoming Eighth Edition of the TNM Classification for Lung Cancer. J Thorac Oncol 2016;11:300–11. doi:10.1016/j.jtho.2015.10.008.

[23] Travis WD, Asamura H, Bankier AA, Beasley MB, Detterbeck F, Flieder DB, et al. The IASLC lung cancer staging project: Proposals for coding T categories for subsolid nodules and assessment of tumor size in part-solid tumors in the forthcoming eighth edition of the TNM classification of lung cancer. J Thorac Oncol 2016;11:1204–23. doi:10.1016/j.jtho.2016.03.025.

[24] Cagle PT, Allen TC, Dacie S, Beth Beasley M, Borczuk AC, Chirieac LR, et al. Revolution in lung cancer new challenges for the surgical pathologist. Arch Pathol Lab Med 2011;135:110–6. doi:10.5858/arpa.2011-0055-LE.

[25] Charloux A, Quoix E, Wolkove N, Small D, Pauli G, Kreisman H. The increasing incidence of lung adenocarcinoma: Reality or artefact? A review of the epidemiology of lung adenocarcinoma. Int J Epidemiol 1997;26:14–23. doi:10.1093/ije/26.1.14.

[26] Davidson MR, Gazdar AF, Clarke BE. The pivotal role of pathology in the management of lung cancer. J Thorac Dis 2013;5 Suppl 5:S463-78. doi:10.3978/j.issn.2072-1439.2013.08.43.

[27] Jain M, Sznajder JI. Bench-to-bedside review: Distal airways in acute respiratory distress syndrome. Crit Care 2007;11:1–8. doi:10.1186/cc5159.

[28] Langer CJ, Besse B, Gualberto A, Brambilla E, Soria JC. The evolving role of histology in the management of advanced non - small-cell lung cancer. J Clin Oncol 2010;28:5311–20. doi:10.1200/JCO.2010.28.8126.

[29] Tsao AS, Scagliotti G V., Bunn PA, Carbone DP, Warren GW, Bai C, et al. Scientific advances in lung cancer 2015. J Thorac Oncol 2016;11:613–38. doi:10.1016/j.jtho.2016.03.012.

[30] Hackshaw AK. Lung cancer and passive smoking. Stat Methods Med Res 1998;7:119–36. doi:10.1177/096228029800700203.

[31] Tammemagi CM, Neslund-Dudas C, Simoff M, Kvale P. Smoking and Lung Cancer Survival: The Role of Comorbidity and Treatment. Chest 2004;125:27–37. doi:10.1378/chest.125.1.27.

[32] Warren GW, Sobus S, Gritz ER. The biological and clinical effects of smoking by patients with cancer and strategies to implement evidence-based tobacco cessation support. Lancet Oncol 2014;15:e568-80. doi:10.1016/S1470-2045(14)70266-9.

[33] Leone FT, Carlsen K-H, Folan P, Latzka K, Munzer A, Neptune E, et al. An Official American Thoracic Society Research Statement: Current Understanding and Future Research Needs in Tobacco Control and Treatment. Am J Respir Crit Care Med 2015;192:e22–41. doi:10.1164/rccm.201506-1081ST.

[34] Coté ML, Liu M, Bonassi S, Neri M, Schwartz AG, Christiani DC, et al. Increased risk of lung cancer in individuals with a family history of the disease: a pooled analysis from the International Lung Cancer Consortium. Eur J Cancer 2012;48:1957–68. doi:10.1016/j.ejca.2012.01.038.

[35] Yamamoto H, Higasa K, Sakaguchi M, Shien K, Soh J, Ichimura K, et al. Novel germline mutation in the transmembrane domain of HER2 in familial lung adenocarcinomas. J Natl Cancer Inst 2014;106:djt338. doi:10.1093/jnci/djt338.

[36] Darby S, Hill D, Auvinen A, Barros-Dios JM, Baysson H, Bochicchio F, et al. Radon in homes and risk of lung cancer: collaborative analysis of individual data from 13 European case-control studies. BMJ 2005;330:223. doi:10.1136/bmj.38308.477650.63.

[37] Rodenhuis S, van de Wetering ML, Mooi WJ, Evers SG, van Zandwijk N, Bos JL. Mutational activation of the K-ras oncogene. A possible pathogenetic factor in adenocarcinoma of the lung. N Engl J Med 1987;317:929–35. doi:10.1056/NEJM198710083171504.

[38] Santos E, Martin-Zanca D, Reddy EP, Pierotti MA, Della Porta G, Barbacid

M. Malignant activation of a K-ras oncogene in lung carcinoma but not in normal tissue of the same patient. Science 1984;223:661–4.

[39] Davies H, Bignell GR, Cox C, Stephens P, Edkins S, Clegg S, et al. Mutations of the BRAF gene in human cancer. Nature 2002;417:949–54. doi:10.1038/nature00766.

[40] Paez JG, Jänne PA, Lee JC, Tracy S, Greulich H, Gabriel S, et al. EGFR Mutations in Lung Cancer: Correlation with Clinical Response to Gefitinib Therapy. Science (80-) 2004;304:1497–500. doi:10.1126/science.1099314.

[41] Lynch TJ, Bell DW, Sordella R, Gurubhagavatula S, Okimoto RA, Brannigan BW, et al. Activating Mutations in the Epidermal Growth Factor Receptor Underlying Responsiveness of Non–Small-Cell Lung Cancer to Gefitinib. N Engl J Med 2004;350:2129–39. doi:10.1056/NEJMoa040938.

[42] Soda M, Choi YL, Enomoto M, Takada S, Yamashita Y, Ishikawa S, et al. Identification of the transforming EML4-ALK fusion gene in non-small-cell lung cancer. Nature 2007;448:561–6. doi:10.1038/nature05945.

[43] Engelman JA, Zejnullahu K, Mitsudomi T, Song Y, Hyland C, Park JO, et al. MET amplification leads to gefitinib resistance in lung cancer by activating ERBB3 signaling. Science 2007;316:1039–43. doi:10.1126/science.1141478.

[44] Stephens P, Hunter C, Bignell G, Edkins S, Davies H, Teague J, et al. Lung cancer: intragenic ERBB2 kinase mutations in tumours. Nature 2004;431:525–6. doi:10.1038/431525b.

[45] Collisson EA, Campbell JD, Brooks AN, Berger AH, Lee W, Chmielecki J, et al. Comprehensive molecular profiling of lung adenocarcinoma. Nature 2014;511:543–50. doi:10.1038/nature13385.

[46] Kohno T, Ichikawa H, Totoki Y, Yasuda K, Hiramoto M, Nammo T, et al. KIF5B-RET fusions in lung adenocarcinoma. Nat Med 2012;18:375–7. doi:10.1038/nm.2644.

[47] Fernandez-Cuesta L, Plenker D, Osada H, Sun R, Menon R, Leenders F, et al. CD74-NRG1 fusions in lung adenocarcinoma. Cancer Discov 2014;4:415–22. doi:10.1158/2159-8290.CD-13-0633.

[48] Vaishnavi A, Capelletti M, Le AT, Kako S, Butaney M, Ercan D, et al. Oncogenic and drug-sensitive NTRK1 rearrangements in lung cancer. Nat Med 2013;19:1469–72. doi:10.1038/nm.3352.

[49] Rekhtman N, Paik PK, Arcila ME, Tafe LJ, Oxnard GR, Moreira AL, et al.

Clarifying the spectrum of driver oncogene mutations in biomarker-verified squamous carcinoma of lung: lack of EGFR/KRAS and presence of PIK3CA/AKT1 mutations. Clin Cancer Res 2012;18:1167–76. doi:10.1158/1078-0432.CCR-11-2109.

[50] Reungwetwattana T, Weroha SJ, Molina JR. Oncogenic pathways, molecularly targeted therapies, and highlighted clinical trials in non-small-cell lung cancer (NSCLC). Clin Lung Cancer 2012;13:252–66. doi:10.1016/j.cllc.2011.09.004.

[51] Ahrendt SA, Decker PA, Alawi EA, Zhu Yr YR, Sanchez-Cespedes M, Yang SC, et al. Cigarette smoking is strongly associated with mutation of the K-ras gene in patients with primary adenocarcinoma of the lung. Cancer 2001;92:1525–30.

[52] Riely GJ, Kris MG, Rosenbaum D, Marks J, Li A, Chitale DA, et al. Frequency and distinctive spectrum of KRAS mutations in never smokers with lung adenocarcinoma. Clin Cancer Res 2008;14:5731–4. doi:10.1158/1078-0432.CCR-08-0646.

[53] Sequist L V, Heist RS, Shaw AT, Fidias P, Rosovsky R, Temel JS, et al. Implementing multiplexed genotyping of non-small-cell lung cancers into routine clinical practice. Ann Oncol Off J Eur Soc Med Oncol 2011;22:2616–24. doi:10.1093/annonc/mdr489.

[54] Odogwu L, Mathieu L, Blumenthal G, Larkins E, Goldberg KB, Griffin N, et al. FDA Approval Summary: Dabrafenib and Trametinib for the Treatment of Metastatic Non-Small Cell Lung Cancers Harboring *BRAF V600E* Mutations. Oncologist 2018;23:740–5. doi:10.1634/theoncologist.2017-0642.

[55] Shigematsu H, Lin L, Takahashi T, Nomura M, Suzuki M, Wistuba II, et al. Clinical and biological features associated with epidermal growth factor receptor gene mutations in lung cancers. J Natl Cancer Inst 2005;97:339–46. doi:10.1093/jnci/dji055.

[56] Cortot AB, Jänne PA. Molecular mechanisms of resistance in epidermal growth factor receptor-mutant lung adenocarcinomas. Eur Respir Rev 2014;23:356–66. doi:10.1183/09059180.00004614.

[57] Herbst RS, Morgensztern D, Boshoff C. The biology and management of non-small cell lung cancer. Nature 2018;553:446–54. doi:10.1038/nature25183.

[58] Camidge DR, Pao W, Sequist L V. Acquired resistance to TKIs in solid

tumours: learning from lung cancer. Nat Rev Clin Oncol 2014;11:473–81. doi:10.1038/nrclinonc.2014.104.

[59] Jänne PA, Yang JC-H, Kim D-W, Planchard D, Ohe Y, Ramalingam SS, et al. AZD9291 in EGFR inhibitor-resistant non-small-cell lung cancer. N Engl J Med 2015;372:1689–99. doi:10.1056/NEJMoa1411817.

[60] Mok TS, Wu Y-L, Ahn M-J, Garassino MC, Kim HR, Ramalingam SS, et al. Osimertinib or Platinum-Pemetrexed in EGFR T790M-Positive Lung Cancer. N Engl J Med 2017;376:629–40. doi:10.1056/NEJMoa1612674.

[61] Kwak EL, Bang Y-J, Camidge DR, Shaw AT, Solomon B, Maki RG, et al. Anaplastic lymphoma kinase inhibition in non-small-cell lung cancer. N Engl J Med 2010;363:1693–703. doi:10.1056/NEJMoa1006448.

[62] Bergethon K, Shaw AT, Ou S-HI, Katayama R, Lovly CM, McDonald NT, et al. ROS1 rearrangements define a unique molecular class of lung cancers. J Clin Oncol 2012;30:863–70. doi:10.1200/JCO.2011.35.6345.

[63] Solomon BJ, Mok T, Kim D-W, Wu Y-L, Nakagawa K, Mekhail T, et al. First-line crizotinib versus chemotherapy in ALK-positive lung cancer. N Engl J Med 2014;371:2167–77. doi:10.1056/NEJMoa1408440.

[64] Dagogo-Jack I, Shaw AT. Crizotinib resistance: implications for therapeutic strategies. Ann Oncol Off J Eur Soc Med Oncol 2016;27 Suppl 3:iii42-iii50. doi:10.1093/annonc/mdw305.

[65] Takeuchi K, Soda M, Togashi Y, Suzuki R, Sakata S, Hatano S, et al. RET, ROS1 and ALK fusions in lung cancer. Nat Med 2012;18:378–81. doi:10.1038/nm.2658.

[66] Beau-Faller M, Ruppert A-M, Voegeli A-C, Neuville A, Meyer N, Guerin E, et al. MET gene copy number in non-small cell lung cancer: molecular analysis in a targeted tyrosine kinase inhibitor naïve cohort. J Thorac Oncol 2008;3:331–9. doi:10.1097/JTO.0b013e318168d9d4.

[67] Dal Bello MG, Alama A, Coco S, Vanni I, Grossi F. Understanding the checkpoint blockade in lung cancer immunotherapy. Drug Discov Today 2017;22:1266–73. doi:10.1016/j.drudis.2017.05.016.

[68] IPCS IPOCS. Biomarkers In Risk Assessment: Validity And Validation. World Health Organization; 2001.

[69] VanderLaan PA, Rangachari D, Majid A, Parikh MS, Gangadharan SP, Kent MS, et al. Tumor biomarker testing in non-small-cell lung cancer: A decade of

change. Lung Cancer 2018;116:90–5. doi:10.1016/j.lungcan.2018.01.002.

[70] Kris MG, Gaspar LE, Chaft JE, Kennedy EB, Azzoli CG, Ellis PM, et al. Adjuvant Systemic Therapy and Adjuvant Radiation Therapy for Stage I to IIIA Completely Resected Non–Small-Cell Lung Cancers: American Society of Clinical Oncology/Cancer Care Ontario Clinical Practice Guideline Update. J Clin Oncol 2017;35:2960–74. doi:10.1200/JCO.2017.72.4401.

[71] Miller V, Bivona T. Clinical and Molecular Biomarkers in Non-Small-Cell Lung Cancer. Lung 2008:1–6.

[72] Grigg C, Rizvi NA. PD-L1 biomarker testing for non-small cell lung cancer: truth or fiction? J Immunother Cancer 2016;4:48. doi:10.1186/s40425-016-0153-x.

[73] Armache J-P, Jarasch A, Anger AM, Villa E, Becker T, Bhushan S, et al. Cryo-EM structure and rRNA model of a translating eukaryotic 80S ribosome at 5.5-A resolution. Proc Natl Acad Sci U S A 2010;107:19748–53.

[74] Ben-Shem A, Jenner L, Yusupova G, Yusupov M. Crystal structure of the eukaryotic ribosome. Science 2010;330:1203–9.

[75] Rabl J, Leibundgut M, Ataide SF, Haag A, Ban N. Crystal structure of the eukaryotic 40S ribosomal subunit in complex with initiation factor 1. Science 2011;331:730–6.

[76] Lafontaine DLJ. Noncoding RNAs in eukaryotic ribosome biogenesis and function. Nat Struct Mol Biol 2015;22:11–9. doi:10.1038/nsmb.2939.

[77] Tafforeau L, Zorbas C, Langhendries J-L, Mullineux S-T, Stamatopoulou V, Mullier R, et al. The Complexity of Human Ribosome Biogenesis Revealed by Systematic Nucleolar Screening of Pre-rRNA Processing Factors. Mol Cell 2013;51:539–51. doi:10.1016/j.molcel.2013.08.011.

[78] Sonenberg N, Hinnebusch AG. Regulation of translation initiation in eukaryotes: mechanisms and biological targets. Cell 2009;136:731–45. doi:10.1016/j.cell.2009.01.042.

[79] Jackson RJ, Hellen CUT, Pestova T V. The mechanism of eukaryotic translation initiation and principles of its regulation. Nat Rev Mol Cell Biol 2010;11:113–27. doi:10.1038/nrm2838.

[80] Klinge S, Voigts-Hoffmann F, Leibundgut M, Arpagaus S, Ban N. Crystal Structure of the Eukaryotic 60S Ribosomal Subunit in Complex with Initiation Factor 6. Science (80-) 2011;334:941–8. doi:10.1126/science.1211204.

[81] Gantenbein N, Bernhart E, Anders I, Golob-Schwarzl N, Krassnig S, Wodlej C, et al. Influence of eukaryotic translation initiation factor 6 on non–small cell lung cancer development and progression. Eur J Cancer 2018;101:165–80. doi:10.1016/j.ejca.2018.07.001.

[82] Hadjiolov AA, Nikolaev N. Maturation of ribosomal ribonucleic acids and the biogenesis of ribosomes. Prog Biophys Mol Biol 1976;31:95–144.

[83] Mullineux S-TT, Lafontaine DLJJ. Mapping the cleavage sites on mammalian pre-rRNAs: Where do we stand? Biochimie 2012;94:1521–32. doi:10.1016/j.biochi.2012.02.001.

[84] Fromont-Racine M, Senger B, Saveanu C, Fasiolo F. Ribosome assembly in eukaryotes. Gene 2003;313:17–42. doi:10.1016/S0378-1119(03)00629-2.

[85] Carron C, O'Donohue M-F, Choesmel V, Faubladier M, Gleizes P-E. Analysis of two human pre-ribosomal factors, bystin and hTsr1, highlights differences in evolution of ribosome biogenesis between yeast and mammals. Nucleic Acids Res 2011;39:280–91. doi:10.1093/nar/gkq734.

[86] Morello LG, Hesling C, Coltri PP, Castilho BA, Rimokh R, Zanchin NIT. The NIP7 protein is required for accurate pre-rRNA processing in human cells. Nucleic Acids Res 2011;39:648–65. doi:10.1093/nar/gkq758.

[87] Schillewaert S, Wacheul L, Lhomme F, Lafontaine DLJ. The Evolutionarily Conserved Protein LAS1 Is Required for Pre-rRNA Processing at Both Ends of ITS2. Mol Cell Biol 2012;32:430–44. doi:10.1128/MCB.06019-11.

[88] Farrar JE, Nater M, Caywood E, McDevitt MA, Kowalski J, Takemoto CM, et al. Abnormalities of the large ribosomal subunit protein, Rpl35a, in Diamond-Blackfan anemia. Blood 2008;112:1582–92. doi:10.1182/blood-2008-02-140012.

[89] Hadjiolova K V, Nicoloso M, Mazan S, Hadjiolov AA, Bachellerie JP. Alternative pre-rRNA processing pathways in human cells and their alteration by cycloheximide inhibition of protein synthesis. Eur J Biochem 1993;212:211–5.

[90] Bowman LH, Rabin B, Schlessinger D. Multiple ribosomal RNA cleavage pathways in mammalian cells. Nucleic Acids Res 1981;9:4951–66.

[91] Silvera D, Formenti SC, Schneider RJ. Translational control in cancer. Nat Rev Cancer 2010;10:254–66. doi:10.1038/nrc2824.

[92] Saxton RA, Sabatini DM. mTOR Signaling in Growth, Metabolism, and

Disease. Cell 2017;168:960–76. doi:10.1016/j.cell.2017.02.004.

[93] Hershey JWB, Sonenberg N, Mathews MB. Principles of translational control: An overview. Cold Spring Harb Perspect Biol 2012;4:1–10. doi:10.1101/cshperspect.a009829.

[94] Hinnebusch AG, Lorsch JR. The mechanism of eukaryotic translation initiation: New insights and challenges. Cold Spring Harb Perspect Biol 2012;4:1–25. doi:10.1101/cshperspect.a011544.

[95] Graifer D, Malygin A, Zharkov DO, Karpova G. Eukaryotic ribosomal protein S3: A constituent of translational machinery and an extraribosomal player in various cellular processes. Biochimie 2014;99:8–18. doi:10.1016/j.biochi.2013.11.001.

[96] Spilka R, Ernst C, Mehta AK, Haybaeck J. Eukaryotic translation initiation factors in cancer development and progression. Cancer Lett 2013;340:9–21. doi:10.1016/j.canlet.2013.06.019.

[97] Maag D, Lorsch JR. Communication between eukaryotic translation initiation factors 1 and 1A on the yeast small ribosomal subunit. J Mol Biol 2003;330:917–24.

[98] Passmore LA, Schmeing TM, Maag D, Applefield DJ, Acker MG, Algire MA, et al. The Eukaryotic Translation Initiation Factors eIF1 and eIF1A Induce an Open Conformation of the 40S Ribosome. Mol Cell 2007;26:41–50. doi:10.1016/j.molcel.2007.03.018.

[99] Golob-Schwarzl N, Schweiger C, Koller C, Krassnig S, Gogg-Kamerer M, Gantenbein N, et al. Separation of low and high grade colon and rectum carcinoma by eukaryotic translation initiation factors 1, 5 and 6. Oncotarget 2017;8:101224–43. doi:10.18632/oncotarget.20642.

[100] Saini AK, Nanda JS, Lorsch JR, Hinnebusch AG. Regulatory elements in eIF1A control the fidelity of start codon selection Met binding by modulating tRNA i to the ribosome 2007;1:97–110. doi:10.1101/gad.1871910.triplets.

[101] Battiste JL, Pestova T V., Hellen CUT, Wagner G. The eIF1A solution structure reveals a large RNA-binding surface important for scanning function. Mol Cell 2000;5:109–19. doi:10.1016/S1097-2765(00)80407-4.

[102] Baird TD, Wek RC. Eukaryotic initiation factor 2 phosphorylation and translational control in metabolism. Adv Nutr 2012;3:307–21. doi:10.3945/an.112.002113.

[103] Liu Y, László C, Liu Y, Liu W, Chen X, Evans SC, et al. Regulation of G(1) arrest and apoptosis in hypoxia by PERK and GCN2-mediated eIF2alpha phosphorylation. Neoplasia 2010;12:61–8.

[104] Lam N, Sandberg ML, Sugden B. High physiological levels of LMP1 result in phosphorylation of eIF2 alpha in Epstein-Barr virus-infected cells. J Virol 2004;78:1657–64.

[105] Lobo MVT, Martín ME, Pérez MI, Alonso FJM, Redondo C, Álvarez MI, et al. Levels, phosphorylation status and cellular localization of translational factor eIF2 in gastrointestinal carcinomas. Histochem J 2000;32:139–50. doi:10.1023/A:1004091122351.

[106] Tejada S, Lobo MVT, García-Villanueva M, Sacristán S, Pérez-Morgado MI, Salinas M, et al. Eukaryotic Initiation Factors (eIF) 2α and 4E Expression, Localization, and Phosphorylation in Brain Tumors. J Histochem Cytochem 2009;57:503–12. doi:10.1369/jhc.2009.952929.

[107] Rosenwald IB, Wang S, Savas L, Woda B, Pullman J. Expression of translation initiation factor eIF-2? is increased in benign and malignant melanocytic and colonic epithelial neoplasms. Cancer 2003;98:1080–8. doi:10.1002/cncr.11619.

[108] Schewe DM, Aguirre-Ghiso JA. Inhibition of eIF2alpha dephosphorylation maximizes bortezomib efficiency and eliminates quiescent multiple myeloma cells surviving proteasome inhibitor therapy. Cancer Res 2009;69:1545–52. doi:10.1158/0008-5472.CAN-08-3858.

[109] Pavitt GD, Ramaiah K V, Kimball SR, Hinnebusch AG. eIF2 independently binds two distinct eIF2B subcomplexes that catalyze and regulate guanine-nucleotide exchange. Genes Dev 1998;12:514–26.

[110] Donzé O, Jagus R, Koromilas AE, Hershey JW, Sonenberg N. Abrogation of translation initiation factor eIF-2 phosphorylation causes malignant transformation of NIH 3T3 cells. EMBO J 1995;14:3828–34.

[111] Masutani M, Sonenberg N, Yokoyama S, Imataka H. Reconstitution reveals the functional core of mammalian eIF3. EMBO J 2007;26:3373–83. doi:10.1038/sj.emboj.7601765.

[112] Dong Z, Zhang J-T. Initiation factor eIF3 and regulation of mRNA translation, cell growth, and cancer. Crit Rev Oncol Hematol 2006;59:169–80. doi:10.1016/j.critrevonc.2006.03.005.

[113] Pestova* T V., Hellen CUT. The structure and function of initiation factors in eukaryotic protein synthesis. Cell Mol Life Sci 2000;57:651–74. doi:10.1007/PL00000726.

[114] Ben-Shem A, Garreau de Loubresse N, Melnikov S, Jenner L, Yusupova G, Yusupov M. The Structure of the Eukaryotic Ribosome at 3.0 A Resolution. Science (80-) 2011;334:1524–9.

[115] Shveygert M, Kaiser C, Bradrick SS, Gromeier M. Regulation of eukaryotic initiation factor 4E (eIF4E) phosphorylation by mitogen-activated protein kinase occurs through modulation of Mnk1-eIF4G interaction. Mol Cell Biol 2010;30:5160–7. doi:10.1128/MCB.00448-10.

[116] Vaysse C, Philippe C, Martineau Y, Quelen C, Hieblot C, Renaud C, et al. Key contribution of eIF4H-mediated translational control in tumor promotion. Oncotarget 2015;6:39924–40. doi:10.18632/oncotarget.5442.

[117] Marintchev A, Edmonds KA, Marintcheva B, Hendrickson E, Oberer M, Suzuki C, et al. Topology and Regulation of the Human eIF4A/4G/4H Helicase Complex in Translation Initiation. Cell 2009;136:447–60. doi:10.1016/j.cell.2009.01.014.

[118] Richter NJ, Rogers GW, Hensold JO, Merrick WC. Further biochemical and kinetic characterization of human eukaryotic initiation factor 4H. J Biol Chem 1999;274:35415–24. doi:10.1074/JBC.274.50.35415.

[119] Rozen F, Edery I, Meerovitch K, Dever TE, Merrick WC, Sonenberg N. Bidirectional RNA helicase activity of eucaryotic translation initiation factors 4A and 4F. Mol Cell Biol 1990;10:1134–44.

[120] Richter-Cook NJ, Dever TE, Hensold JO, Merrick WC. Purification and characterization of a new eukaryotic protein translation factor. Eukaryotic initiation factor 4H. J Biol Chem 1998;273:7579–87.

[121] Capossela S, Muzio L, Bertolo A, Bianchi V, Dati G, Chaabane L, et al. Growth Defects and Impaired Cognitive–Behavioral Abilities in Mice with Knockout for Eif4h, a Gene Located in the Mouse Homolog of the Williams-Beuren Syndrome Critical Region. Am J Pathol 2012;180:1121–35. doi:10.1016/j.ajpath.2011.12.008.

[122] Wu D, Matsushita K, Matsubara H, Nomura F, Tomonaga T. An alternative splicing isoform of eukaryotic initiation factor 4H promotes tumorigenesis in vivo and is a potential therapeutic target for human cancer. Int J Cancer

2011;128:1018–30. doi:10.1002/ijc.25419.

[123] Paulin FE., Campbell LE, O'Brien K, Loughlin J, Proud CG. Eukaryotic translation initiation factor 5 (eIF5) acts as a classical GTPase-activator protein. Curr Biol 2001;11:55–9. doi:10.1016/S0960-9822(00)00025-7.

[124] Wei J, Jia M, Zhang C, Wang M, Gao F, Xu H, et al. Crystal structure of the C-terminal domain of the ε subunit of human translation initiation factor eIF2B. Protein Cell 2010;1:595–603. doi:10.1007/s13238-010-0070-6.

[125] Yamamoto H, Unbehaun A, Loerke J, Behrmann E, Collier M, Bürger J, et al. Structure of the mammalian 80S initiation complex with initiation factor 5B on HCV-IRES RNA. Nat Struct Mol Biol 2014;21:721–7. doi:10.1038/nsmb.2859.

[126] Si K, Chaudhuri J, Chevesich J, Maitra U. Molecular cloning and functional expression of a human cDNA encoding translation initiation factor 6. Proc Natl Acad Sci U S A 1997;94:14285–90.

[127] Miluzio A, Beugnet A, Volta V, Biffo S. Eukaryotic initiation factor 6 mediates a continuum between 60S ribosome biogenesis and translation. EMBO Rep 2009;10:459–65. doi:10.1038/embor.2009.70.

[128] Groft CM, Beckmann R, Sali A, Burley SK. Crystal structures of ribosome anti-association factor IF6. Nat Struct Biol 2000;7:1156–64. doi:10.1038/82017.

[129] Rose AS, Bradley AR, Valasatava Y, Duarte JM, Prlić A, Rose PW. Web-based molecular graphics for large complexes. Proc. 21st Int. Conf. Web3D Technol. - Web3D '16, New York, New York, USA: ACM Press; 2016, p. 185–6. doi:10.1145/2945292.2945324.

[130] Rose AS, Hildebrand PW. NGL Viewer: a web application for molecular visualization. Nucleic Acids Res 2015;43:W576–9. doi:10.1093/nar/gkv402.

[131] Valenzuelas DM, Chaudhurig A, Maitra U. Eukaryotic ribosomal aubunit anti-association activity of calf liver Is contained in a single polypeptide Chain Protein of MI. = 25,500 (eukaryotic initiation factor 6). J Biol Chem 1982;257:7712–9.

[132] Sanvito F, Vivoli F, Gambini S, Santambrogio G, Catena M, Viale E, et al. Expression of a Highly Conserved Protein , p27 BBP , during the Progression of Human Colorectal Cancer. Cancer Res 2000;60:510–6.

[133] Miluzio A, Beugnet A, Grosso S, Brina D, Mancino M, Campaner S, et al. Impairment of cytoplasmic eIF6 activity restricts lymphomagenesis and tumor progression without affecting normal growth. Cancer Cell 2011;19:765–75.

doi:10.1016/j.ccr.2011.04.018.

[134] Miluzio A, Oliveto S, Pesce E, Mutti L, Murer B, Grosso S, et al. Expression and activity of eIF6 trigger malignant pleural mesothelioma growth in vivo. Oncotarget 2015;6:37471–85. doi:10.18632/oncotarget.5462.

[135] Ceci M, Gaviraghi C, Gorrini C, Sala LA, Offenhäuser N, Marchisio PC, et al. Release of eIF6 (p27BBP) from the 60S subunit allows 80S ribosome assembly. Nature 2003;426:579–84. doi:10.1038/nature02160.

[136] Chendrimada TP, Finn KJ, Ji X, Baillat D, Gregory RI, Liebhaber SA, et al. MicroRNA silencing through RISC recruitment of eIF6. Nature 2007;447:823–8. doi:10.1038/nature05841.

[137] Benelli D, Cialfi S, Pinzaglia M, Talora C, Londei P. The translation factor eIF6 is a Notch-dependent regulator of cell migration and invasion. PLoS One 2012;7:e32047. doi:10.1371/journal.pone.0032047.

[138] Finch AJ, Hilcenko C, Basse N, Drynan LF, Goyenechea B, Menne TF, et al. Uncoupling of GTP hydrolysis from eIF6 release on the ribosome causes Shwachman-Diamond syndrome. Genes Dev 2011;25:917–29. doi:10.1101/gad.623011.

[139] Sanvito F, Piatti S, Villa A, Bossi M, Lucchini G, Marchisio PC, et al. The β4 integrin interactor p27(BBP/eIF6) is an essential nuclear matrix protein involved in 60S ribosomal subunit assembly. J Cell Biol 1999;144:823–37. doi:10.1083/jcb.144.5.823.

[140] Si K, Maitra U. The Saccharomyces cerevisiae homologue of mammalian translation initiation factor 6 does not function as a translation initiation factor. Mol Cell Biol 1999;19:1416–26.

[141] Menne TF, Goyenechea B, Sánchez-Puig N, Wong CC, Tonkin LM, Ancliff PJ, et al. The Shwachman-Bodian-Diamond syndrome protein mediates translational activation of ribosomes in yeast. Nat Genet 2007;39:486–95. doi:10.1038/ng1994.

[142] Basu U, Si K, WARNER JR, Maitra U. The Saccharomyces cerevisiae TIF6 Gene Encoding Translation Initiation Factor 6 Is Required for 60S Ribosomal Subunit Biogenesis. Society 2001;75:1453–62. doi:10.1128/MCB.21.5.1453.

[143] Gatza ML, Silva GO, Parker JS, Fan C, Perou CM. An integrated genomics approach identifies drivers of proliferation in luminal-subtype human breast cancer. Nat Genet 2014;46:1051–9. doi:10.1038/ng.3073.

[144] Nanda JS, Cheung Y-N, Takacs JE, Martin-Marcos P, Saini AK, Hinnebusch AG, et al. eIF1 Controls Multiple Steps in Start Codon Recognition during Eukaryotic Translation Initiation. J Mol Biol 2009;394:268–85. doi:10.1016/J.JMB.2009.09.017.

[145] Miyazaki S, Imatani A, Ballard L, Marchetti A, Buttitta F, Albertsen H, et al. The Chromosome Location of the Human Homolog of the Mouse Mammary Tumor-Associated GeneINT6and Its Status in Human Breast Carcinomas. Genomics 1997;46:155–8. doi:10.1006/GENO.1997.4996.

[146] Yu Y, Marintchev A, Kolupaeva VG, Unbehaun A, Veryasova T, Lai S-C, et al. Position of eukaryotic translation initiation factor eIF1A on the 40S ribosomal subunit mapped by directed hydroxyl radical probing. Nucleic Acids Res 2009;37:5167–82. doi:10.1093/nar/gkp519.

[147] Mohammad-Qureshi SS, Haddad R, Hemingway EJ, Richardson JP, Pavitt GD. Critical contacts between the eukaryotic initiation factor 2B (eIF2B) catalytic domain and both eIF2beta and -2gamma mediate guanine nucleotide exchange. Mol Cell Biol 2007;27:5225–34. doi:10.1128/MCB.00495-07.

[148] Jiang H-Y, Jiang L, Wek RC. The eukaryotic initiation factor-2 kinase pathway facilitates differential GADD45a expression in response to environmental stress. J Biol Chem 2007;282:3755–65. doi:10.1074/jbc.M606461200.

[149] Horzinski L, Huyghe A, Cardoso M-C, Gonthier C, Ouchchane L, Schiffmann R, et al. Eukaryotic Initiation Factor 2B (eIF2B) GEF Activity as a Diagnostic Tool for EIF2B-Related Disorders. PLoS One 2009;4:e8318. doi:10.1371/journal.pone.0008318.

[150] Wang X, Proud CG. A novel mechanism for the control of translation initiation by amino acids, mediated by phosphorylation of eukaryotic initiation factor 2B. Mol Cell Biol 2008;28:1429–42. doi:10.1128/MCB.01512-07.

[151] Saletta F, Rahmanto YS, Richardson DR. The translational regulator eIF3a: The tricky eIF3 subunit! Biochim Biophys Acta - Rev Cancer 2010;1806:275–86. doi:10.1016/j.bbcan.2010.07.005.

[152] Sha Z, Brill LM, Cabrera R, Kleifeld O, Scheliga JS, Glickman MH, et al. The eIF3 Interactome Reveals the Translasome, a Supercomplex Linking Protein Synthesis and Degradation Machineries. Mol Cell 2009;36:141–52. doi:10.1016/J.MOLCEL.2009.09.026.

[153] Walsh D, Perez C, Notary J, Mohr I. Regulation of the translation initiation

factor eIF4F by multiple mechanisms in human cytomegalovirus-infected cells. J Virol 2005;79:8057–64. doi:10.1128/JVI.79.13.8057-8064.2005.

[154] Kroczynska B, Kaur S, Katsoulidis E, Majchrzak-Kita B, Sassano A, Kozma SC, et al. Interferon-dependent engagement of eukaryotic initiation factor 4B via S6 kinase (S6K)- and ribosomal protein S6K-mediated signals. Mol Cell Biol 2009;29:2865–75. doi:10.1128/MCB.01537-08.

[155] Cheng S, Sultana S, Goss DJ, Gallie DR. Translation initiation factor 4B homodimerization, RNA binding, and interaction with Poly(A)-binding protein are enhanced by zinc. J Biol Chem 2008;283:36140–53. doi:10.1074/jbc.M807716200.

[156] Pavitt GD, Yang W, Hinnebusch AG. Homologous segments in three subunits of the guanine nucleotide exchange factor eIF2B mediate translational regulation by phosphorylation of eIF2. Mol Cell Biol 1997;17:1298–313. doi:10.1128/MCB.17.3.1298.

[157] Homma MK, Wada I, Suzuki T, Yamaki J, Krebs EG, Homma Y. CK2 phosphorylation of eukaryotic translation initiation factor 5 potentiates cell cycle progression. Proc Natl Acad Sci U S A 2005;102:15688–93. doi:10.1073/pnas.0506791102.

[158] Jennings MD, Pavitt GD. eIF5 has GDI activity necessary for translational control by eIF2 phosphorylation. Nature 2010;465:378–81. doi:10.1038/nature09003.

[159] Gandin V, Miluzio A, Barbieri AM, Beugnet A, Kiyokawa H, Marchisio PC, et al. Eukaryotic initiation factor 6 is rate-limiting in translation, growth and transformation. Nature 2008;455:684–8. doi:10.1038/nature07267.

[160] Rush J, Moritz A, Lee KA, Guo A, Goss VL, Spek EJ, et al. Immunoaffinity profiling of tyrosine phosphorylation in cancer cells. Nat Biotechnol 2005;23:94–101. doi:10.1038/nbt1046.

[161] Rosenwald IB, Hutzler MJ, Wang S, Savas L, Fraire AE. Expression of eukaryotic translation initiation factors 4E and 2alpha is increased frequently in bronchioloalveolar but not in squamous cell carcinomas of the lung. Cancer 2001;92:2164–71.

[162] Dellas A, Torhorst J, Bachmann F, Bðnziger R, Schultheiss E, Burger MM. Expression of p150 in cervical neoplasia and its potential value in predicting survival. Cancer 1998;83:1376–83. doi:10.1002/(SICI)1097-

0142(19981001)83:7<1376::AID-CNCR15>3.0.CO;2-1.

[163] Bachmann F, Bänziger R, Burger MM. Cloning of a novel protein overexpressed in human mammary carcinoma. Cancer Res 1997;57:988–94.

[164] Marchetti A, Buttitta F, Pellegrini S, Bertacca G, Callahan R. Reduced expression of INT-6/eIF3-p48 in human tumors. Int J Oncol 2001;18:175–9.

[165] Nupponen NN, Isola J, Visakorpi T. Mapping the amplification ofEIF3S3 in breast and prostate cancer. Genes, Chromosom Cancer 2000;28:203–10. doi:10.1002/(SICI)1098-2264(200006)28:2<203::AID-GCC9>3.0.CO;2-X.

[166] Savinainen KJ, Linja MJ, Saramäki OR, Tammela TLJ, Chang GTG, Brinkmann AO, et al. Expression and copy number analysis of TRPS1, EIF3S3 and MYC genes in breast and prostate cancer. Br J Cancer 2004;90:1041–6. doi:10.1038/sj.bjc.6601648.

[167] Nupponen NN, Porkka K, Kakkola L, Tanner M, Persson K, Borg Å, et al. Amplification and Overexpression of p40 Subunit of Eukaryotic Translation Initiation Factor 3 in Breast and Prostate Cancer. Am J Pathol 1999;154:1777–83. doi:10.1016/S0002-9440(10)65433-8.

[168] Li BD L., Liu L, Dawson M, De Benedetti A. Overexpression of eukaryotic initiation factor 4E (eIF4E) in breast carcinoma. Cancer 1997;79:2385–90. doi:10.1002/(SICI)1097-0142(19970615)79:12<2385::AID-CNCR13>3.0.CO;2-N.

[169] Golob-Schwarzl N, Krassnig S, Toeglhofer AM, Park YN, Gogg-Kamerer M, Vierlinger K, et al. New liver cancer biomarkers: PI3K/AKT/mTOR pathway members and eukaryotic translation initiation factors. Eur J Cancer 2017;83:56–70. doi:10.1016/j.ejca.2017.06.003.

[170] Wang H, Ru Y, Sanchez-Carbayo M, Wang X, Kieft JS, Theodorescu D. Translation initiation factor eIF3b expression in human cancer and its role in tumor growth and lung colonization. Clin Cancer Res 2013;19:2850–60. doi:10.1158/1078-0432.CCR-12-3084.

[171] Lin L, Holbro T, Alonso G, Gerosa D, Burger MM. Molecular interaction between human tumor marker protein p150, the largest subunit of eIF3, and intermediate filament protein K7. J Cell Biochem 2001;80:483–90.

[172] Scoles DR, Yong WH, Qin Y, Wawrowsky K, Pulst SM. Schwannomin inhibits tumorigenesis through direct interaction with the eukaryotic initiation factor subunit c (eIF3c). Hum Mol Genet 2006;15:1059–70.

doi:10.1093/hmg/ddl021.

[173] Rothe M, Ko Y, Albers P, Wernert N. Eukaryotic initiation factor 3 p110 mRNA is overexpressed in testicular seminomas. Am J Pathol 2000;157:1597–604. doi:10.1016/S0002-9440(10)64797-9.

[174] Pincheira R, Chen Q, Zhang JT. Identification of a 170-kDa protein over-expressed in lung cancers. Br J Cancer 2001;84:1520–7. doi:10.1054/bjoc.2001.1828.

[175] Buttitta F, Martella C, Barassi F, Felicioni L, Salvatore S, Rosini S, et al. Int6 expression can predict survival in early-stage non-small cell lung cancer patients. Clin Cancer Res 2005;11:3198–204. doi:10.1158/1078-0432.CCR-04-2308.

[176] Cappuzzo F, Varella-Garcia M, Rossi E, Gajapathy S, Valente M, Drabkin H, et al. MYC and EIF3H Coamplification significantly improve response and survival of non-small cell lung cancer patients (NSCLC) treated with gefitinib. J Thorac Oncol 2009;4:472–8. doi:10.1097/JTO.0b013e31819a5767.

[177] Brass N, Ukena I, Remberger K, Mack U, Sybrecht GW, Meese EU. DNA amplification on chromosome 3q26.1-q26.3 in squamous cell carcinoma of the lung detected by reverse chromosome painting. Eur J Cancer 1996;32:1205–8. doi:10.1016/0959-8049(96)00016-0.

[178] Comtesse N, Keller A, Diesinger I, Bauer C, Kayser K, Huwer H, et al. Frequent overexpression of the genes FXR1, CLAPM1 and EIF4G located on amplicon 3q26-27 in squamous cell carcinoma of the lung. Int J Cancer 2007;120:2538–44. doi:10.1002/ijc.22585.

[179] Doldan A, Chandramouli A, Shanas R, Bhattacharyya A, Leong SPL, Nelson MA, et al. Loss of the eukaryotic initiation factor 3f in melanoma. Mol Carcinog 2008;47:806–13. doi:10.1002/mc.20436.

[180] Okamoto H, Yasui K, Zhao C, Arii S, Inazawa J. PTK2 and EIF3S3 genes may be amplification targets at 8q23–q24 and are associated with large hepatocellular carcinomas. Hepatology 2003;38:1242–9. doi:10.1053/JHEP.2003.50457.

[181] Joseph P, Lei Y-X, Ong T. Up-regulation of expression of translation factors – a novel molecular mechanism for cadmium carcinogenesis. Mol Cell Biochem 2004;255:93–101. doi:10.1023/B:MCBI.0000007265.38475.f7.

[182] Matsuda S, Katsumata R, Okuda T, Yamamoto T, Miyazaki K, Senga T, et al.

Molecular cloning and characterization of human MAWD, a novel protein containing WD-40 repeats frequently overexpressed in breast cancer. Cancer Res 2000;60:13–7.

[183] Rauch J, Ahlemann M, Schaffrik M, Mack B, Ertongur S, Andratschke M, et al. Allogenic antibody-mediated identification of head and neck cancer antigens. Biochem Biophys Res Commun 2004;323:156–62. doi:10.1016/j.bbrc.2004.08.071.

[184] Gray SG, Kytola S, Lui WO, Larsson C, Ekstrom TJ. Modulating IGFBP-3 expression by trichostatin A: potential therapeutic role in the treatment of hepatocellular carcinoma. Int J Mol Med 2000;5:33–74. doi:10.3892/ijmm.5.1.33.

[185] Bernardini S, Melino G, Saura F, Annicchiarico-Petruzzelli M, Motti C, Cortese C, et al. Expression of Co-factors (SMRT and Trip-1) for Retinoic Acid Receptors in Human Neuroectodermal Cell Lines. Biochem Biophys Res Commun 1997;234:278–82. doi:10.1006/BBRC.1997.6626.

[186] Silvera D, Arju R, Darvishian F, Levine PH, Zolfaghari L, Goldberg J, et al. Essential role for eIF4GI overexpression in the pathogenesis of inflammatory breast cancer. Nat Cell Biol 2009;11:903–8. doi:10.1038/ncb1900.

[187] Sorrells DL, Ghali GE, De Benedetti A, Nathan C-A, Li BD. Progressive amplification and overexpression of the eukaryotic initiation factor 4E gene in different zones of head and neck cancers. J Oral Maxillofac Surg 1999;57:294–9. doi:10.1016/S0278-2391(99)90676-6.

[188] Rosso P, Cortesina G, Sanvito F, Donadini A, Di Benedetto B, Biffo S, et al. Overexpression of p27BBP in head and neck carcinomas and their lymph node metastases. Head Neck 2004;26:408–17. doi:10.1002/hed.10401.

[189] Noske A, Lindenberg JL, Darb-Esfahani S, Weichert W, Buckendahl A-C, Röske A, et al. Activation of mTOR in a subgroup of ovarian carcinomas: correlation with p-eIF-4E and prognosis. Oncol Rep 2008;20:1409–17.

[190] Tu L, Liu Z, He X, He Y, Yang H, Jiang Q, et al. Over-expression of eukaryotic translation initiation factor 4 gamma 1 correlates with tumor progression and poor prognosis in nasopharyngeal carcinoma. Mol Cancer 2010;9:78. doi:10.1186/1476-4598-9-78.

[191] Tunca B, Tezcan G, Cecener G, Egeli U, Zorluoglu A, Yilmazlar T, et al. Overexpression of CK20, MAP3K8 and EIF5A correlates with poor prognosis

in early-onset colorectal cancer patients. J Cancer Res Clin Oncol 2013;139:691–702. doi:10.1007/s00432-013-1372-x.

[192] Lee NP, Tsang FH, Shek FH, Mao M, Dai H, Zhang C, et al. Prognostic significance and therapeutic potential of eukaryotic translation initiation factor 5A (eIF5A) in hepatocellular carcinoma. Int J Cancer 2010;127:968–76. doi:10.1002/ijc.25100.

[193] Harris MN, Ozpolat B, Abdi F, Gu S, Legler A, Mawuenyega KG, et al. Comparative proteomic analysis of all-trans-retinoic acid treatment reveals systematic posttranscriptional control mechanisms in acute promyelocytic leukemia. Blood 2004;104:1314–23. doi:10.1182/blood-2004-01-0046.

[194] Flavin RJ, Smyth PC, Finn SP, Laios A, O'Toole SA, Barrett C, et al. Altered eIF6 and Dicer expression is associated with clinicopathological features in ovarian serous carcinoma patients. Mod Pathol 2008;21:676–84. doi:10.1038/modpathol.2008.33.

[195] Seki N, Takasu T, Mandai K, Nakata M, Saeki H, Heike Y, et al. Expression of eukaryotic initiation factor 4E in atypical adenomatous hyperplasia and adenocarcinoma of the human peripheral lung. Clin Cancer Res 2002;8:3046–53.

[196] Wang R, Geng J, Wang J, Chu X, Geng H, Chen L. Overexpression of eukaryotic initiation factor 4E (eIF4E) and its clinical significance in lung adenocarcinoma. Lung Cancer 2009;66:237–44. doi:10.1016/j.lungcan.2009.02.001.

[197] Yang SX, Hewitt SM, Steinberg SM, Liewehr DJ, Swain SM. Expression levels of eIF4E, VEGF, and cyclin D1, and correlation of eIF4E with VEGF and cyclin D1 in multi-tumor tissue microarray. Oncol Rep 2007;17:281–7.

[198] Konicek BW, Stephens JR, McNulty AM, Robichaud N, Peery RB, Dumstorf C a., et al. Therapeutic inhibition of MAP kinase interacting kinase blocks eukaryotic initiation factor 4E phosphorylation and suppresses outgrowth of experimental lung metastases. Cancer Res 2011;71:1849–57. doi:10.1158/0008-5472.CAN-10-3298.

[199] Khoury T, Alrawi S, Ramnath N, Li Q, Grimm M, Black J, et al. Eukaryotic Initiation Factor-4E and Cyclin D1 Expression Associated with Patient Survival in Lung Cancer. Clin Lung Cancer 2009;10:58–66. doi:10.3816/CLC.2009.n.009.

[200] Li Y, Fan S, Koo J, Yue P, Chen Z (Georgia), Owonikoko TK, et al. Elevated expression of eukaryotic translation initiation factor 4E is associated with proliferation, invasion and acquired resistance to erlotinib in lung cancer. Cancer Biol Ther 2012;13:272–80. doi:10.4161/cbt.18923.

[201] Parsyan A, Reckamp KL. Cancers of the Respiratory System. Transl. Its Regul. Cancer Biol. Med., Dordrecht: Springer Netherlands; 2014, p. 557–74. doi:10.1007/978-94-017-9078-9_27.

[202] Demosthenous C, Han JJ, Stenson MJ, Maurer MJ, Wellik LE, Link B, et al. Translation initiation complex eIF4F is a therapeutic target for dual mTOR kinase inhibitors in non-Hodgkin lymphoma. Oncotarget 2015;6:9488–501. doi:10.18632/oncotarget.3378.

[203] Li Y, Yue P, Deng X, Ueda T, Fukunaga R, Khuri FR, et al. Protein phosphatase 2A negatively regulates eukaryotic initiation factor 4E phosphorylation and eIF4F assembly through direct dephosphorylation of Mnk and eIF4E. Neoplasia 2010;12:848–55.

[204] Seki N, Takasu T, Sawada S, Nakata M, Nishimura R, Segawa Y, et al. Prognostic significance of expression of eukaryotic initiation factor 4E and 4E binding protein 1 in patients with pathological stage I invasive lung adenocarcinoma. Lung Cancer 2010;70:329–34. doi:10.1016/j.lungcan.2010.03.006.

[205] Yin J-Y, Shen J, Dong Z-Z, Huang Q, Zhong M-Z, Feng D-Y, et al. Effect of eIF3a on Response of Lung Cancer Patients to Platinum-Based Chemotherapy by Regulating DNA Repair. Clin Cancer Res 2011;17:4600–9. doi:10.1158/1078-0432.CCR-10-2591.

[206] He Y, Correa AM, Raso MG, Hofstetter WL, Fang B, Behrens C, et al. The role of PKR/eIF2α signaling pathway in prognosis of Non-Small cell lung cancer. PLoS One 2011;6:e24855. doi:10.1371/journal.pone.0024855.

[207] Xu G, Yu H, Shi X, Sun L, Zhou Q, Zheng D, et al. Cisplatin sensitivity is enhanced in non-small cell lung cancer cells by regulating epithelial-mesenchymal transition through inhibition of eukaryotic translation initiation factor 5A2. BMC Pulm Med 2014;14:174. doi:10.1186/1471-2466-14-174.

[208] Wen Q, Wang W, Luo J, Chu S, Chen L, Xu L, et al. CGP57380 enhances efficacy of RAD001 in non-small cell lung cancer through abrogating mTOR inhibition-induced phosphorylation of eIF4E and activating mitochondrial

apoptotic pathway. Oncotarget 2016;7:27787–801. doi:10.18632/oncotarget.8497.

[209] Chen L, Tian G, Shao C, Cobos E, Gao W. Curcumin modulates eukaryotic initiation factors in human lung adenocarcinoma epithelial cells. Mol Biol Rep 2010;37:3105–10. doi:10.1007/s11033-009-9888-5.

[210] Győrffy B, Surowiak P, Budczies J, Lánczky A. Online Survival Analysis Software to Assess the Prognostic Value of Biomarkers Using Transcriptomic Data in Non-Small-Cell Lung Cancer. PLoS One 2013;8:e82241. doi:10.1371/journal.pone.0082241.

[211] Andersen CL, Jensen JL, Ørntoft TF. Normalization of Real-Time Quantitative Reverse Transcription-PCR Data: A Model-Based Variance Estimation Approach to Identify Genes Suited for Normalization, Applied to Bladder and Colon Cancer Data Sets. Cancer Res 2004;64:5245–50. doi:10.1158/0008-5472.CAN-04-0496.

[212] Livak KJ, Schmittgen TD. Analysis of Relative Gene Expression Data Using Real-Time Quantitative PCR and the 2−ΔΔCT Method. Methods 2001;25:402–8. doi:10.1006/meth.2001.1262.

[213] Liu Y, Sturgis CD, Grzybicki DM, Jasnosz KM, Olson PR, Tong M, et al. Microtubule-Associated Protein-2: A New Sensitive and Specific Marker for Pulmonary Carcinoid Tumor and Small Cell Carcinoma. Mod Pathol 2001;14:880–5. doi:10.1038/modpathol.3880406.

[214] Olsen BB, Wang S-Y, Svenstrup TH, Chen BP, Guerra B. Protein kinase CK2 localizes to sites of DNA double-strand break regulating the cellular response to DNA damage. BMC Mol Biol 2012;13:7. doi:10.1186/1471-2199-13-7.

[215] Dimri GP, Lee X, Basile G, Acosta M, Scott G, Roskelley C, et al. A biomarker that identifies senescent human cells in culture and in aging skin in vivo. Proc Natl Acad Sci U S A 1995;92:9363–7.

[216] Giannakakou P, Robey R, Fojo T, Blagosklonny M V. Low concentrations of paclitaxel induce cell type-dependent p53, p21 and G1/G2 arrest instead of mitotic arrest: molecular determinants of paclitaxel-induced cytotoxicity. Oncogene 2001;20:3806–13. doi:10.1038/sj.onc.1204487.

[217] Hatzenpichler R, Orphan VJ. Detection of Protein-Synthesizing Microorganisms in the Environment via Bioorthogonal Noncanonical Amino Acid Tagging (BONCAT), Springer, Berlin, Heidelberg; 2015, p. 145–57.

doi:10.1007/8623_2015_61.

[218] Fan S, Ramalingam SS, Kauh J, Xu Z, Khuri FR, Sun S-Y. Phosphorylated eukaryotic translation initiation factor 4 (eIF4E) is elevated in human cancer tissues. Cancer Biol Ther 2009;8:1463–9.

[219] He L-R, Zhao H-Y, Li B-K, Liu Y-H, Liu M-Z, Guan X-Y, et al. Overexpression of eIF5A-2 is an adverse prognostic marker of survival in stage I non-small cell lung cancer patients. Int J Cancer 2011;129:143–50. doi:10.1002/ijc.25669.

[220] Golob-Schwarzl N, Schweiger C, Koller C, Krassnig S, Gogg-Kamerer M, Gantenbein N, et al. Suppl.Separation of low and high grade colon and rectum carcinoma by eukaryotic translation initiation factors 1, 5 and 6. Oncotarget 2017;8:101224–43. doi:10.18632/oncotarget.20642.

[221] Rowinsky EK, Donehower RC. Paclitaxel (Taxol). N Engl J Med 1995;332:1004–14. doi:10.1056/NEJM199504133321507.

[222] Mollinedo F, Gajate C. Microtubules, microtubule-interfering agents and apoptosis. Apoptosis 2003;8:413–50.

[223] Greenberg VL, Zimmer SG. Paclitaxel induces the phosphorylation of the eukaryotic translation initiation factor 4E-binding protein 1 through a Cdk1-dependent mechanism. Oncogene 2005;24:4851–60. doi:10.1038/sj.onc.1208624.

[224] Vivanco I, Sawyers CL. The phosphatidylinositol 3-Kinase–AKT pathway in human cancer. Nat Rev Cancer 2002;2:489–501. doi:10.1038/nrc839.

[225] Sun QL, Sha HF, Yang XH, Bao GL, Lu J, Xie YY. Comparative proteomic analysis of paclitaxel sensitive A549 lung adenocarcinoma cell line and its resistant counterpart A549-Taxol. J Cancer Res Clin Oncol 2011;137:521–32. doi:10.1007/s00432-010-0913-9.

[226] Giancotti FG. Signal transduction by the alpha 6 beta 4 integrin: charting the path between laminin binding and nuclear events. J Cell Sci 1996;109 (Pt 6:1165–72.

[227] Timmer RT, Lax SR, Hughes DL, Merrick WC, Ravel JM, Browning KS. Characterization of wheat germ protein synthesis initiation factor eIF-4C and comparison of eIF-4C from wheat germ and rabbit reticulocytes. J Biol Chem 1993;268:24863–7.

[228] Wei C-L, Kainuma M, Hershey JWB. Characterization of Yeast Translation

Initiation Factor 1A and Cloning of Its Essential Gene*. 1995.

[229] Benne R, Brown-Luedi ML, Hershey JWB. Purification and Characterization of Protein Synthesis Initiation Factors eIF-1, eIF=4C, eIF=4D, and eIF-5 from Rabbit Reticulocytes*. vol. 253. 1978.

[230] Bernhart E, Damm S, Heffeter P, Wintersperger A, Asslaber M, Frank S, et al. Silencing of protein kinase D2 induces glioma cell senescence via p53-dependent and -independent pathways. Neuro Oncol 2014;16:933–45. doi:10.1093/neuonc/not303.

8 Appendix

8.1 Ethical Vote NSCLC

Ethikkommission

Medizinische Universität Graz

Auenbruggerplatz 2, A-8036 Graz
ethikkommission@medunigraz.at
Tel.: +43 / 316 / 385-13928, Fax: -14348

FOLGEVOTUM
gültig bis 26.03.2019

EK-Nummer:	27-240 ex 14/15
Studientitel:	Biochemical and genetic contribution of eukaryotic translation Initiation Factors (eIFs) to lung carcinoma
Prüfer:	Prof.Dr.Dr. PhD Johannes Haybäck Medizinische Universität Graz
Sponsor:	Institut für Pathologie; Med. Univ. Graz
Ansprechpartner:	Dr.Dr. PhD Johannes Haybäck, 8036 Graz, Auenbruggerplatz 25
CRO:	-
Antragsteller:	Institut für Pathologie, Medizinische Universität Graz
Ansprechpartner:	Nadine Gantenbein, MSc. BSc.

Die o.a. Studie wurde von der Ethikkommission erstmals im 'expedited Review' am 06.03.2015 behandelt. Die Ethikkommission ist zu folgendem Schluss gekommen:

Es besteht kein Einwand gegen die Durchführung der Studie in der vorliegenden Form.

Kommissionsmitglieder, die für diesen Tagesordnungspunkt als befangen anzusehen waren und daher gemäß Geschäftsordnung an der Entscheidungsfindung und Abstimmung nicht teilgenommen haben: keine

Zur Beurteilung vorliegende Dokumente:

Dokumente eingegangen am 13.02.2015, begutachtet im 'expedited Review' am 06.03.2015	
✓ Antragsformular ECS Unterschriftenseiten	13.02.2015
✓ Antragsformular ECS	13.02.2015
✓ Originalprotokoll Studienprotokoll_eIFs_Lunge_Version 1.0 Version 1.0	02.02.2015
✓ CV CV_Haybaeck_Johannes Version 1.0	22.01.2015
✓ Sonstiges: Ethikvotum_EPO_Xenografts Version 1.0	17.01.2015
✓ Sonstiges: Ansuchen um Erlass der Bearbeitungsgebüren Version 1.0	22.01.2015
✓ Sonstiges: 20150204_Stellungnahme_Biobank_1008_15_Lunge_normal_Haybaeck_FV Version 1.0	10.02.2015
Dokumente eingegangen am 24.03.2015, begutachtet im 'expedited Review' am 26.03.2015	
✓ Sonstiges: Stellungnahme - Pathologie	23.03.2015
Dokumente eingegangen am 26.06.2015, begutachtet im 'expedited Review' am 07.07.2015	
✓ Originalprotokoll 2.0/undatiert	
✓ Protokoll Amendment 1.0	26.06.2015
✓ Informed Consent Form 1.0	25.06.2015
✓ Sonstiges: Zustimmungserklärung/Thoraxchirurgie 1.0	
Dokumente eingegangen am 16.07.2015, begutachtet im 'expedited Review' am 07.08.2015	
✓ Originalprotokoll 3.0	16.07.2015
✓ Informed Consent Form post O.P. 1.0	16.07.2015

Dokumente eingegangen am 15.02.2016 (in der nächsten Begutachtung mitbegutachtet)	
✓ Protokoll Amendment 2.0	12.02.2016
✓ Informed Consent Form post O.P. 2.0	10.02.2016
✓ Informed Consent Form Lungenkarzinom 2,.0	10.02.2016
✓ Sonstiges: Zustimmungserklärung LKH Graz Süd West - Prof Lax	24.08.2015
✓ Sonstiges: Tumor Tissue Checklist HayLab-Lung 1.0	
✓ Sonstiges: SOP - Lung autopsy tissue sampling	
Dokumente eingegangen am 22.02.2016, begutachtet im 'expedited Review' am 29.02.2016	
✓ Originalprotokoll 4.0	10.02.2016
Dokumente eingegangen am 02.03.2016, begutachtet im 'expedited Review' am 14.03.2016	
✓ Zwischenbericht	02.03.2016
Dokumente eingegangen am 02.02.2017 (in der nächsten Begutachtung mitbegutachtet)	
✓ Cover Letter Amendment	02.02.2017
Originalprotokoll 5.0	03.02.2017
✓ Informed Consent Form post O.P. 3.0	02.02.2017
✓ Informed Consent Form Lungenkarzinom 3.0	02.02.2017
Dokumente eingegangen am 08.02.2017, begutachtet im 'expedited Review' am 10.02.2017	
✓ Originalprotokoll 5.0	02.02.2017
Dokumente eingegangen am 13.03.2017 (in der nächsten Begutachtung mitbegutachtet)	
✓ Cover Letter Amendment	13.03.2017
Originalprotokoll 5.0	02.02.2017
✓ Zwischenbericht	13.03.2017
Dokumente eingegangen am 21.03.2017, begutachtet im 'expedited Review' am 27.03.2017	
✓ Originalprotokoll 6.0	12.03.2017
Dokumente eingegangen am 22.03.2018, begutachtet im 'expedited Review' am 29.03.2018	
✓ Zwischenbericht	11.03.2018

Datum Erstvotum: 26.03.2015

Die Ethikkommission geht - rechtlich unverbindlich - davon aus, dass es sich um keine klinische Prüfung nach AMG bzw. MPG handelt.

Es handelt sich um eine Studie im Rahmen einer Dissertation.

Das Votum der Ethikkommission berührt in keiner Weise die alleinige Verantwortung der Prüferin / des Prüfers / der Prüfer für die ordnungsgemäße Durchführung der Studie unter Einhaltung aller einschlägiger gesetzlicher Bestimmungen und Richtlinien.

Weiters machen wir darauf aufmerksam, dass der Kommission unverzüglich zu melden sind:

- Abweichungen vom Protokoll aus Sicherheitsgründen oder Protokolländerungen

- Änderungen, die das Risiko der Teilnehmer/-innen erhöhen oder die Durchführung der Studie wesentlich beeinflussen

- Mutmaßliche unerwartete schwerwiegende Nebenwirkungen - SUSARs (AMG-Studien ab 1.5.2004) oder schwerwiegende unerwünschte Ereignisse - SAEs (andere Studien)

- Jegliche Information über sonstige Umstände, die die Sicherheit der Teilnehmer/-innen oder die Durchführung der Studie beeinträchtigen können

8.2 Buffer Solution

Table 7 SDS-Gel Solution

Gel type	Components for 1 gel	
Separation gel 12.5%	3.28 ml	ddH_2O (Millipore)
	2.5 ml	Tris 1.5 M pH 8.8
	4.06 ml	30% Acrylamide / Bis Solution (37.5:1)
	100 µl	10% SDS
	100µl	APS
	7.5 µl	TEMED
Separation gel 8%	4.6 ml	ddH_2O (Millipore)
	2.5 ml	Tris 1.5 M pH 8.8
	2.7 ml	Acrylamide
	100 µl	10% SDS
	100µl	APS
	6 µl	TEMED
Stacking Gel	3.1 ml	ddH_2O (Millipore)
	1.25 ml	Tris 1.5 M pH 6.8
	0.5 ml	Acrylamide
	50 µl	10% SDS
	25 µl	APS
	7.5 µl	TEMED

Table 8 Buffer and Solutions

Buffer/ Solution	Component	Amount	Final Conc.
NP-40 Lysis Buffer (1 L)	1M Tris HCl (pH 7.5)	50 ml	50 mM
	5M NaCl	30 ml	150 mM
	NP-40	5 ml	0.5%
	ddH_2O	Add up to 500 ml	
Final lysis buffer (10ml)	0.1M Pefabloc	100µl	1 mM
	1 M DTT	10 µl	1 mM
	1 tablet of Complete Mini and PhosSTOP dissolved in 1mL ddH_2O	1 ml	
	NP-40 Lysis buffer	9 ml	
SDS-Running Buffer 10x	Tris HCl (pH 8.4)	30.29 g	250 mM
	Glycine	14.13 g	192 mM
	SDS	10 g	1%
	ddH2O		Ad to 1L
Towbin Transfer Buffer	Tris	3.03 g	250 mM
	Glycine	14.26 g	190 mM
	Methanol	20%	1%
TBS-Tween 0.1%	Tris	24.2 g	0.2 M
	NaCl	80.0 g	1.4 M
	Tween-20	1 ml	0.1%
	ddH2O		Ad to 1L

8.3 Appendix tables

Table 9 One-Way ANOVA statistical data of eIF6 knockdown in A549 cell line

Day 3		**p-value**
Living cells	siScr. vs. sieIF6_1	ns
	siScr. vs. sieIF6_2	p< 0.001
	siScr. vs. sieIF6_1+2	p< 0.001
Early apoptotic cells	siScr. vs. sieIF6_1	p<0.05
	siScr. vs. sieIF6_2	p<0.001
	siScr. vs. sieIF6_1+2	p< 0.01
Late apoptotic cells	siScr. vs. sieIF6_1	ns
	siScr. vs. sieIF6_2	ns
	siScr. vs. sieIF6_1+2	ns
Necrotic cells	siScr. vs. sieIF6_1	ns
	siScr. vs. sieIF6_2	ns
	siScr. vs. sieIF6_1+2	ns
Day 5		**p-value**
Living cells	siScr. vs. sieIF6_1	p< 0.001
	siScr. vs. sieIF6_2	p< 0.001
	siScr. vs. sieIF6_1+2	p< 0.001
Early apoptotic cells	siScr. vs. sieIF6_1	ns
	siScr. vs. sieIF6_2	p< 0.01
	siScr. vs. sieIF6_1+2	ns
Late apoptotic cells	siScr. vs. sieIF6_1	p< 0.001
	siScr. vs. sieIF6_2	p< 0.001
	siScr. vs. sieIF6_1+2	p< 0.001
Necrotic cells	siScr. vs. sieIF6_1	ns
	siScr. vs. sieIF6_2	ns
	siScr. vs. sieIF6_1+2	ns

Table 10 qRT-PCR Primers

Primer name	**Sequence (5´->3´)**
Actin FW	ACA GCC TGG ATA GCA ACG TAC
Actin REV	CGT GCT GCT GAC CGA GG
SDHA FW	TGGTTGTCTTTGGTCGGG
SDHA REV	GCGTTTGGTTTAATTGGAGGG
IPO8 FW+REV	Qiagen #QT00071246
eIF6 FW	CCGCGTGCGGAGCTTGTTA
eIF6 REV	CGCCCTCGAACACACTGTAGAAGT

Table 11 siRNA constructs

siRNA	Sequence (5´->3´)	Order Number
Hs_EIF1AX_6 (eIF1A_1)		SI03187961
Hs_EIF1AX_9 (eIF1A_2)		SI04215869
Hs_ITGB4BP_5 (eIF6_1)	CTGCTTTGCCAAGCTCACCAA	SI03096331
HS_ITGB4BP_6 (eIF6_2)	CTGGTGCATCCCAAGACTTCA	SI03099768
AllStars Negative		1027280
AllStars Negative 488-Alexa-labeled		1027292

Table 12 Northernblot oligonucleotides

Primer name	Sequence (5´->3´)
ITS1	CCTCGCCCTCCGGGCTCCGTTAATGATC
ITS2	CTGCGAGGGAACCCCCAGCCGCGCA

Table 13 Antibody used in this study

Antibody	P- site	Dilution	Host	Cat.no.	Company
p-4E-BP1	Ser65	1:1000	Rabbit	#9456	Cell Signaling Technology
4E-BP1	-	1:1000	Rabbit	#9452	Cell Signaling Technology
p-mTOR	Ser2448	1:1000	Rabbit	#5536	Cell Signaling Technology
mTOR (7C10)	-	1:1000	Rabbit	#2983	Cell Signaling Technology
p-AKT	Ser473	1:1000	Rabbit	#4058	Cell Signaling Technology
AKT	-	1:1000	Rabbit	#9272	Cell Signaling Technology
p-P70S6K	Thr421/ Ser424	1:1000	Rabbit	#9204	Cell Signaling Technology
P70S6K	-	1:1000	Rabbit	#9202	Cell Signaling Technology
p-PTEN	Ser380	1:1000	Rabbit	#9551	Cell Signaling Technology
PTEN	-	1:1000	Rabbit	#9559	Cell Signaling Technology
P53 (7F5)	-	1:1000	Rabbit	#2527	Cell Signaling Technology
MDM2	-	1:1000	Mouse	sc-965	Santa Cruz Biotechnology
eIF1A	-	1:1000	Rabbit	Ab177939	Abcam
eIF2α (D7D3)	-	1:1000	Rabbit	#5324	Cell Signaling Technology
p-eIF2α (D9G8)	Ser51	1:1000	Rabbit	#3398	Cell Signaling Technology
eIF3A	-	1:1000	Rabbit	#2538	Cell Signaling Technology
eIF3B (eIF3η D-9)	-	1:1000	Mouse	Sc-137215	Santa Cruz Biotechnology
eIF3C	-	1:1000	Rabbit	#2068	Cell Signaling Technology
eIF3D (eIF3ζ H-300)	-	1:1000	Rabbit	Sc-28856	Santa Cruz Biotechnology
eIF3H (D9C1)	-	1:1000	Rabbit	#3413	Cell Signaling Technology
eIF3I (eIF3β A-8)	-	1:1000	Mouse	Sc-374153	Santa Cruz Biotechnology
eIF3J	-	1:1000	Rabbit	#3261	Cell Signaling Technology
eIF3K (2313C2a)	-	1:1000	Mouse	Sc-81262	Santa Cruz Biotechnology
eIF3M (V-21)	-	1:1000	Rabbit	Sc-133541	Santa Cruz Biotechnology
eIF4A1	-	1:1000	Rabbit	#2490	Cell Signaling Technology

p-eIF4B	Ser406	1:1000	Rabbit	#5399	Cell Signaling Technology
eIF4B	-	1:1000	Rabbit	#3592	Cell Signaling Technology
eIF4E	-	1:1000	Rabbit	#9742	Cell Signaling Technology
p-eIF4G	Ser1108	1:1000	Rabbit	#2441	Cell Signaling Technology
eIF4G	-	1:1000	Rabbit	#2498	Cell Signaling Technology
eIF4H	-	1:1000	Rabbit	#3469	Cell Signaling Technology
eIF5	-	1:1000	Rabbit	GTX114923	GeneTex
eIF6	-	1:1000	Rabbit	GTX63642	GeneTex
GAPDH	-	1:2000	Rabbit	#2118	Cell Signaling Technology
p-RPS6	Ser235/236	1:1000	Rabbit	#2211	Cell Signaling Technology
RPS6	-	1:1000	Rabbit	ab40820	Abcam
cleaved caspase 3	-	1:1000	Rabbit	#9664	Cell Signaling Technology
PARP	-	1:1000	Rabbit	#9542	Cell Signaling Technology
p21	-	1:1000	Rabbit	#2847	Cell Signaling Technology

8.4 Protocols

8.4.1 RNA Isolation

1) Homogenization

- Tissue:
- Homogenize tissue samples (50-100 mg) in 1ml of Trizol
- 2-3 times Magna Lyser 30 sec at 6500rpm
- Cell pellet:
- Resuspend pellet in 1 ml of Trizol

2) Phase separation

- Incubate 10min RT
- Add 200µl chloroform (per 1 ml Trizol) and shake vigorously by hand for 15 sec
- Incubate at RT for 2-3 min centrifuge at full speed for 15 min at 4°C
- Mixture separates into a lower red phenol-chlorophorm phase, in an interphase and in a colorless upper aqueous phase containing RNA

3) RNA precipitation

- Transfer aqueous phase to fresh tube with 500µl isopropyl alcohol
- Shake vigorously by hand (you can see a cloudiness)
- Incubate at RT for 10 min
- Centrifuge at full speed 20 min at 4°C

4) RNA wash

- Remove supernatant and wash the RNA pellet 1-2 x with 1ml of 80% ethanol, centrifuge at full speed for 5 min at 4°C

5) Dissolving the RNA

- Briefly dry the RNA pellet, dry pellet at 37°C for 5min (Don´t let the RNA pellet dry completely as this will greatly decrease its solubility)
- Dissolve RNA pellet in H_2Ofresenius by passing the solution a few times through a pipette tip (no pellet visible 30µl of water, tissue samples around 300-400µl of water)
- Incubate for 10 min at 58°C
- After the incubation step put RNA on ice
- RNA can be stored at -80°C

8.4.2 Click iT® HPG Protocol for A549 and H520 cell line in 12 Wells (6 Wells for each construct)

Prepare:

a. HPG solution: Solubilize the Click-iT® (Cat no. C10186) metabolic labeling reagent with DMSO to make a 10mM stock (higher stock solution is not soluble). This process ensures that the DMSO concentration is not more than 0.1–0.2% in the cell culture. Aliquot and store any unused reagent at –20°C. When stored as directed, this stock solution is stable for up to 1 year. [Orig. Protocol Step 1.1.]
b. Dilute 10x Click-iT® cell reaction buffer (Component A) to 1x
c. Solubilize Click-iT® cell buffer additive (Component C) with 4mL deionized H_2O
d. Cycloheximide (CycHx) solution 5mg/mL in H_2O Fresenius.
e. Lysis buffer: Tris-HCl,1% SDS, -> Add shortly before needed Benzonase, Phosphatase Inhib., Protease Inhib. to the lysis Buffer

Buffer/ Solution	Component	[µl]
100µl Lysis Buffer	A-Proteinin	0,1
	Pepstastin	0,1
	Leupeptid	0,1
	PMFS	1
	Phosphate inhib,	1
	Benzoase	1,8
	Puffer (50mM Tris-HCl pH. 8.0 + 0,1% SDS)	94,9
100µl HPG 1:10 Dilution	HPG Met (-) Medium	10 90

Protocol:

1. Wash cells once with warm PBS, add 500µl/well methionine-free medium to the cells and incubate the cells at 37°C for **overnight** (o/n) to deplete methionine reserves. [Orig. Protocol Step 1.2.]
2. After o/n add 500µM CycHx (10µl of stock)/well for *inhibited translation control* to untreated control cells.
3. After **1h** CycHx add the **10µM** concentration of Click-iT® HPG labeling reagent per well, gently mix, and incubate at 37°C, 5% CO_2 for 2 hours (can be extended to 4h). [Orig. Protocol Step 1.3.]
4. Prepare final lysis buffer at the end of incubation time, by adding protease and phosphatase inhibitors at appropriate concentrations to 1% SDS in 50 mM Tris-HCl, pH 8.0. You need 50 µl lysis buffer for 3-5 12-Wells. [Orig Protocol Step 5.1.]
5. Put the Plates on Ice, remove the medium and wash the cells three times with Ice cold PBS.
6. Add lysis buffer to the well and scrape cells, transfer lysate into a tube.
7. Sonicate the cells in Sonication Bath 20-50 seconds. [Orig Protocol Step 5.4.]
8. Vortex the lysate for 5 minutes. [Orig Protocol Step 5.5.]
9. Centrifuge the cell lysate at 13.000 RPM at 4°C for 5 minutes. [Orig Protocol Step 5.6.]
10. Transfer the supernatant to a clean tube and take aliquot to determine the protein concentration. The protein sample is now ready for reaction with an azide or alkyne detection molecule. If you are not immediately using the prepared protein sample for the Click-iT® detection reaction, store the sample at –20°C for up to 2 weeks. If you wish to store the sample for more than 2 weeks, proceed to precipitate the sample. [Orig Protocol Step 5.7.]
    Click IT Reaction (Cat. no.: C10276): PROTECT from LIGHT, work in Room with reduced light and aluminium foil around the tubes.
11. Up to 200 µg in a maximum volume of 50 µL of azide- or alkyne-labeled protein in 50 mM Tris-HCl, pH 8.0, containing up to 1% SDS.

100 µL of the Click-iT® reaction buffer
Sufficient volume of 18 megaOhm water for a final volume of 160 µL.

12. Cap the tube and vortex for 5 seconds.
13. Add 10 µL of $CuSO_4$ (Component B) and vortex for 5 seconds.
14. Add 10 µL of Click-iT® reaction buffer additive 1 solution and vortex for 5 seconds. Wait for 2-3 minutes, but not longer than 5 minutes, before proceeding to step 16.
15. Add 20 µL of Click-iT® reaction buffer additive 2 solution and vortex for 5 seconds. This solution turns bright orange.
16. Vortex continuously or rotate in the dark end-over-end for 20 minutes using a rotator. Using tetramethylrhodamine (TAMRA) as the detection reagent, **protect this solution from light.**

Preparing Sample for 1D or 2D Analysis:

17. Add 600 µL of methanol to the reaction mixture and vortex briefly.
18. Add 150 µL of chloroform and vortex briefly.
19. Add 400 µL of 18 megaOhm water and vortex briefly.
20. Centrifuge for 5 minutes at 13,000–18,000 × g, then carefully remove and discard as much of
    the upper aqueous phase as possible while leaving the interface layer containing the protein precipitate intact. Note: The upper phase is bright orange. The lower phase is pink if TAMRA is used or colorless if biotin is used.
21. Add 450 µL of methanol to the tube and vortex briefly.
22. Centrifuge for 5 minutes at 13,000–18,000 × g to pellet the protein. Discard the supernatant.
23. Add 450 µL of methanol to the tube and vortex briefly. Centrifuge and discard the supernatant. This second methanol wash step serves to remove residual reaction components.
24. Cover the tube with a lint-free tissue and keep the tube cap open. Allow the pellet to air-dry, for 15 minutes to overnight.
    If you won't proceed with gel electrophorese, cap the tube and store the sample at –20°C until use.
25. Resolubilize the precipitated sample in gel electrophoresis sample loading buffer. A target concentration of approximately 1–2 mg/mL is suggested.
    For 1D SDS gels, vortex the sample for 10 minutes followed by heating for 10 minutes at 70°C.
26. Briefly, spin the protein sample before loading to remove any unsolubilized material.
27. Recommended loading amounts for 1D minigels are 5–20 µg.
28. Perform electrophoresis as recommended by the manufacturer. **PROTECT from LIGHT (Aluminum Foil around electrophoresis chamber)**
29. Following electrophoresis, remove the gel from the cassette. **PROTECT from LIGHT**
30. Image Bis-Tris gels immediately after removal from the cassette or after a short 5-minute water wash. If imaged immediately, use water to rinse some of the SDS on the side of the gel. **PROTECT from LIGHT**
31. Wash the Tris-Glycine gels for 5 minutes with deionized water and image. **PROTECT from LIGHT**
32. If the TAMRA detection reagent was used, image directly or perform a western transfer procedure. If biotin detection reagent was used, perform a western transfer procedure.
33. After imaging gels with TAMRA-labeled samples, the samples can be fixed and stained with SYPRO® Ruby total protein stain, Pro-Q® Emerald glycoprotein stain, or Pro-Q® Diamond phosphoprotein stain, or bands can be excised for subsequent mass spectrometry analysis.

8.4.3 eIF Silencing A549 in 12 well plates

Material:

Medium:

DMEM/Hams F12 (Gibco #11330-057) + 10% FBS (FBS South American EU Approved Lotnr: 42Q8257K RESERVEnr.: 1150145 S2, #10270106) + 1% Penicillin- Streptomycin (10,000 U/mL) (#15140-122)

Transfection reagent:

Oligofectamine™ Transfection Reagent (Life technologies # 12252-011)

siRNA: all from Qiagen

eIF1A Constructs:

Hs_EIF1AX_6 FlexiTube siRNA # SI03187961

Hs_EIF1AX_9 FlexiTube siRNA # SI04215869

eIF6 Constructs:

Hs_ITGB4BP_5 FlexiTube siRNA # SI03096331

HS_ITGB4BP_6 FlexiTube siRNA # SI03099768

Scrambled siRNA:

AllStars Negative Control siRNA (5 nmol) siRNA # 1027280

Silencing A549 in 12 Well Plates workflow:

1. Serum starvation 24h before seeding out cells
2. 20´000 cell/well should be seeded out and then let them attach and grow for 24h
3. Transfection: Aspirate the medium and give “Serum, P/S free Medium” in all wells. Controls 600µl and for transfection wells 522 µl.
   Transfection Mix: first mix siRNA and Medium-> vortex carefully -> then give OF to the mix and incubate 15 min RT
   - Add 78µl of transfection mix per well and incubate for 4h in the incubator
   - Add 400µl of Medium with 20% FBS final volume is 1000µl
4. Harvest cells after 3 days and 5 days:
   Cells are washed with PBS
   Trypsinized and for each sample 3 wells were pooled and then centrifuged
   Cell pellet was washed with PBS two times
   Cell pellet was flash frozen and stored at -80°C

Transfection scheme:

Following is calculated for 600µl transfection end volume.

	Medium[µl]	Oligofectamine [µl]	siRNA
Control	78	-	-
MOK	74	4	-
Scrambled	74 - siRNA	4	20nM end conc.
eIF1A_6	74 - siRNA	4	20nM end conc.
eIF1A_9	74 - siRNA	4	20nM end conc.
eIF1A_6+9	74 - siRNA	4	10nM eIF1A_6 +10mM eIF1A_9 (20nM end conc.)
eIF6_5	74 - siRNA	4	20nM end conc.
eIF6_6	74 - siRNA	4	20nM end conc.
eIF6_5+6	74 - siRNA	4	10nM eIF6_5 +10mM eIF6_6 (20nM end conc.)

8.4.4 eIF Silencing H520 in 12 well plates

Material:

Medium:

DMEM + 10% FBS (FBS South American EU Approved Lotnr: 42Q8257K RESERVEnr.: 1150145 S2, #10270106) + 1% Penicillin- Streptomycin (10,000 U/mL) (#15140-122)

Transfection reagent:

Oligofectamine™ Transfection Reagent (Life technologies # 12252-011)

siRNA: all from Qiagen

eIF1A Constructs:

Hs_EIF1AX_6 FlexiTube siRNA # SI03187961

Hs_EIF1AX_9 FlexiTube siRNA # SI04215869

eIF6 Constructs:

Hs_ITGB4BP_5 FlexiTube siRNA # SI03096331

HS_ITGB4BP_6 FlexiTube siRNA # SI03099768

Scrambled siRNA:

AllStars Negative Control siRNA (5 nmol) siRNA # 1027280

Silencing A549 in 12 Well Plates workflow:

1. Serum starvation 24h before seeding out cells
2. 80´000 cell/well should be seeded out and then let them attach and grow for 24h (USE ACCUTASE, no Trypsin)
3. Transfection in 12 Well Plates: Aspirate the medium and give “Serum, P/S free Medium” in all wells. Controls 600µl and for transfection wells 522 µl.
   Transfection Mix: first mix siRNA and Medium-> vortex carefully -> then give OF to the mix and incubate 15 min RT
   Add 78µl of transfection mix per well and incubate for 4h in the incubator
   Add 400µl of Medium with 20% FBS final volume is 1000µl
4. Harvest cells after 3 days and 5 days:
   Cells are washed with PBS
   Use Accutase to detache the cells and for each sample 3 wells were pooled and then centrifuged
   Cell pellet was washed with PBS two times
   Cell pellet was flash frozen and stored at -80°C

Transfection scheme:

Following is calculated for 600µl transfection end volume.

	Medium[µl]	Oligofectamine [µl]	siRNA
Control	78	-	-
MOK	74	4	-
Scrambled	74 - siRNA	4	20nM end conc.
eIF1A_6	74 - siRNA	4	20nM end conc.
eIF1A_9	74 - siRNA	4	20nM end conc.
eIF1A_6+9	74 - siRNA	4	10nM eIF1A_6 +10mM eIF1A_9 (20nM end conc.)
eIF6_5	74 - siRNA	4	20nM end conc.
eIF6_6	74 - siRNA	4	20nM end conc.
eIF6_5+6	74 - siRNA	4	10nM eIF6_5 +10mM eIF6_6 (20nM end conc.)

8.4.5 Annexin V / PI stain

1. Pre-cool FACS tubes on ICE
2. Add supernatant of cells and centrifuge for 3 min at 900 rpm at room temperature.
3. In the meantime detach cells with 250 µl trypsin (A549) or 250 µl accutase (H520) and stop the enzymatic activity with 250 µl medium + FBS.
4. Discard supernatant from FACS tubes after centrifugation and add cell suspension from 3.
5. Centrifuge for 3 min at 900 rpm at room temperature.
6. Discard supernatant carefully after centrifugation and resuspend cells in 250-300 µl PBS
7. Centrifuge for 3 min at 900 rpm at room temperature.
8. Discard supernatant carefully after centrifugation and resuspend cells in 250-300 µl PBS
9. Centrifuge for 3 min at 900 rpm at room temperature.
10. Discard supernatant carefully after centrifugation and resuspend cells 100 µl 1x Binding buffer + 2.5 µl Annexin V and 2.5 µl PI per tube (Protect from light)
    For single stain: use only Annexin V or PI
11. Incubate for 15 min in the dark at room temperature. (Protect from light)
12. Add 150µl 1x binding buffer (Protect from light)
13. Measure samples at the FACS (Protect from light)

Addition to 10.: Dilute Binding buffer with ddH2O

For 10 tubes:
1 ml 1x Binding buffer
25 µl Annexin V
25 µl PI

8.4.6 Cell Staining for Senescence a Galactosidase Activity Assay

1. Four days after transfection of cells in 12-well plates, aspirate the medium from the cells
2. Wash cells with PBS three times to remove the cell culture medium
3. Discard PBS
4. Add fixation solution to the cells and incubate at room temperature for 3- 5 minutes,
5. Wash cells twice with PBS
6. Add staining solution to the cell culture dish.
7. Incubate at least for 2 hours at 37 °C WITHOUT CO_2, but it depends on the cell line. In Case of the A549 cells it was 8 hours and for the H520 it was 4 hours.

Table 14 Cell Staining Assay Solutions

Solution/Buffer	Component	Amount	Final Conc.
Staining Solution (5 ml) Prepare solution on day of experiment Protect from light	X-Gal Solution 100 mM Cyanoferrate [$K_3Fe(CN)_6$] 100 mM Cyanoferrate [$K_4Fe(CN)_6$] Citrate buffer pH 6.0 5 M NaCl 1 M $MgCl_2$ ddH_2O	125 µl 250 µl 250 µl 2 ml 150 µl 10 µl 2.215 ml	1 mg/ml 5 mM 5 mM 30 mM 150 mM 2 mM -
X-Gal Solution in DMF (Dimethylformamide)	X-Gal (5-bromo-4-chloro-3-indoly D-galactopyranoside) solve in DMF Store at -20 °C, is not stable in water	20 mg in 1 ml	20 mg/ml
Cyanoferrate [$K_3Fe(CN)_6$] Protect from light	Solve salt in ddH_2O	329 mg in 10 ml	100 mM
Cyanoferrate [$K_4Fe(CN)_6$] Protect from light	Solve salt in ddH_2O	422,4 mg in 10 ml	100 mM
Citrate buffer pH 6.0	Citric Acid Sodium Phosphate (Na_2HPO_4) for pH adjustment (pH 6.0)		0.1 M 0.2 M

8.4.7 Polysomeprofiling for A549 and H520

UP-Scale silencing in 100 mm Dish:

A549:

1. Serum starvation 24h before seeding out cells
2. 1,6 * 10^5 cell/dish should be seeded out and then let them attach and grow for 24h
3. Transfection: Aspirate the medium and give “Serum free, P/S free Medium” in all wells. Give 6960 µl of “Serum free, P/S free Medium” to the well before adding transfection mix.
4. Transfection Mix: first mix siRNA and Medium-> vortex carefully -> then give OF to the mix and incubate 15 min RT
5. Add 1´040 µl of transfection mix per well and incubate for 4h in the incubator
6. Add 2´000 µl of 50% FBS final volume is 10ml with 10% FBS.
7. Let them grow until day 3

H520:

1. Serum starvation 24h before seeding out cells
2. 9,0 * 10^5 cell/dish should be seeded out and then let them attach and grow for 24h
3. Transfection: Aspirate the medium and give “Serum free, P/S free Medium” in all wells. Give 6960 µl of “Serum free, P/S free Medium” to the well before adding transfection mix.
4. Transfection Mix: first mix siRNA and Medium-> vortex carefully -> then give OF to the mix and incubate 15 min RT
5. Add 1´040 µl of transfection mix per well and incubate for 4h in the incubator
6. Add 2´000 µl of 50% FBS final volume is 10ml with 10% FBS.
7. Let them grow until day 3

Oligofectamine:

Normally 4 µl OF in 0,6 mL is used for 100 mm Dish we will use 8mL silencing volume.

$$\begin{aligned} 4\mu l\ OF &= 0{,}6\ ml \\ x\ \mu l\ OF &= 8\ ml \\ \underline{x &= 53{,}3\ \mu l\ OF} \end{aligned}$$

Because of previous tests with more OF we take 60 µl OF per Dish if one uses 10ml silencing volume. Reference: “RNA Silencing: Methods and Protocols” by Gordon Carmichael

SiRNA concentration:

20µM stock solution

Silencing concentration per well or dish is 20nM:

$$\begin{aligned} 2 * 10^4 * x &= 20nM * 10´000\ \mu l \\ x &= \frac{20nM * 10´000\ \mu l}{2 * 10^4} \\ x &= 8\ \mu l \end{aligned}$$

Total:
In total 10 Dish per eIF will be transfected. We used only the pool variant where we combine both siRNAs. 4µl of construct A + 4µl of construct B = 8µl siRNA.

$$10{,}2 * 8\mu l = \mathbf{80}\ \mu \boldsymbol{l\ siRNA\ in\ total}$$
$$10{,}2 * 53{,}3\ \mu l\ OF = \mathbf{533}\ \mu \boldsymbol{l\ OF\ in\ total}$$

	Medium [µl]	**Oligofectamine [µl]**	**siRNA [µl]**
MOCK	10064,3	543,66	-
eIF1A_6+9	9982,7	543,66	40,8 + 40,8
eIF6_5+6	9982,7	543,66	40,8 + 40,8

Cell harvesting
-grow the cells in 100 mm^2 dishes (10 dishes for one lysate) up to around 80% confluency
-add Cycloheximide to a concentration of 100ug/ml (from fresh prepared 5mg/ml solution in water), incubate 15min at 37°C
- Cells were washed twice in cold PBS containing 100µg/ml cycloheximide
-scrape cells with 1 ml of lysis buffer
- Pipet 20 times up and down.
Lysates were centrifuged at 14000g for 7min 4°C
OD 260nm should be measured and noted for later,
Supernatants were aliquoted to 100µl aliquots and then flash frozen in liquid nitrogen and stored at -80°C until used.

Lysis buffer:

Stock Solutions	**Final Conc.**	**1mL Buffer for 10 Petridish:**
200 mM HEPES pH7.4	20mM HEPES pH7.4	100 µl
1 M KCl	200mM KCl	200 µl
150 mM $MgCl_2$	15mM $MgCl_2$	100 µl
-	1% Triton-X-100	10 µl
5mg/ml (always fresh)	100ug/ml Cycloheximide	20 µl
1 pill (1ml) Complete EDTA-free protease inhibitor	1x Complete EDTA-free protease inhibitor	100 µl
1 M DTT	1mM DTT	1 µl
100mM PMSF	10mM PMSF	100 µl
-	Aqua Dest.	369 µl

Gradient buffer:

50mM Tris HCl pH 7.4

12mM $MgCl_2$

50nM NH_4Cl

1mM DTT

For 150ml 40% final Gradient Buffer add 60g of Sucrose, 3 ml CycHx (15mg- end conc.100µg/ml) and 150 µl DTT. This solution you can dilute to all other gradient conc. you need. For each gradient tube 2,2 mL of solution can be filled in. We had following 5 gradients: 15%; 21,25%; 27,5%; 33,75%; 40%

Always start with the highest conc. In this case 40%.

	15%	21,25%	27,5%	33,75%	40%
40% Solution	18,75 ml	26,6 ml	34,4 ml	42,4 ml	-
AD Buffer	31,25 ml	23,4 ml	15,6 ml	7,8 ml	-

Fill 2,2 ml in the tube and then freeze tube with solution at -80°C after 4-5 h, you can get the tube out and make the second gradient conc. and freeze again. With this procedure it is possible to do 2 gradients per day at maximum.

Gradient loading:

4-6 OD Units harvested cells should be used for Polysome Profiling. For example:

1ml Sample has OD_{260} of 54,1

$$OD\ 54{,}1 = 1000\ \mu l$$
$$OD\ 4 = x\ \mu l$$
$$x = \frac{1000 * 4}{54{,}1}$$
$$x = 73{,}93$$

For calculation always refer to the original volume of the sample.

Ultra-centrifugation

The supernatant was layered onto 15%-40% sucrose gradients, and then tubes were centrifuged in a SW41Ti rotor (Beckman, Villepinte, France) for 150 min at 160000 g (38´500 rpm), 4°C without breaking. (we start brake at 25´000 rpm with SLOW).

After 2h of centrifugation one can start washing the ISCO with hot tab water.

Profile detection and fraction collection

Polysomal profiles were analysed via an ISCO density gradient analyser unit, which analyses and simultaneously blots ribosomal distribution measured by an UA-6 detector with 254 nm filter (Teledyne ISCO, Nebraska, USA).

Device adjustments:
Pump:60
Intensity:0,2
Noise:0,5
Paper:60
Fraction: 0,4
Auto baseline – press the button and arrange the marker where you think it is best.

Have Eppis prepared with fraction number and sample ID, were Lids are cut. Keep both pieces to put them into the collector.

TCA precipitation:
All fractions were Trichloroacetic acid precipitated with 50% TCA solution, which should have an end concentration of 10-15%. Incubation over night at -20°C to concentrate proteins for gel electrophoresis.
Next day centrifuge full speed 10 min at 4°C and then wash the cells 2 times with ice cold Fresenius water. Then resuspend pellet in 20µl 2x Loading dye.

8.4.8 Paclitaxel treatment of A549 cells

Paclitaxel Treatment of A549 cells Date:

First day:

1. Trypsinize T175 Flask and harvest cells
2. Count cells
3. Seed out $1.5x10^6$ cells in 2ml medium per 6-well
4. Incubation 37°C 5% CO_2 for 24h

Next day:

5. Freshly prepare paclitaxel solutions and dilutions
6. Start Treatment

Take microscope pictures every 24h before harvesting cells.

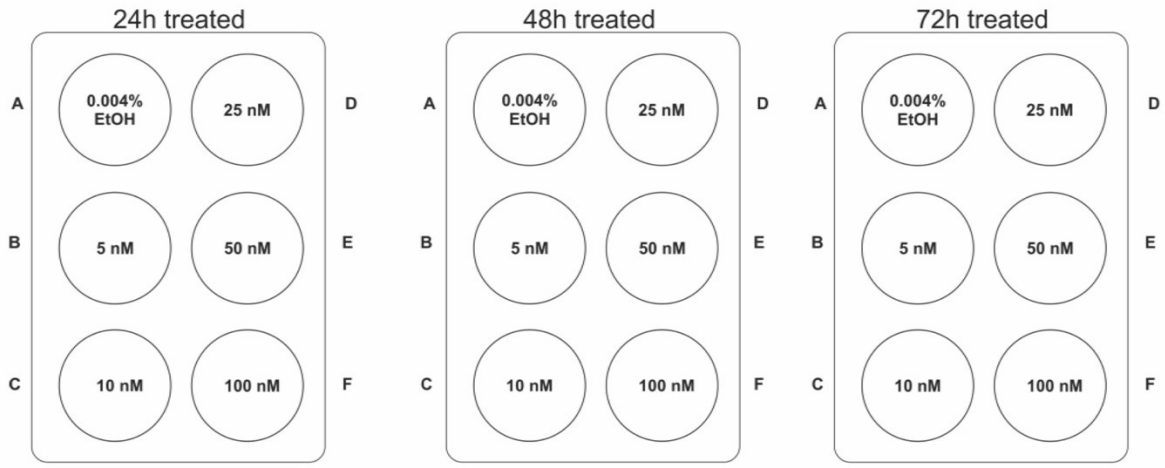

8.5 Reagents

Table 15 List of Reagents used in this work

Reagent	Source	Identifier
Radioactivity	Hartman	SRP401
Oligofectamine™ Transfection Reagent	Life technologies	12252-011
FITC Annexin V Apoptosis Detection Kit	Biolegend	#640932
Guava ViaCount Reagent for Flow Cytometry	Merck-Millipore	#4000-0040
Nonfat dried milk powder	AppliChem	A0830,1000
High Capacity cDNA Reverse Transcriptase Kit	Applied Biosystems	4368814
Micro Amp Fast Optical 96-Well Plate	Applied Biosystems	4311971
4x Laemmli Sample Buffer	Biorad	161-0747
Bio-Rad Protein Assay Dye Reagent Concentrate	BioRad	500-0006
TEMED	BioRad	161-0800
30% Acrylamide / Bis Solution	BIO-RAD	161-0158
Cell Scrapper	Corning	3010
Amersham ECL Prime Western blotting detection Reagent	GE Healthcare	RPN 2236
Amersham ECL Select Western blotting detection Reagent	GE Healthcare	RPN 2235
FBS South American EU Approved Lotnr: 42Q8257K RESERVEnr.: 1150145 S2	Gibco	10270106
DMEM/F-12, HEPES	Gibco life technologies	11330-057
Penicillin-Streptomycin (10,000 U/mL)	Gibco Life technologies	15140-122
Trypsin-EDTA (0.05%), phenol red	Gibco Life technologies	25300-054
DMEM, high glucose, HEPES	Gibco Life technologies	42430-082
DPBS 1x (Dulbecco's Phosphate buffered saline)	Gibco Life technologies	14190-169
RPMI 1640 Medium	Gibco Life technologies	21875-091
Hamilton 50µl tips without filter	Hamilton	235966
PageRuler™ Prestained Protein Ladder, 10 to 180 kDa	Life Technologies	26616
Oligofectamine™ Transfection Reagent	Life technologies	12252-011
Power SYBR Green PCR Master Mix	Life technologies	4368706

Reagent	Source	Identifier
TBE Buffer (Tris-borate-EDTA) (10X)	Life Technologies	B52
Sodium Chloride	Merck	1.064.045.000
TRIS	Merck	1.083.865.000
Tween 20	Merck	8.170.721.000
Guava ViaCount Reagent for Flow Cytometry, 100 tests	Merck	4000-0040
Immobilon-P Membrane, PVDF 0.45µm*26.5cm*3.75m roll	Millipore	IPVH00010
Complete Tablets Mini EDTA-free, Easypack	Roche	4693159001
Magnalyser green beads	Roche	3358941001
PhosSTOP Easypack	Roche	4906837001
Cycloheximide	Roth	8682.1
Rotiphorese® 10x SDS-PAGE	Roth	3060.2
Ponceau S solution	Sigma	P7170-1L
Potassium chloride	Sigma	P5405-250G
DMSO	Sigma Aldrich	D8418-50ml
Giemsa Stain, Modified Solution	Sigma Aldrich	48900-500ML-F
Pefabloc® SC-Roche	Sigma Aldrich	11585916001
Accutase® solution	Sigma Aldrich	A6964-100ML
Formaldehyde solution	Sigma-Aldrich	F1635
Tris(hydroxymethyl)aminomethane	Sigma-Aldrich	252859-500G
Restore Plus Western Blot Stripping Buffer	Thermo Scientific	46430
RNase Inhibitor	Thermo Scientific	N8080119
TRIzol® Reagent	Thermo Scientific	15596-018

8.6 Instruments and Devices

Table 16 List of Instruments used in this Work

Device	Producer	Place
Beckman Ultra Centrifuge with SW41Ti Rotor	Beckman	Villepinte, France
Biofuge Fresco	Heraeus	Hanau, Deutschland
Biospectrometer	Eppendorf	Hamburg, Deutschland
Electrophoresis Power supply EPS 301	GE Healthcare	Little Chalfont, UK
GeneAmp 9700 Thermocycler	Applied Biosystems	Foster City, USA
Guava EasyCyte 8	Millipore	Massachusetts, USA
Image Quant Las 500	GE Healthcare	Little Chalfont, UK
MagNA LYSER	Roche Diagnostics	Risch-Rotkreuz, Switzerland
Mini-Shaker MS1	Ika	North Carolina, USA
NanoDROP 1000	Thermo Fischer scientific	Massachusetts, USA
Quant Studio 7 Flex	Applied Biosystems	Foster City, USA
Semi-dry Blotting Unit V20-SDB	Scieplas	Cambridge, UK
Semi-Micro Analytical Balance GR200EC	A&D Company	Tokyo, JAPAN
Teledyne ISCO	ISCO International	Illinois, USA
Thermomixer comfort	Thermo Fischer scientific	Massachusetts, USA
Typhoon 9400	Amersham	Little Chalfont, UK
Vertical Shaker Duomax 1030	Heidolph	Schwabach, Deutschland
Vertikales Mini-Elektrophoresesystem SE250	Hoefer Inc.	Richmond, USA
Ventana Immunostainer XT	Roche Diagnostics	Risch-Rotkreuz, Switzerland

8.7 Software

Table 17 Software used in this work

Software	Source	Download
Graphpad PRISM 5.0	GraphPad software Inc.	https://www.graphpad.com/
IBM SPSS 23 -Software	SPSS, Inc. Chicago, IL	https://www.ibm.com/analytics/at/de/technology/spss/
InCyte 3.1	Millipore	Millipore
Kaplan-Meier Plotter software	[210]	http://kmplot.com/analysis/index.php?p=service&cancer=lung
Normfinder Software Excel Add-In v0.953	[211]	https://moma.dk/normfinder-software